AD_____

Award Number: DAMD17-01-1-0108

TITLE: Tumor Oxygen Dynamics as a Prognostic Indicator of Effective Antiangiogenic Therapy

PRINCIPAL INVESTIGATOR: Dawen Zhao, M.D., Ph.D.

CONTRACTING ORGANIZATION: The University of Texas Southwestern Medical Center at Dallas
Dallas, TX 75390-9105

REPORT DATE: May 2003

TYPE OF REPORT: Annual Summary

PREPARED FOR: U.S. Army Medical Research and Materiel Command
Fort Detrick, Maryland 21702-5012

REPORT DOCUMENTATION PAGE

Form Approved
OMB No. 074-0188

1. AGENCY USE ONLY (Leave blank)	2. REPORT DATE	3. REPORT TYPE AND DATES COVERED
	May 2003	Annual Summary (1 May 2001 - 30 Apr 2003)

4. TITLE AND SUBTITLE
Tumor Oxygen Dynamics as a Prognostic Indicator of Effective Antiangiogenic Therapy

5. FUNDING NUMBERS
DAMD17-01-1-0108

6. AUTHOR(S)
Dawen Zhao, M.D., Ph.D.

7. PERFORMING ORGANIZATION NAME(S) AND ADDRESS(ES)
The University of Texas Southwestern Medical Center at Dallas
Dallas, TX 75390-9105

E-Mail: dawen.zhao@utsouthwestern.edu

8. PERFORMING ORGANIZATION REPORT NUMBER

9. SPONSORING / MONITORING AGENCY NAME(S) AND ADDRESS(ES)
U.S. Army Medical Research and Materiel Command
Fort Detrick, Maryland 21702-5012

10. SPONSORING / MONITORING AGENCY REPORT NUMBER

11. SUPPLEMENTARY NOTES
Original contain color plates: All DTIC reproductions will be in black and white.

12a. DISTRIBUTION / AVAILABILITY STATEMENT
Approved for Public Release; Distribution Unlimited

12b. DISTRIBUTION CODE

13. ABSTRACT (Maximum 200 Words)
Tumor survival, growth and metastasis depend critically on the development of new blood vessels: so called angiogenesis. One major goal of this project is to fully understand and precisely assess the dynamic changes in blood perfusion and oxygenation, both during normal growth and following anti-angiogenic therapy in diverse prostate tumors with differential characteristics, so that we may predict response and optimize the therapy. Applying non-invasive MRI techniques, we successfully detected differential vasculature and oxygenation among prostate tumor lines with different degrees of aggressiveness. The slower growing and well differentiated H and HI tumors are better vascularized and oxygenated than the fast growing and anaplastic AT1 and metastatic MAT-Lu tumors. These MRI data has been validated by histological studies and irradiation. The metronomic therapy significantly inhibited the AT1 tumor growth. The dynamic contrast enhanced (DCE) MRI was capable of detecting early changes in tumor vasculature cause by the metronomic treatment. Histological studies verified formation of dramatic central necrosis, increased apoptosis, and decreased vascular density and proliferating rate in the treated tumors. Good correlation of the MRI data with tumor growth delay suggested that the non-invasive MRI could predict anti-angiogenic treatment efficacy.

14. SUBJECT TERMS
Magnetic resonance imaging (MRI), pO2, hypoxic maker, VEGF, Anti-angiogenic therapy

15. NUMBER OF PAGES
80

16. PRICE CODE

17. SECURITY CLASSIFICATION OF REPORT	18. SECURITY CLASSIFICATION OF THIS PAGE	19. SECURITY CLASSIFICATION OF ABSTRACT	20. LIMITATION OF ABSTRACT
Unclassified	Unclassified	Unclassified	Unlimited

Table of Contents

Background:

The diagnosis and treatment of cancers are beginning to be influenced by new ideas and discoveries emerging from the field of angiogenesis. Folkman and his colleagues hypothesized that since tumors require a blood supply to grow, inhibiting the growth of new blood vessels, i.e., antiangiogenesis, should prevent growth and metastasis of the primary tumor (1). Recently, Folkman's and Kerbel's laboratories (2-4) have shown that extended administration of certain cytotoxic agents at very low doses known as 'metronomic' chemotherapy, increase the antiangiogenic activity of the drugs. Traditional methods for detection of therapeutic response generally rely on a gross decrease in tumor size. Although these methods are useful for assessing response at the end of treatment, little information is available early in the course of treatment. MRI has the ability to detect treatment-induced changes occurring within the tumor prior to a decrease in tumor size. One major goal of this project is to fully understand and precisely assess the dynamic changes in blood perfusion and oxygenation, both during normal growth and following anti-angiogenic therapy in several prostate tumors with differential characteristics, so that we may predict response and optimize the therapy.

Body:

Initial preparation for research in Year 1 started with animal handling, tumor implantation, and perfusion. I received accreditation from the Institutional Animal Care and Research Advisory committee Board (IACRAC) to proceed with my animal studies. I successfully implanted an orthotopic prostate tumor by injecting minced tumor tissues into rat prostate gland.

I am receiving training and becoming proficient in state of the art MRI techniques. *FREDOM* (Fluorocarbon Relaxometry using Echo planar imaging for Dynamic Oxygen Mapping) with hexafluorobenzene, as a reporter molecule, exploits the exceptional response of the ^{19}F NMR spin-lattice relaxation rate to changes in oxygen tension. Echo planar MRI provides measurements with high temporal resolution (~8 mins) and a spatial resolution (>100 x 4 mm^3 voxels). This facilitates sequential reproducible measurements (±1-2 torr) (5, 6). Dynamic contrast enhanced (DCE) MRI based on the transport properties of gadolinium-DTPA (Gd-DTPA) has been used as a method in the clinic to provide an indication of tumor vasculature and perfusion by imaging the uptake, or leakage, of contrast agent into tumor interstitial space (7, 8). Blood Oxygen Level Dependent (BOLD) MRI is a totally non-invasive approach to provide a qualitative evaluation of blood oxygen level in tumor (9). The large paramagnetic susceptibility of deoxyhemoglobin produces large magnetic field gradients between blood vessels and surrounding tissues. I am applying these MR techniques to extensively study oxygenation and vasculature in prostate tumors. Our results obtained using *FREDOM* showed better tissue oxygen tension in well differentiated and slower growing Dunning R3327 prostate rat H and HI tumors, compared with anaplastic or metastatic, faster growing AT1 and MAT-Lu tumors. Most interestingly, by using *FREDOM* to track oxygen dynamics in specific tumor regions, we found that most hypoxic regions in the H and HI tumor responded to oxygen or carbogen inhalation to become well oxygenated, while those in the AT1 and MAT-Lu tumors showed little response to respiratory intervention (See Appended publications for details). Results of BOLD and DCE MRI, providing information about qualitative vascular oxygenation and perfusion, also showed that the H tumors are better oxygenated and perfused than the AT1 tumors. Also, I have performed extensive studies on tumor blood vessels, perfusion, and hypoxia in the Dunning prostate tumors. Immunohistochemical studies of tumor hypoxia and vasculature using hypoxic marker pimonidazole and endothelium marker CD31 showed that a higher labeling index of pimonidazole and lower vascular density in the AT1 than the H and HI tumors. Comparable results by cellular and molecular biology support our MRI findings.

In Year 2, I started the proposed metronomic therapy. Our results showed the metronomic dose (20 mg/kg/day, p.o. in drinking water) of the conventional chemotherapeutic drug, cyclophosphamide (CTX), significantly inhibited tumor growth of the AT1 tumors. By combining the metronomic CTX with the antiangiogenic agent, thalidomide, a synergistic effect has been achieved (Fig. 1). In contrast,

despite tremendous tumor growth delay in the conventional MTD dose of CTX group (150 mg/kg twice per week, i.p.), all the animals (n=6) died from this highly toxic dose within 12 days.

Fig.1

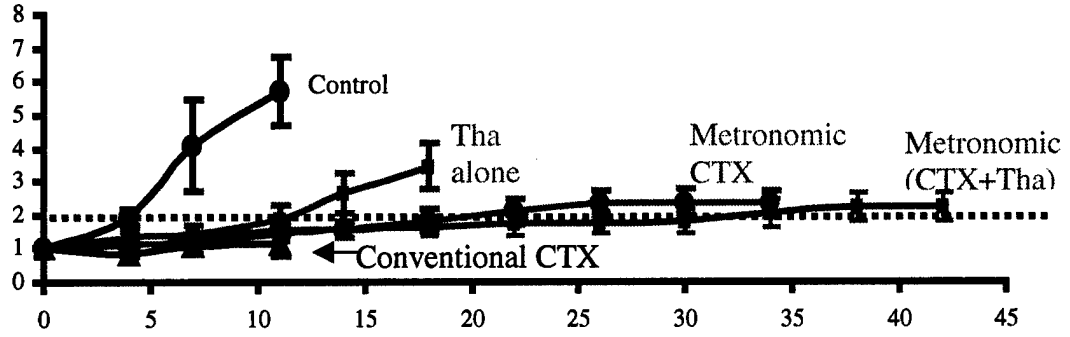

MRI studies were performed on 1 day before and 7~10 days after the treatment with the metronomic CTX and thalidomide. By applying multiple slices DCE MRI, I am able to detect heterogeneity within the tumor. Following up the treated tumors, significant decrease in signal enhancement in the central region of tumor was observed, compared with the pretreated same tumors. Some tumors even showed essentially no change in signal intensity after Gd-DTPA injection (Fig.2). The MRI results correlated well with the outcome of the treatment for individual tumors.

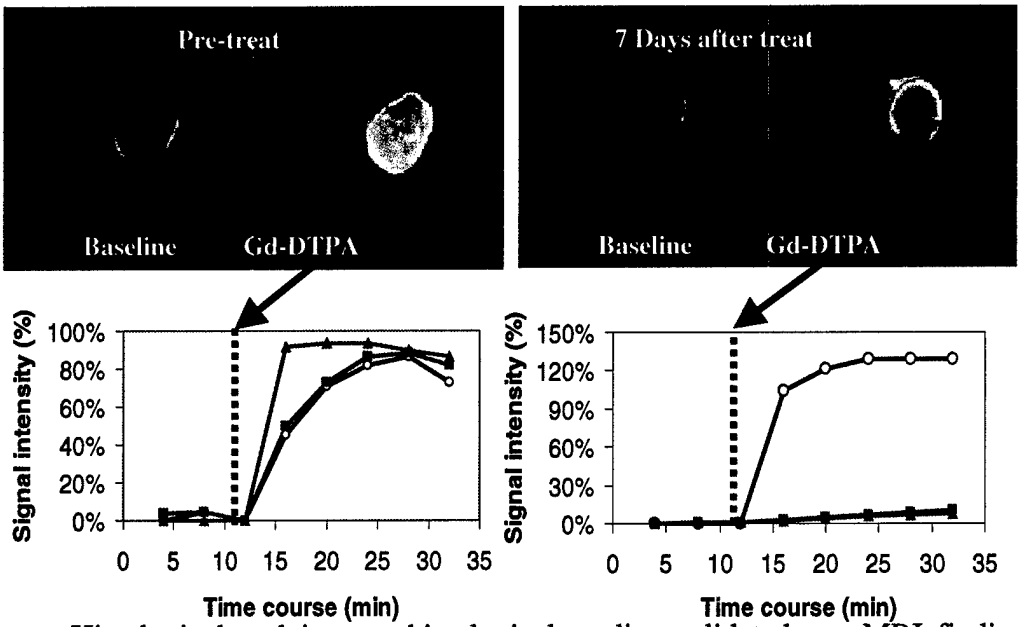

Figure 2. Dynamic contrast enhanced proton MRI of Dunning prostate rat tumor in pedicle in foreback of rat. Pre-treatment: there is uniform enhancement of all three tumor slices following Gd-DTPA infusion. After 7 days treatment, only the rim enhances.

Histological and immunohistological studies validated our MRI findings, showing that dramatic central necrotic tissues developed after the metronomic treatment and significantly increased apoptosis and VEGF expression, and decreased vascular density and tumor proliferating rate. More interestingly, vascular thrombosis was observed in numerous tumor microvessels accompanying with the treatment.

During the past two year studies, **three peer reviewed papers and five abstracts have been generated from this research endeavor (10-17).**

Fig. 3

a) b) c)

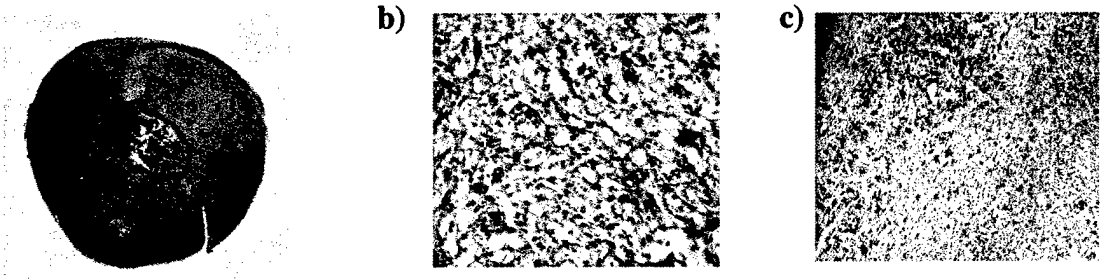

Fig.3 Significant central necrosis was found in a typical AT1 tumor 7 days after the treatment with combination of metronomic CTX and thalidomide (a). Anti-CD31 staining (b) showed significant decrease in vascular density compared with the untreated control tumor. There was significantly increased apoptotic tumor cells detected by anti-caspase 3 (c).

Key Research Accomplishments

1. **Learned animal tumor implantation**
   Implantation of Dunning prostate R3327 rat tumor
2. **Learned and becoming proficient in the state of art NMR techniques**
   a. *FREDOM* (Fluorocarbon Relaxometry using Echo planar imaging for Dynamic Oxygen Mapping)
   b. *BOLD* (blood oxygen level dependent) MRI
   c. Dynamic contrast enhanced (DCE) MRI
   d. Learned operating system of new Varian MR
3. **Assessment of tumor perfusion and oxygenation during normal growth of prostate tumors**
   3.1. MR approaches
   a. Better tissue oxygen tension in Dunning R3327 prostate rat H and HI tumors, compared with AT1 and MAT-Lu tumors.
   b. Most hypoxic regions in the H and HI tumor responded to oxygen or carbogen inhalation to become well oxygenated, while those in the AT1 and MAT-Lu tumors showed little response to respiratory intervention.
   c. Results of BOLD and DCE MRI, providing information about qualitative vascular oxygenation and perfusion.

   3.2. Correlation of MR findings with biological studies
   a. Immunohistochemical studies of tumor hypoxia and vasculature using hypoxic marker pimonidazole and endothelium marker CD31 supported our MR findings.
   b. Administration of perfusion marker Hoechst dye 33342 showed a good correlation between perfused vessels and total vessels (CD31) in the HI tumors.
   c. RT-PCR showed no significant difference in HIF-1α gene expression between H and AT1 tumor.
4. **Experimental metronomic therapy and MRI evaluation**
   4.1. Tumor growth delay and histological studies
   a. Significant tumor growth delay achieved in the anaplastic and faster growing Dunning prostate AT1 tumors treated with metronomic dose of cyclophosphamide (CTX) alone or combined with thalidomide.
   b. Histological studies verified the metronomic treatment induced dramatic central necrosis with a thin peripheral rim.
   c. Immunohistochemical staining showed that significantly increased apoptosis (Caspase 3) in tumor and endothelial cells, and decreased vascular density (CD31) and proliferation (PCNA).
   d. A large number of thromboses were observed in the tumor blood vessels treated with the metronomic approach.

   4.2. MRI evaluation
   a. Dynamic contrast enhanced (DCE) MRI was capable of detecting physiological changes underlying tumor growth delay.
   b. DCE MRI studies showed that significant decrease in signal enhancement occurred between 7 and 10 days after the start of metronomic treatment.

Reportable Outcomes

Reportable outcomes that have resulted from this research endeavor include:

Peer Reviewed Publications:

1. **Zhao, D.**, Constantinescu, A., Hahn, E. W., and Mason, R. P. Differential oxygen dynamics in the two Dunning prostate R3327 rat tumor sublines (MAT-Lu and HI) with respect to growth and respiratory challenge. *Int. J. Radiat. Oncol. Biol. Phys.* 53, 744-56, 2002.
2. **Zhao, D.**, Constantinescu, A., Hahn, E. W., and Mason, R. P. Correlation of tumor oxygen dynamics with radiation response of the Dunning prostate R3327-HI tumors. *Radiat. Res.* 159, 621-31, 2003.
3. **Zhao, D.**, Ran, S., Constantinescu, A., Hahn, E. W., and Mason, R. P. Tumor oxygen dynamics: in vivo MRI monitoring and correlation with histological findings. *Neoplasia* in press 2003.
4. **Zhao, D.**, Constantinescu, A., Hahn, E.W., and Mason, R.P. MRI evaluation of metronomic chemotherapy: the antitumor effects of combined low-dose cyclophosphamide and thalidomide on prostate tumors. Manuscript in preparation.

Abstracts (Published Conference Proceedings):

1. **Zhao, D.**, Jiang, L., Constantinescu, A., Hahn, E.W., and Mason, R.P. In vivo MRI monitoring of prostate tumor vasculature and oxygen dynamics. *AACR New Discoveries in Prostate Cancer Biology and Treatment*, # B-56, Naples, FL, Dec 2001.
2. **Zhao, D.**, Ran, S., Constantinescu, A., Hahn, E.W., and Mason, R.P. In vivo MRI monitoring of tumor oxygen dynamics and correlation with histological findings. *4th International Symposium on Anti-Angiogenic Agents*, Dallas, TX, Jan 2002.
3. **Zhao, D.**, Hahn, E.W., Constantinescu, A., Ran, S., and Mason, R.P. Comparison of hypoxia and microvascular density in the slow growing well differentiated H vs. the faster growing anaplastic AT1 Dunning prostate R3327 rat tumor. *49th Radiat. Res. Soc.* # P10-87, Reno, NV, Apr 2002.
4. **Zhao, D.**, Constantinescu, A., Chang, K., Gall, K., Hahn, E.W., and Mason, R.P. Measurement of tumor oxygen dynamics correctly predicts beneficial adjuvant intervention for radiotherapy in Dunning prostate R3327-HI tumors. *10th ISMRM*, #2149, Honolulu, Hawaii, May 2002.
5. **Zhao, D.**, Ran, S., Constantinescu, A., Hahn, E.W., and Mason, R.P. MRI evaluation of metronomic chemotherapy: the antitumor effects of combined low-dose cyclophosphamide and thalidomide on prostate tumors. *8th International Workshop on Tumor Microenvironment and Its Impact on Cancer Therapies*, Pg V-3, Miami, FL, May 2003.

Conclusion:

Results reported here were successful in terms of the outlined tasks cited in the original Statement Of Work. Eight publications have resulted from this research endeavor during the past two years. Our results suggest that the metronomic approach is very effective on our prostate rat tumors, which has been verified by tumor growth delay and histological and immunohistochemical studies. More importantly, our MRI approaches predict anti-angiogenic treatment efficacy by evaluating the physiological changes during the early stage of the treatment. I expect such MR studies will facilitate further understanding and assessment of the dynamic changes in blood perfusion and oxygenation following anti-angiogenic or vascular therapy on prostate cancer.

Based on the training and success of the Fellowship, and with the goal of developing my career as a prostate cancer researcher, I applied for the 2003 DOD Prostate Cancer Research New Investigator Award. Unfortunately, my 'very good' score (2.2) was not funded. However, I was successful in gaining a 2003 DOD Breast Cancer research initiative Idea Award. This will allow me to continue to develop an academic cancer research career. Moreover, while 80% of my effort will be devoted to the breast cancer research, I will spend the other 20% time in continuing to pursue prostate cancer research with the collaboration with my colleague, Dr. Ralph Mason.

References:

1. Folkman, J. Anti-angiogenesis: new concept for therapy of solid tumors, Ann. Surg. *175:* 409-416, 1972.

2. Browder, T., Butterfield, C. E., Kraling, B. M., Shi, B., Marshall, B., O'Reilly, M. S., and Folkman, J. Antiangiogenic Scheduling of Chemotherapy Improves Efficacy aganinst Experimental Drug-resistant Cancer, Cancer Res. *60:* 1878-1886, 2000.
3. Klement, G., Baruchel, S., Rak, J., Man, S., Clark, K., Hicklin, D. J., Bohlen, P., and Kerbel, R. S. Continuous low-dose therapy with vinblastine and VEGF receptor-2 antibody induces sustained tumorregression without over toxicity, J. Clin. Invest. *105:* R15-24, 2000.
4. Man, S., Bocci, G., Francia, G., Green, S. K., Jothy, S., Hanahan, D., Bohlen, P., Hicklin, D. J., Bergers, G., and Kerbel, R. S. Antitumor effects in mice of low-dose (metronomic) cyclophosphamide administered continuously through drinking water, Cancer Res. *62:* 2731-5, 2002.
5. Mason, R. P., Rodbumrung, W., and Antich, P. P. Hexafluorobenzene: a sensitive ^{19}F NMR indicator of tumor oxygenation, NMR Biomed. *9:* 125-134, 1996.
6. Hunjan, S., **Zhao, D.**, Constantinescu, A., Hahn, E. W., Antich, P. P., and Mason, R. P. Tumor Oximetry: demonstration of an enhanced dynamic mapping procedure using fluorine-19 echo planar magnetic resonance imaging in the Dunning prostate R3327-AT1 rat tumor, Int. J. Radiat. Oncol. Biol. Phys. *49:* 1097-1108, 2001.
7. Taylor, J. S. and Reddick, W. E. Evolution from empirical dynamic contrast-enhanced magnetic resonance imaging to pharmacokinetic MRI, Adv. Drug Delivery Reviews. *41:* 91-110, 2000.
8. Evelhoch, J. L., Gillies, R. J., Karczmar, G. S., Koutcher, J. A., Maxwell, R. J., Nalcioglu, O., Raghunand, N., Ronen, S. M., Ross, B. D., and Swartz, H. M. Application of magnetic resonance in model systems: cancer therapeutics, Neoplasia. *152:* 152-65, 2000.
9. Robinson, S. P., Howe, F. A., Rodrigues, L. M., Stubbs, M., and Griffiths, J. R. Magnetic resonance imaging techniques for monitoring changes in tumor oxygenation and blood flow, Semin. Radiat. Oncol. *8:* 198-207, 1998.
10. **Zhao, D.**, Constantinescu, A., Hahn, E. W., and Mason, R. P. Differential oxygen dynamics in the two Dunning prostate R3327 rat tumor sublines (MAT-Lu and HI) with respect to growth and respiratory challenge. *Int. J. Radiat. Oncol. Biol. Phys.* in the press 2002.
11. **Zhao, D.**, Constantinescu, A., Hahn, E. W., and Mason, R. P. Correlation of tumor oxygen dynamics with radiation response of the Dunning prostate R3327-HI tumors. *Radiat. Res.* Submitted 2002.
12. **Zhao, D.**, Ran, S., Constantinescu, A., Hahn, E. W., and Mason, R. P. Tumor oxygen dynamics: in vivo MRI monitoring and correlation with histological findings. *Neoplasia* in press 2003.
13. **Zhao, D.**, Jiang, L., Constantinescu, A., Hahn, E.W., and Mason, R.P. In vivo MRI monitoring of prostate tumor vasculature and oxygen dynamics. *AACR New Discoveries in Prostate Cancer Biology and Treatment*, # B-56, Naples, FL, Dec 2001.
14. **Zhao, D.**, Ran, S., Constantinescu, A., Hahn, E.W., and Mason, R.P. In vivo MRI monitoring of tumor oxygen dynamics and correlation with histological findings. *4th International Symposium on Anti-Angiogenic Agents*, Dallas, TX, Jan 2002.
15. **Zhao, D.**, Hahn, E.W., Constantinescu, A., Ran, S., and Mason, R.P. Comparison of hypoxia and microvascular density in the slow growing well differentiated H vs. the faster growing anaplastic AT1 Dunning prostate R3327 rat tumor. *49th Radiat. Res. Soc.* # P10-87, Reno, NV, Apr 2002.
16. **Zhao, D.**, Constantinescu, A., Chang, K., Gall, K., Hahn, E.W., and Mason, R.P. Measurement of tumor oxygen dynamics correctly predicts beneficial adjuvant intervention for radiotherapy in Dunning prostate R3327-HI tumors. *10th ISMRM*, #2149, Honolulu, Hawaii, May 2002.
17. **Zhao, D.**, Ran, S., Constantinescu, A., Hahn, E.W., and Mason, R.P. MRI evaluation of metronomic chemotherapy: the antitumor effects of combined low-dose cyclophosphamide and thalidomide on prostate tumors. *8th International Workshop on Tumor Microenvironment and Its Impact on Cancer Therapies*, Pg V-3, Miami, FL, May 2003.

Appendices

Int. J. Radiation Oncology Biol. Phys., Vol. 53, No. 3, pp. 744–756, 2002

0360-3016/02/$–see front matter

ELSEVIER

PII S0360-3016(02)02822-5

BIOLOGY CONTRIBUTION

DIFFERENTIAL OXYGEN DYNAMICS IN TWO DIVERSE DUNNING PROSTATE R3327 RAT TUMOR SUBLINES (MAT-Lu AND HI) WITH RESPECT TO GROWTH AND RESPIRATORY CHALLENGE

DAWEN ZHAO, M.D., PH.D., ANCA CONSTANTINESCU, PH.D., ERIC W. HAHN, PH.D., AND RALPH P. MASON, PH.D.

Advanced Radiological Sciences, Department of Radiology, The University of Texas Southwestern Medical Center, Dallas, TX

Purpose: Since hypoxia may influence tumor response to therapy and prognosis, we have compared oxygenation of tumors known to exhibit differential growth rate and tissue differentiation.

Methods and Materials: Regional tumor oxygen tension was measured using ^{19}F nuclear magnetic resonance echo planar imaging relaxometry of hexafluorobenzene, which provided dynamic maps with respect to respiratory intervention. Investigations used two Dunning prostate R3327 rat tumor sublines: the fast growing, highly metastatic MAT-Lu and the moderately well-differentiated, slower growing HI.

Results: Both sublines showed significantly higher oxygen tension in smaller tumors (<2 cm^3) than in larger tumors (>3.5 cm^3). Pooled data showed that MAT-Lu tumors exhibited greater hypoxia compared with the size-matched HI tumors ($p < 0.0001$). Respiratory challenge (oxygen or carbogen) produced significant increases in mean pO_2 for tumors of both sublines ($p < 0.0001$). However, initially hypoxic regions displayed very different behavior in each subline: those in the HI tumors responded rapidly with significant elevation in pO_2, while those in the MAT-Lu tumors showed little response to respiratory intervention.

Conclusions: These results concur with hypotheses that hypoxia is related to tumor growth rate and degree of differentiation. Under baseline conditions, the differences were subtle. However, response to respiratory intervention revealed highly significant differences, which, if held valid in the clinic, could have prognostic value.

Oxygen, Magnetic resonance imaging, Prostate tumor, Hypoxia, Differentiation.

INTRODUCTION

Hypoxia in solid tumors has been widely recognized as a potent factor, which leads to resistance to radiotherapy (1, 2), photodynamic therapy (3), and some anticancer drugs (1). Further, recent studies suggest that tumor hypoxia might also be associated with malignant progression in solid tumors (4, 5). Therefore, accurate measurement of tumor oxygenation, assessment of levels of hypoxia in individual tumors, and the development of effective methods to reduce the hypoxic fraction may well contribute to therapeutic outcome. Given the importance of oxygen, many techniques for monitoring oxygen tension (pO_2) have been developed (6). While each method has specific attributes, many are highly invasive and impractical for longitudinal studies of specific regions of interest. Nuclear magnetic resonance (NMR) is entirely noninvasive: ^{31}P NMR provides an indirect estimate of hypoxia based on phosphorylation potential (7), but the measured metabolic hypoxia occurs at a higher pO_2 than radiobiological hypoxia, and some studies have shown a lack of correlation between high-energy phosphate metabolites and pO_2 (8). Blood Oxygen Level Dependent (BOLD) contrast proton magnetic resonance imaging (MRI) provides an indication of tumor vascular oxygenation, and heterogeneity, in response to intervention, but the method does not provide pO_2 values and interpretation may be complicated by flow, hence, the concept FLOOD (FLOw and Oxygenation Dependent contrast) (9).

We recently demonstrated the feasibility of measuring tumor oxygenation based on ^{19}F NMR echo planar imaging (EPI) after direct intratumoral injection (i.t.) of hexafluorobenzene (HFB) (10, 11), for which we have chosen the

Reprint requests to: Ralph P. Mason, Ph.D., C. Chem., Department of Radiology, U.T. Southwestern Medical Center, 5323 Harry Hines Blvd., Dallas, TX 75390-9058. Tel: (214) 648-8926; Fax: (214) 648-2991; E-mail: Ralph.Mason@UTSouthwestern.edu

Presented in part at the Forty-seventh Annual Meeting of the Radiation Research Society, Albuquerque, NM, April 2000.

This work was supported in part by NIH RO1 CA79515, the American Cancer Society (RPG-97-116-010CCE), and a postdoctoral fellowship from the DOD Prostate Cancer Initiative (DAMD 170110108) (DZ). NMR experiments were performed at the Mary Nell and Ralph B. Rogers MR Center, an NIH BRTP Facility P41-RR02584.

Acknowledgments—We are grateful to Drs. Peter Antich and Peter Peschke for collegial support and Drs. Sophia Ran and Mark Jeffrey for technical assistance.

Received Nov 16, 2001, and in revised form Mar 6, 2002. Accepted for publication Mar 8, 2002.

acronym *FREDOM* (Fluorocarbon Relaxometry using Echo planar imaging for Dynamic Oxygen Mapping). This technique allows us to assess baseline pO_2 at multiple locations within a tumor, and to follow dynamic changes in response to interventions. Hexafluorobenzene has many strengths as a reporter molecule; it is readily available, cheap, and nontoxic. In terms of NMR, the sixfold symmetry provides a single ^{19}F signal offering maximum signal to noise, and the long relaxation times (T1 and T2) facilitate echo planar imaging. The spin lattice relaxation rate R1 is very sensitive to changes in pO_2, but shows minimal response to variations in temperature. HFB is readily administered through a fine needle and remains at the site of administration for several hours ($t_{1/2}$ typically 600 min) (12).

We have now applied the technique to investigate oxygen distribution and dynamics in two rat prostate tumor sublines exhibiting diverse characteristics. Although the baseline oxygenation of the moderately well-differentiated subline (HI) has been investigated previously using electrodes (13), we are unaware of previous investigations of oxygenation in the highly metastatic and poorly differentiated MAT-Lu subline. Furthermore, comparison of response to interventions, here respiratory challenge with oxygen and carbogen, is now established using a single technique for comparison of both sublines.

METHODS AND MATERIALS

Experiments were approved by the Institutional Animal Care and Research Advisory Committee.

Tumor model

Two sublines of the Dunning prostate R3327 adenocarcinoma were selected: HI, a moderately well-differentiated, slower growing, hormone-insensitive, nonmetastatic subline with tumor volume doubling time (VDT) of 9 days (14), and MAT-Lu, a highly metastatic, poorly differentiated subline with VDT of 2.7 days (15). Tumors were implanted in a skin pedicle surgically created on the foreback of adult male Copenhagen-2331 rats (~250 g, Harlan), as described in detail elsewhere (16). Tumors were allowed to grow and investigated by MRI when about 1.5 cm^3 or when greater than 3.5 cm^3 volume (~15 mm or greater than 20 mm diameter). In total, we investigated seven HI tumors including three small (size range 1.1–1.7 cm^3) and four large (range 3.5–4.6 cm^3), and eight MAT-Lu tumors including four small (range 1.2–1.9 cm^3) and four large tumors (range 3.7–5.0 cm^3). In preparation for MRI, each rat was given 200 μL ketamine hydrochloride (100 mg/mL, Aveco, Fort Dodge, IA) as a relaxant (i.p.). The rats were maintained under general gaseous anesthesia with FO_2 = 33% (fraction of inhaled O_2: 0.3 dm^3/min O_2, 0.6 dm^3/min N_2O, and 0.5% methoxyflurane [MF]; Pittman-Moore, Washington Crossing, NJ) using a small animal anesthesia unit. Hexafluorobenzene (45 μL, Lancaster, Gainesville, FL), was deoxygenated by bubbling nitrogen for 5 min before use, and injected directly into the tumors using a Hamilton syringe (Reno, NV) with a custom-made fine sharp needle (32G). The HFB was deliberately deposited in both the central and peripheral regions of the tumors to ensure that the interrogated regions would be representative of the whole tumor and for comparison with the oxygen electrode method. Generally, HFB was administered along two or three tracks in the form of a fan in a single central plane of the tumor sagittal to the rat's body. The needle was inserted manually to penetrate across the whole tumor and withdrawn ~1 mm to reduce pressure, and 3 μL HFB was deposited. The needle was repeatedly withdrawn a further 2–3 mm and additional HFB was deposited. Each rat was placed on its side in a cradle with a thermal blanket to maintain body temperature. A fiber optic probe was placed in the rectum to monitor core temperature.

Assessment of HFB distribution

Magnetic resonance experiments were performed using an Omega CSI 4.7 horizontal bore magnet system with actively shielded gradients (Bruker Instrument Inc., Fremont, CA). A tunable ($^1H/^{19}F$) single-turn solenoid coil (2 or 3 cm in diameter matched to the tumor size) was placed around the tumor-bearing pedicle. Shimming was performed on the ^1H signal (200.11 MHz) of the tissue water to a typical linewidth of 115 Hz. Proton images were obtained for anatomic reference using a three-dimensional (3D) spin-echo sequence. Imaging parameters were: repetition time (TR) = 150 ms; echo time (TE) = 8 ms; pulse width $\pi/2$ = 32 μs with 128 × 64 × 8 data points over a 40 mm field of view in plane, and 40 mm thickness, providing 312 μm × 624 μm × 5 mm digital resolution. Two transients were acquired at each phase-encoding increment, giving a total acquisition time of 2.5 min. The coil was retuned in place to 188.27 MHz, and corresponding ^{19}F MR images were obtained as a 3D data set with 128 × 32 × 8 data points and gradients compensated for the difference in gyromagnetic ratios, yielding 312 μm × 1.2 mm × 5 mm resolution. For ^{19}F MRI, a driven-equilibrium sequence was applied with TR = 150 ms, TE = 8 ms, $\pi/2$ = 50 μs excitation pulse and 16 transients at each increment, giving a total accumulation time of 10 min for the 3D data set. Driven equilibrium both enhanced the efficiency of data acquisition and provided signal corresponding primarily to spin density. Data were processed using sine-bell apodization and zero filling in the first phase-encode dimension.

Tumor oximetry

FREDOM. Following conventional MR imaging, tumor oxygenation was estimated on the basis of ^{19}F pulse burst saturation recovery (PBSR) EPI relaxometry of the HFB, as described previously (11). The *ARDVARC* (Alternated R1 Delays with Variable Acquisitions to Reduce Clearance effects) data acquisition protocol was applied to optimize data quality. This approach provided pO_2 maps with 1.25 mm in-plane voxel resolution in 8 min with typically ~50–150 individual pO_2 measurements (voxels per tumor). The spin-lattice relaxation rate [R1 (s^{-1}) = 1/T1] was estimated

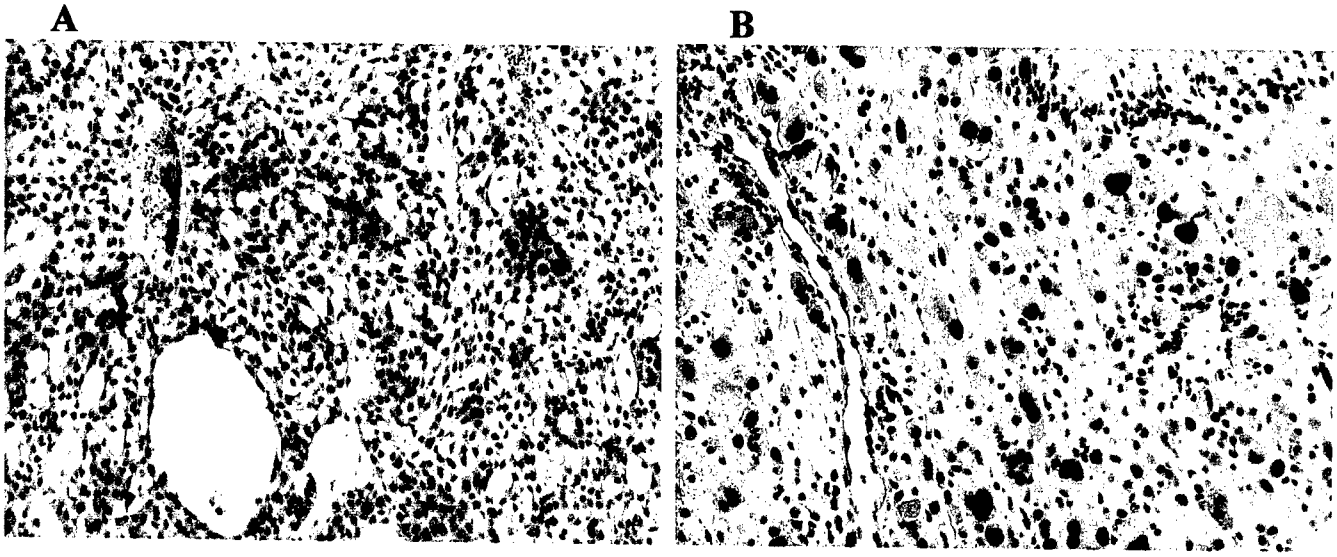

Fig. 1. Immunohistochemical comparison of HI and MAT-Lu tumors. PCNA is detected in nucleus of tumor cells. A representative HI tumor (A) with labeling index 15%, and a MAT-Lu (B) showing 40% positive index. Original magnification ×100.

on a voxel-by-voxel basis using a three-parameter monoexponential function, and pO_2 was estimated using the relationship pO_2 (mm Hg) = (R1–0.0835)/0.001876 (11). Three consecutive baseline pO_2 measurements were made over 24 min, while the rat breathed FO_2 = 33%. The inhaled gas was then sequentially altered to provide different inhaled FO_2, although the MF concentration was maintained constant at 0.5%. Inhaled gas was switched to 100% O_2 and pO_2 maps were immediately acquired with no equilibration period. Five consecutive maps were acquired over 40 min. The gas was then returned to baseline, followed by carbogen (95% O_2/5% CO_2), and finally, baseline again. In each case, gas was maintained for 40 min with five pO_2 determinations. The statistical significance of changes in oxygenation was assessed using an analysis of variance (ANOVA) on the basis of the Fisher's protected least significant difference (PLSD) test (Statview, SAS Institute, Cary, NC). Where appropriate, the Student's *t* test was applied.

Electrode measurements. After MRI measurement, one representative rat from each tumor subline was selected for electrode measurement using a non-Clark style oxygen needle electrode with a 0.7-mm-diameter tip (Product No. 768–22, Diamond General, Ann Arbor, MI) linked to a Chemical Microsensor (Diamond General). Calibration was performed using saline solutions equilibrated with air, 5% O_2, and 100% nitrogen at 37°C. After calibration, the needle electrode was inserted into the tumor, while a reference electrode was placed rectally. The pO_2 values were obtained at varying depths in two parallel tracks. In total, five locations in each tumor were studied. At each location within the tumor, the respiratory challenge sequence used for MRI was performed. After a change in inhaled gas, there was an equilibration period of 15 min and then pO_2 was recorded.

Immunohistochemistry

After MRI investigations, tumor tissues were surgically removed, fixed in 10% formalin for 24 h, and embedded in paraffin. Tissue sections (4 μm) were treated in boiling citrate buffer (0.1 M; pH 6.0) for 15 min and blocked in normal goat serum for 20 min. A primary antibody (1:50 dilution) against proliferating cell nuclear antigen (PCNA; BD Biosciences, San Diego, CA) was added and incubated overnight at 4°C in a humid box. Slides were then incubated with horseradish peroxidase (HRP)-conjugated goat anti-mouse secondary antibody (1: 100 dilution; Serotec, Raleigh, NC) for 1 h at 37°C. After a phosphate-buffered saline (PBS) wash, sections were immersed in the AEC substrate (3-amino-9-ethylcarbazole, Vector Laboratories, Inc., Burlingame, CA) for 15 min at room temperature. Finally, sections were counterstained with hematoxylin and mounted with Universal Mount. The positive and negative labeled nuclei were counted under microscopy. In total, 1000 nuclei were counted for each slide section; the labeling index was expressed as the percentage of positive cells for PCNA.

RESULTS

Histology shows distinctly different characteristics for the two sublines: the HI appears moderately well-differentiated with uniform sized tumor cells, pseudoglandular structures, and large vesicles (Fig. 1A). By comparison, the MAT-Lu appears poorly differentiated with cellular and nuclear variations in size and shape and no glandular structure (Fig. 1B). PCNA immunostaining also shows a higher proliferation rate in the MAT-Lu than the HI tumors (Fig. 1).

Hexafluorobenzene was readily observed by ^{19}F MRI after direct intratumoral injection, as shown for representative tumors in Fig. 2. Overlay of ^{19}F signal on the corresponding ^{1}H images indicates that HFB occurred in multiple

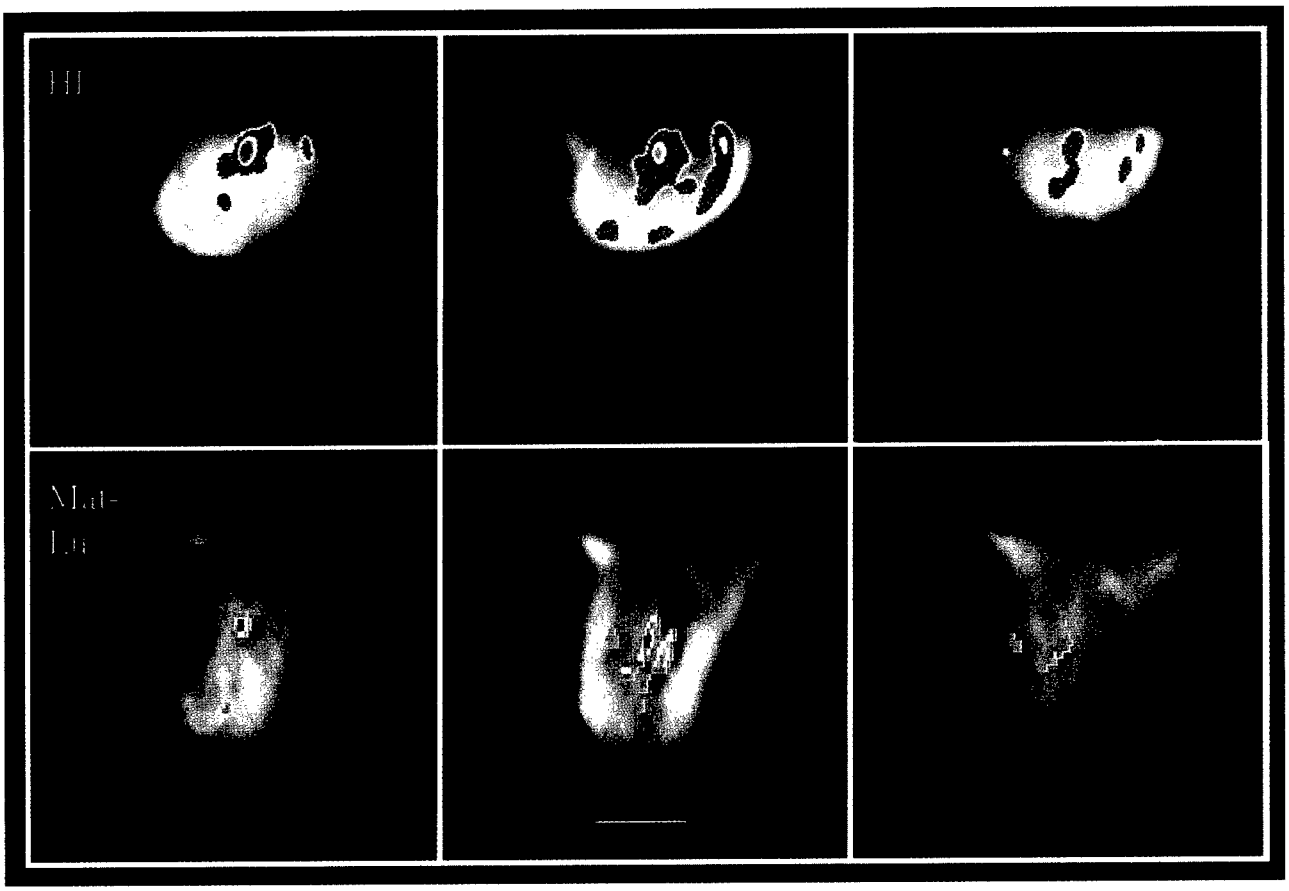

Fig. 2. MR images showing the distribution of hexafluorobenzene (45 μL) in representative large R3327 Dunning prostate rat tumors. Upper: HI (3.5 cm^3) and lower: MAT-Lu (3.8 cm^3). Three contiguous slices showing ^{19}F MRI signal density overlaid on the corresponding ^1H MR slices. HFB was detected from approximately 8% of the HI and 6% of the MAT-Lu tumor, predominantly in one plane. Each slice was 5 mm thick with in-plane resolution of 312 × 624 μm (^1H) or 312 × 1200 μm (^{19}F). Bar represents 1 cm.

discrete regions and was localized predominantly in the central slices with less signal in peripheral regions. In the series of EPI relaxation data sets, typically ~50–300 voxels provided an R1 fit, and potential pO_2 value. Because even noise may give an apparent relaxation curve (R1) fit, data were selected within a region of interest, and having T1 error < 2.5 s. With respect to respiratory interventions, only those voxels which provided consistently reliable data throughout all measurements were included for further analysis. The number of such acceptable voxels ranged from 18 to 84 per tumor.

Figure 3 shows typical pO_2 maps of the selected regions obtained from the two tumors in Fig. 2. For the series of 23 pO_2 maps obtained with various inhaled gases, 39 voxels in the HI tumor and 52 voxels in the MAT-Lu tumor were considered reliable. Oxygen tension changed significantly when the rats inhaled oxygen or carbogen. Dynamic changes in mean pO_2 accompanying respiratory challenge in these two tumors are shown in Fig. 4. For the HI tumor, mean baseline pO_2 = 20 ± 5 (± SE) mm Hg (median pO_2 = 11 mm Hg), increased significantly within 8 min of switching the inspired oxygen from FO_2 = 33% to 100%, and the pO_2 reached 119 ± 10 mm Hg ($p < 0.0001$; median pO_2 = 58 mm Hg) after 40 min. Return to 33% O_2 produced a significant decline in pO_2 from the peak within 8 min, reaching a value of pO_2 = 33 ± 3 mm Hg by 40 min (median pO_2 = 39 mm Hg). Challenge with carbogen likewise produced a significant increase in pO_2 within 8 min and by 40 min reached a value of 113 ± 13 mm Hg ($p < 0.0001$; median pO_2 = 60 mm Hg). Again pO_2 declined significantly upon returning to FO_2 = 33%. Baseline pO_2 in the MAT-Lu tumor was lower (mean = 11 ± 1 mm Hg; median = 8 mm Hg). But as with the HI, pO_2 steadily increased over 40 min upon altering inhaled gas to oxygen or carbogen (mean = 30 ± 3 mm Hg, median = 18 mm Hg; 47 ± 4 mm Hg, median pO_2 = 23 mm Hg, respectively; $p < 0.0001$). However, the mean values were always significantly lower than those in the size-matched HI tumor ($p < 0.0001$).

Data for small and large tumors in the HI and MAT-Lu sublines are pooled as histograms in Fig. 5 and summarized in Table 1. Using the pooled data, the small HI tumors had a mean baseline pO_2 of 32 ± 1 mm Hg (median = 29 mm Hg), which was significantly greater than the larger HI tumors, which had a value of 14 ± 1 mm Hg (median = 7 mm Hg; $p < 0.0001$). For the MAT-Lu subline, small

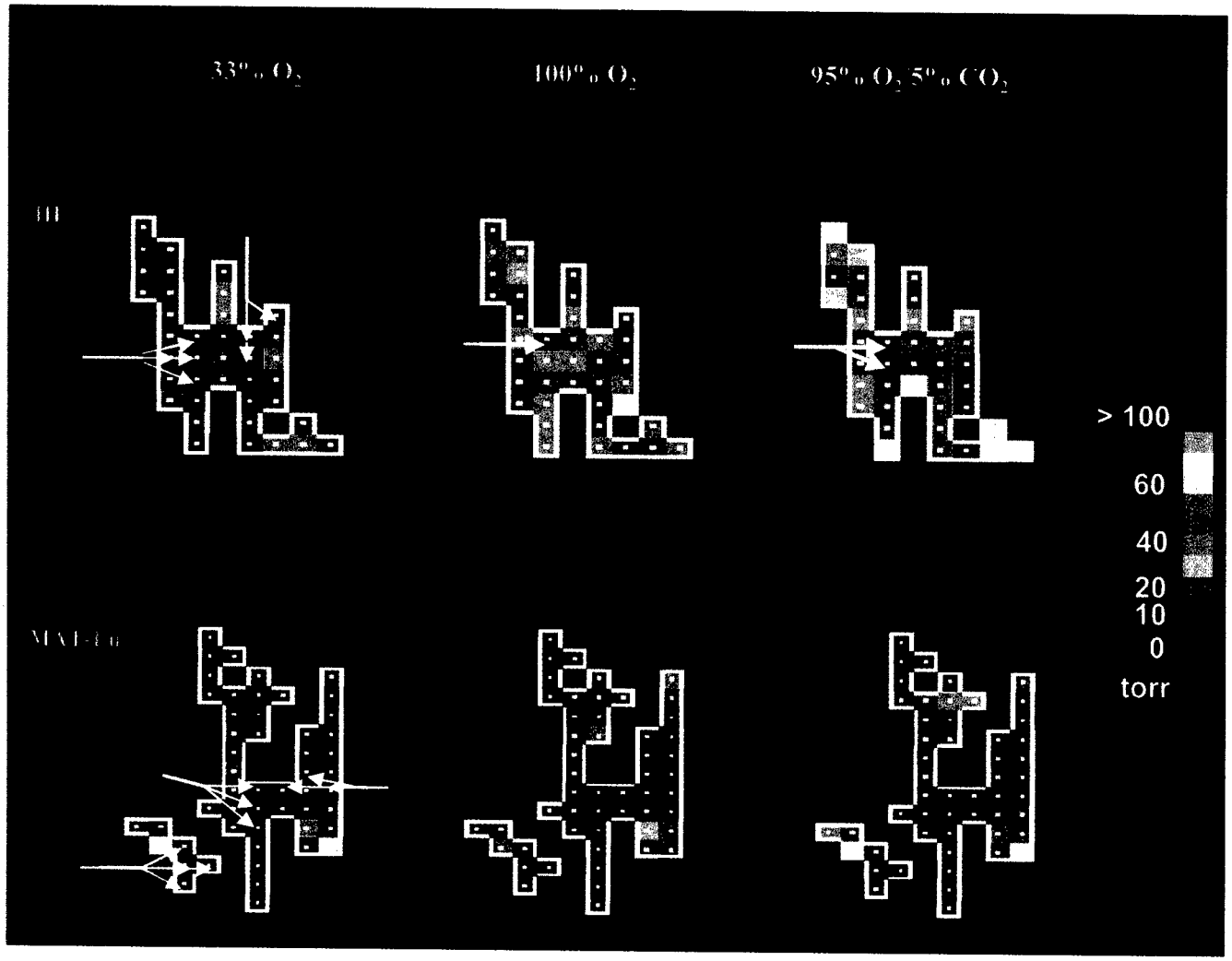

Fig. 3. pO_2 maps of selected regions from the tumors shown in Fig. 2 with respect to respiratory challenge. 39 voxels from the HI and 52 voxels from the MAT-Lu tumor were selected on the basis of consistently reliable data throughout all measurements. Maximum mean pO_2 increases with respect to respiratory challenges were found 40 min after breathing 100% oxygen or carbogen in both of these two tumors. Arrows indicate hypoxic voxels with $pO_2 < 10$ mm Hg.

tumors had a mean pO_2 of 25 ± 1 mm Hg (median = 23 mm Hg), which was significantly greater than for the large MAT-Lu tumors (mean = 8 ± 1 mm Hg, median = 4 mm Hg; $p < 0.0001$). Comparison of the pooled mean baseline pO_2 between the two sublines showed that both the small and large groups of MAT-Lu tumors had significantly lower mean pO_2 than the size-matched HI groups ($p < 0.0001$; Table 1). All the tumors in the two sublines except one large MAT-Lu showed significant increases in global mean pO_2 with oxygen or carbogen inhalation ($p < 0.001$). In six of the seven HI tumors and five of the eight MAT-Lu tumors, the maximum mean pO_2 values were observed while the rats breathed carbogen. Most interestingly, hypoxic fraction, specifically $pO_2 < 10$ mm Hg (HF_{10}), in the large HI tumors decreased from 59% to 24% with oxygen and to 22% with carbogen inhalation, whereas in the large MAT-Lu tumors the final HF_{10} values were still over 37%. We also analyzed our pO_2 data by comparing the differences in individual tumors as shown in Table 2. As with the pooled data, for both the HI and MAT-Lu tumors, the large tumors were significantly more hypoxic when breathing 33% O_2 than the smaller tumors (Table 2). When breathing oxygen or carbogen, the mean and median pO_2 increased significantly for both the small and large HI tumors. The HF_{10} was significantly reduced in the large HI tumors. For the MAT-Lu tumors, the only significant change was an increase in the mean and median pO_2 in the large tumors with carbogen inhalation.

A major strength of the *FREDOM* approach is the ability to follow individual tumor regions. Thus, we selected those voxels from the baseline pO_2 maps, which were radiobiologically hypoxic ($pO_2 < 10$ mm Hg) in all three baseline measurements (24 min), to assess the influence of respiratory challenge. Inspection of the representative tumors in Fig. 3 shows that pO_2 increased significantly in the majority of the initially hypoxic voxels in the HI tumor ($p < 0.01$), whereas there was no significant response to oxygen or carbogen in the MAT-Lu. Data are summarized in Fig. 6.

For comparison, the traditional polarographic method was performed on one tumor from each subline after the

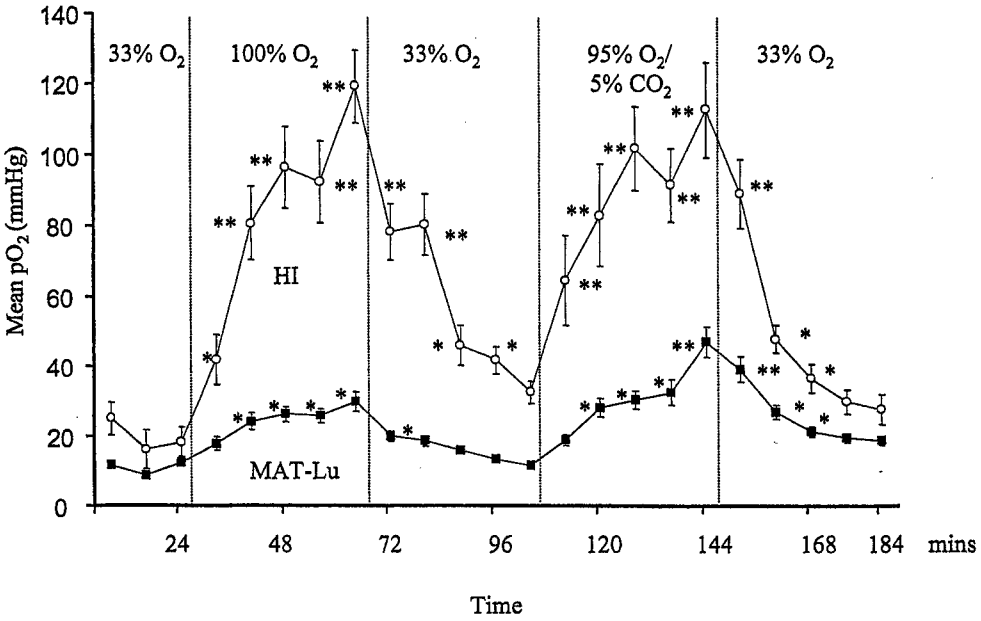

Fig. 4. Mean ± SE pO_2 obtained from sequential maps of the HI (○) and the MAT-Lu (■) tumors shown in Figs. 1 and 2 with respect to respiratory challenge. $*p < 0.001$, $**p < 0.0001$ compared to mean baseline.

NMR experiment (Fig. 7). All interrogated regions in the HI tumor, irrespective of baseline pO_2, showed a remarkable increase in pO_2 in response to oxygen or carbogen. However, only the relatively well-oxygenated regions (>10 mm Hg) in the MAT-Lu responded.

DISCUSSION

The oxygen tension dynamics observed here demonstrate that response to gaseous intervention can be very different for sublines of a single parental tumor type. The relatively hypoxic regions of the well-differentiated HI subline responded to elevated inhaled oxygen, whereas those of the undifferentiated MAT-Lu subline did not. Tumors of a given subline behaved consistently.

In common with our previous investigations of the undifferentiated anaplastic Dunning prostate R3327-AT1 subline (VDT ~5 days) (10, 11), we found that the larger tumors of each subline were significantly more hypoxic than smaller ones (Tables 1 and 2). Indeed, this is a general observation across most experimental tumor types, based on observations using various oximetry techniques (17–21), although exceptions have been reported (22). In response to respiratory challenge with oxygen or carbogen, as we also reported for the AT1 subline (11), for both the HI and MAT-Lu sublines the pooled data showed a significant increase in mean pO_2, irrespective of tumor size.

Under baseline conditions, the MAT-Lu tumors were significantly less well-oxygenated than the HI (Table 1). Large and small tumors responded to oxygen and carbogen, but MAT-Lu tumors consistently remained significantly less well-oxygenated than HI tumors. Further, the baseline radiobiologically hypoxic MAT-Lu voxels (<10 mm Hg) showed no significant increase in mean pO_2 (Fig. 6), a finding that coincides with our previous observations in the AT1 tumor (11, 23). In contrast, initially hypoxic voxels in the HI showed a rapid, and highly significant, response to respiratory challenge. This observation was confirmed using the traditional oxygen electrodes (Fig. 7), and previously using the fiber optic OxyLite (Oxford Optronix, Oxford, UK) (24). Such remarkable differences in behavior surely reflect intrinsic differences in the vascular architecture and perhaps the metabolic rate.

Previously, Eble *et al.* (13) compared oxygenation of the HI and undifferentiated AT1 (VDT ~5 days) Dunning prostate sublines using the Eppendorf Histograph. As we report here, they found that the slower growing, better differentiated tumor was better oxygenated. Likewise, Chapman *et al.* (22, 25, 26) found that the well-differentiated H subline (VDT 20 days) was better oxygenated than the AT1, as assessed by the Eppendorf electrode or by indirect means such as misonidazole binding and ^{31}P NMR. By contrast, Thews *et al.* (27) reported that a better differentiated rhabdomyosarcoma subline (F1) of the BA-HAN-1 was slightly less well-oxygenated than an undifferentiated counterpart subline (G8). While Thews' results show the opposite trend with differentiation, it is important to note that the F1 and G8 sublines each grow relatively rapidly (VDT 2.5–3 days). In the series of Dunning prostate tumors, VDTs range from 2.7 days (MAT-Lu) to 5 days (AT1), 9 days (HI), and 20 days (H). Comparing our current results with our own previous data from the undifferentiated AT1 with the same anesthesia protocol (10) reveals that correlations of hypoxia and growth rate or level of histologic differentiation are not always straightforward. Previously, we reported that smaller vs. larger AT1 tumors respectively

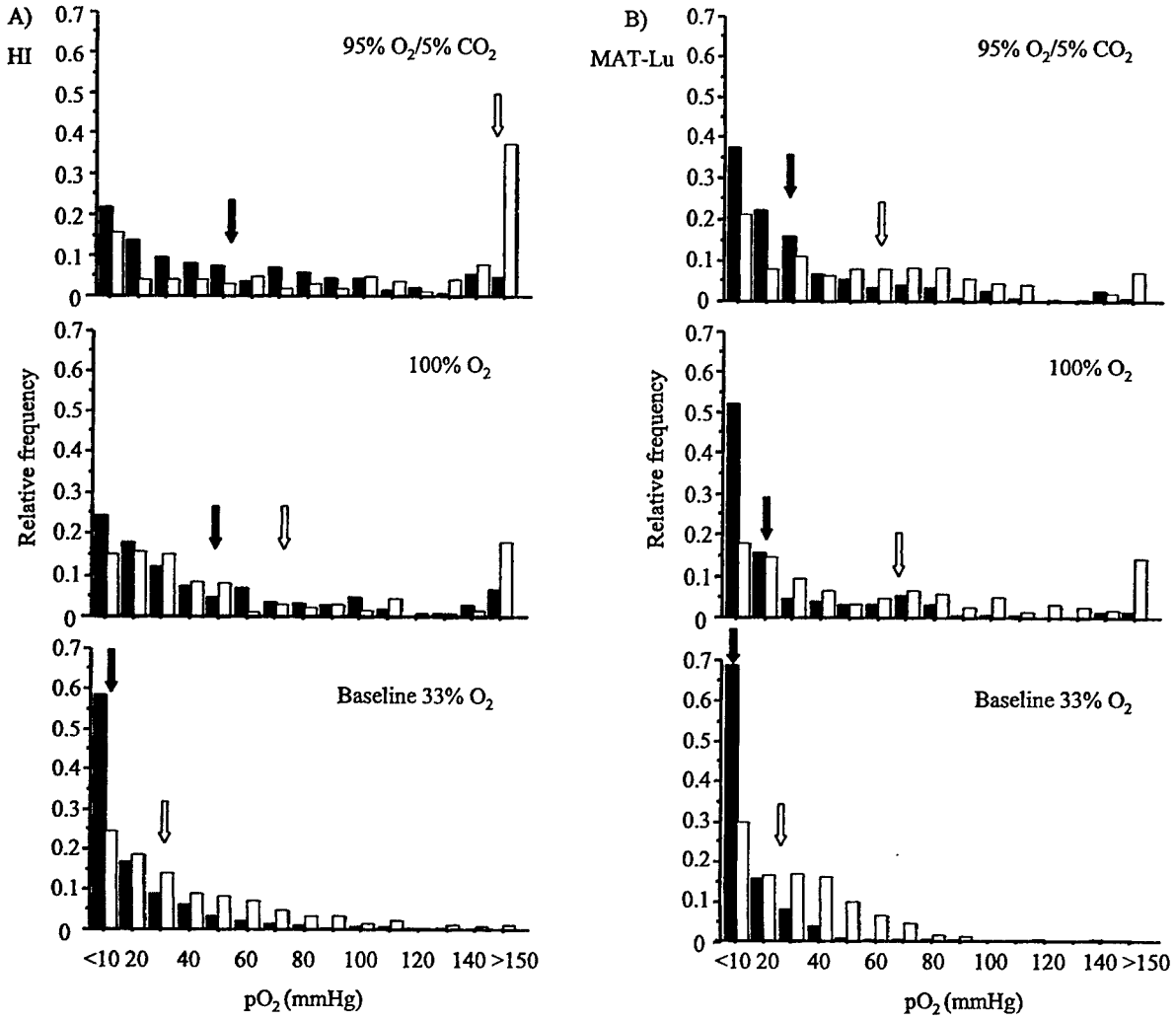

Fig. 5. Histograms of pooled pO_2 observed by *FREDOM* for all 15 tumors with respect to respiratory challenge. (A) Seven HI tumors including 4 large (solid) and 3 small (open). (B) Eight MAT-Lu tumors including 4 large (solid) and 4 small (open). Lowest frame: Rats inhaled 33% O_2. Middle frame: Maximum value when rats inhaled 100% O_2. Top frame: Maximum values when rats inhaled 95% O_2/5% CO_2. Arrows indicate mean values in large (solid) and small tumors (open), respectively.

had mean pO_2 = 39 vs. 3 torr, median pO_2 = 15 vs. 2 torr, and HF_{10} 44% and 82%. Thus, the AT1 apparently is more hypoxic than the MAT-Lu even though it grows more slowly. We believe the most valuable observation is that for both AT1 and MAT-Lu tumors, the initially hypoxic regions respond little to elevated oxygen inhalation, whereas the slower growing well-differentiated HI responds with a significant decline in HF_{10}. Thus, while growth rate and degree of differentiation each appear related to tumor oxygenation, we find the most pronounced effect is on the oxygen dynamics with respect to intervention.

In line with the observed VDT, histology using the proliferation marker PCNA showed a higher proliferation rate in the poorly oxygenated MAT-Lu than the relatively better oxygenated HI tumors. This result is in line with an *in vitro* study by Young *et al.* (28), who reported that hypoxia induced DNA overreplication. Likewise, Nordsmark *et al.* (29) reported that rapidly proliferating human soft tissue sarcomas from a clinical study were more hypoxic. Recent studies suggest that tumor hypoxia can enhance malignant progression and increase aggressiveness and metastasis (30, 31). In terms of the Dunning prostate R3327 rat tumors, Peschke *et al.* (14) found higher bromodeoxyuridine (BrdU) labeling in the fast growing and anaplastic AT1 subline compared with the slower growing and relatively well-differentiated H and HI sublines, which are relatively better oxygenated. However, some investigators have reported a lack of correlation between tumor oxygenation and proliferation in animals or patients (32). Future study regarding the relationship between these two factors is clearly needed.

Several reports based on the Eppendorf Histograph system have now shown that the level of hypoxia is related to clinical prognosis. Höckel *et al.* (33) found better disease-free and overall survival for patients with cervical cancer when median $pO_2 > 10$ mm Hg. Other reports have indicated similar findings, although alternate threshold parameters such as HF_5 (hypoxic fraction < 5 mm Hg) or $HF_{2.5}$ (hypoxic fraction < 2.5 mm Hg) have been favored over

Table 1. Summary of the pooled pO_2 data in R3327 Dunning prostate rat tumor sublines*

Tumor sublines	Size†	Baseline (33% O_2) pO_2 (mm Hg) Mean ± SE	Median	HF (%) < 10 mm Hg	< 5 mm Hg	Oxygen challenge pO_2 (mm Hg) Mean ± SE	Median	HF (%) < 10 mm Hg	< 5 mm Hg	Carbogen challenge pO_2 (mm Hg) Mean ± SE	Median	HF (%) < 10 mm Hg	< 5 mm Hg
HI	Small	32 ± 1	29	24	16	75 ± 9‖	39	15	7	148 ± 12‖¶	111	16	5
	Large	14 ± 1‡	7	59	42	49 ± 4‡‖	26	24	13	53 ± 4‡‖	38	22	8
MAT-Lu	Small	25 ± 1§	23	30	21	68 ± 5‖	44	18	12	63 ± 5§‖	46	21	15
	Large	8 ± 1‡§	4	68	53	22 ± 4‡§‖	9	52	43	28 ± 4‡§‖	18	38	33

Abbreviation: HF = hypoxic fraction.

*The average number of voxels used to determine the mean and median pO_2 values for each gas was 198 for the small HI tumors, 226 for the large HI tumors, 229 for the small MAT-Lu tumors, and 148 for the large MAT-Lu tumors. These measurements reflect tumor size and tissue types irrespective of individual tumor, and indicate intratumoral heterogeneity.

† Small: volume < 2 cm^3; Large: volume > 3.5 cm^3.

‡ $p < 0.0001$ from small.

§ $p < 0.0001$ from HI.

‖ $p < 0.0001$ from baseline.

¶ $p < 0.0001$ from oxygen.

median value as a prognostic threshold (34, 35). Based on such findings, prospective clinical trials may now use pO_2 measurements for individual therapy planning. Clearly, the ability to differentiate those patients with well vs. poorly oxygenated tumors would be important in itself, but an even more powerful capability would be to assess the heterogeneity of the tumors and to determine whether hypoxic regions (voxels) are capable of responding to oxygen or carbogen.

There is increasing evidence suggesting that tumor metastasis may be associated with a hypoxic microenvironment (30, 31). An *in vivo* experimental study by Jaeger *et al.* showed that hypoxic murine KHT-C tumors are more likely to metastasize (36). Many clinical studies have also demonstrated a positive relationship between the presence of hypoxia and poor outcome associated with malignant progression and metastasis in several cancers, e.g., advanced squamous cell carcinoma of the cervix (33, 37), sarcomas and carcinomas from head, neck, and soft tissue (38). A hypoxic microenvironment is reported to induce increased expression of a group of genes, e.g., VEGF (vascular endothelial growth factor), PAI-1 (plasminogen activator inhibitor-1), and p53, which are associated with an increased malignant phenotype (39–42).

The clinical progression of prostatic cancer among patients remains by and large unpredictable. In some patients, the cancer metastasizes rapidly, killing the patient in less than a year, whereas in other patients the disease may remain localized for many years (43). Knowledge of the etiologic factors and biologic properties that predispose cells to malignant transformation remains essentially unknown (44). Thus, research that reveals factors, either temporal or causal, which can be linked to the onset of a metastatic potential, would surely be of great value. For instance, Movsas' study (45) using the Eppendorf Histograph reported that increasing levels of hypoxia were related to increasing clinical stage of human prostate carcinomas. This finding may simply support our findings, relating increasing size to greater tumor hypoxia. In the present study, we chose to compare the moderately well-differenti-

Table 2. Comparison of pO_2 data in individual R3327 Dunning prostate rat tumors*

Tumor subline	Size†	No.	Baseline (33% O_2) pO_2 (mm Hg) Mean ± SE	Median	HF (%) < 10 mm Hg	< 5 mm Hg	Oxygen challenge pO_2 (mm Hg) Mean ± SE	Median	HF (%) < 10 mm Hg	< 5 mm Hg	Carbogen challenge pO_2 (mm Hg) Mean ± SE	Median	HF (%) < 10 mm Hg	< 5 mm Hg
HI	Small	3	39 ± 11	38 ± 15	15 ± 3	11 ± 4	106 ± 40§	68 ± 42	6 ± 3	5 ± 3	163 ± 64§	112 ± 10§	5 ± 3	3 ± 3
	Large	4	13 ± 3‡	7 ± 2‡	53 ± 4‡	40 ± 3‡	54 ± 14§	36 ± 11	20 ± 9§	14 ± 4§	58 ± 12§	41 ± 15§	15 ± 8§	10 ± 4
MAT-Lu	Small	4	24 ± 4	20 ± 5	23 ± 8	17 ± 7	60 ± 19	45 ± 20	14 ± 6	11 ± 6	59 ± 7	40 ± 14	14 ± 8	10 ± 5
	Large	4	8 ± 1‡	4 ± 1‡	58 ± 7‡	51 ± 8‡	27 ± 6	19 ± 7	40 ± 11	36 ± 10	43 ± 17§	39 ± 20§	34 ± 8	29 ± 6

Abbreviation: HF = hypoxic fraction.

* These data reflect individual tumors and provide an indication of intertumoral heterogeneity.

† Small: volume < 2 cm^3; Large: volume > 3.5 cm^3.

‡ $p < 0.05$ from small.

§ $p < 0.05$ from baseline.

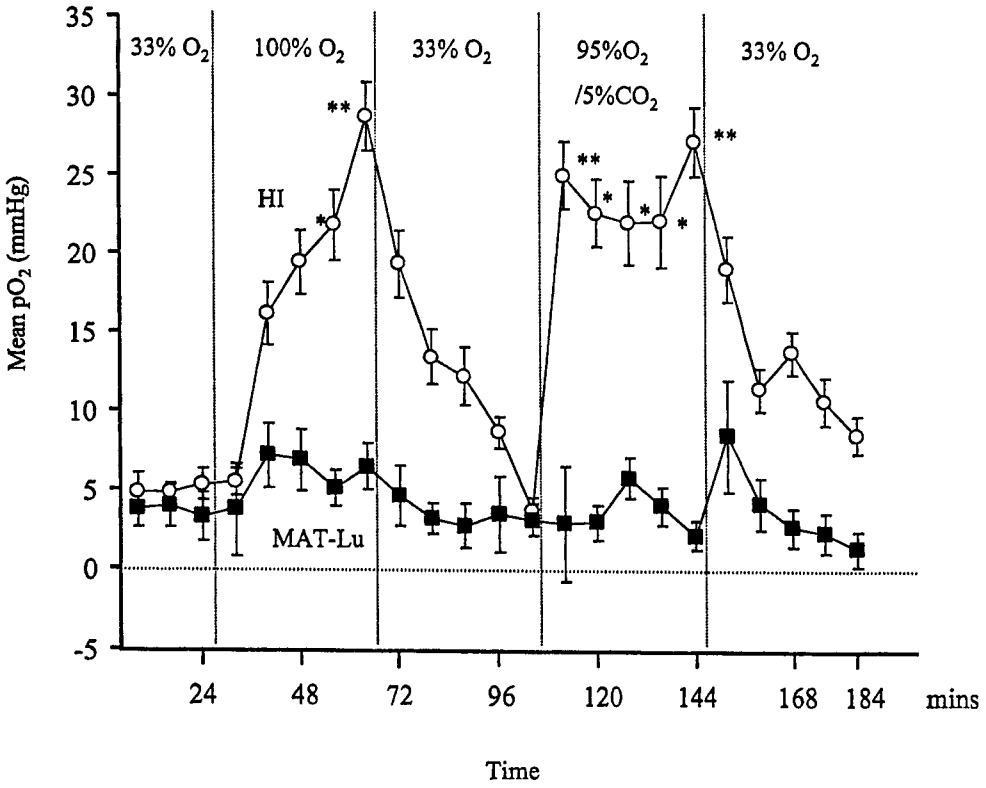

Fig. 6. Mean ± SE pO_2 in all the hypoxic voxels (<10 mm Hg) from each tumor in Fig. 2 with respect to respiratory challenge. Significant increases in mean pO_2 of the 7 hypoxic HI (○) voxels in response to 100% O_2 or 95% O_2/5% CO_2 challenge (*$p < 0.05$; **$p < 0.01$). No increase was observed in mean pO_2 of the 10 hypoxic MAT-Lu (■) voxels.

ated HI and poorly differentiated and highly metastatic MAT-Lu sublines, both derived from Dunning R3327 prostatic tumor (15), to investigate the extent of hypoxia. This study was not designed to investigate the correlation between hypoxia and tumor malignant progression, but clearly there is a need for further investigation to separate the phenotypic characteristics of differentiation, growth rate, and metastatic tendency. We propose to undertake further studies comparing the Dunning prostate AT2.1, AT6.3, and G sublines (4) to test these issues.

Many experimental and clinical studies have demonstrated that reoxygenation of hypoxic tumor cells contributes to improved radiation sensitivity for tumor therapy (46, 47). Therefore, how this population of cells responds to respiratory challenge is particularly important. If the findings we present here are confirmed in prostate cancer patients, it would suggest therapeutic value of monitoring tumor baseline and dynamic pO_2. Tumors like the HI can be modulated and might be expected to show improved response to radiotherapy with oxygen or carbogen inhalation before therapy; in tumors like MAT-Lu one might expect little advantage, indicating a need for an alternative approach.

In recent clinical trials, carbogen has been favored over oxygen, as an adjuvant intervention to enhance radiotherapy. Here, except in the small HI tumors, which exhibited significantly higher mean pO_2 in response to carbogen than oxygen, we have found no significant difference between the two gases, in terms of pO_2 values and hypoxic fraction. A recent report by Hartmann *et al.* (48) showed that hyperbaric oxygen, but not carbogen, significantly increased the median pO_2, leading to better radiation response in the rhabdomyosarcoma R1H. Further studies will be required to validate this observation, including reversing the order of administered gases, since a conditioning effect could have been generated here. We also note that changes in pO_2 were still occurring at 40 min, when we ceased our interventions here (Fig. 4). Others have reported a differential response to oxygen or carbogen in clinical gynecological tumors, where inhalation of either gas elevated median and mean pO_2, but only carbogen was effective at eliminating the hypoxic fraction (49). Such an observation was also reported for human glioma xenografts (50). Others have reported that response can depend on tumor type and site of implantation (51). In some cases, vasoactive agents have been shown to have differential activity against small and large tumors; e.g., angiotensin II led to reduced pO_2 in small DS-sarcomas (0.75 cm^3), but increased pO_2 in larger tumors (1.8 cm^3) (21). This was attributed to the relative role of preexisting host vessels vs. newly formed vessels lacking innervation and a responsive musculature. Here, in the HI tumor, we see that carbogen was equally effective in small or large tumors, consistent with the highly differentiated morphology and well-developed vasculature. Data obtained for the HI tumor here are very similar to results obtained previously with this tumor subline when rats were breathing an alternative an-

HI

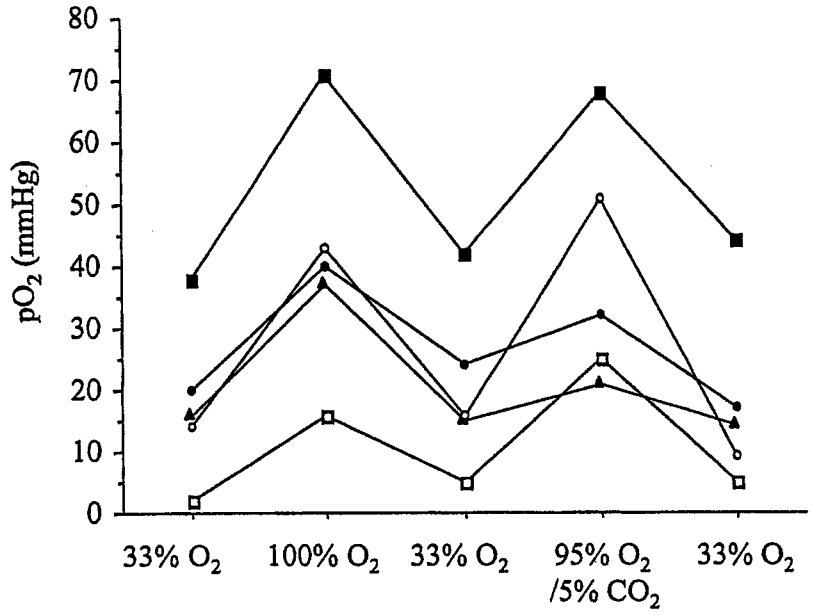

MAT-Lu

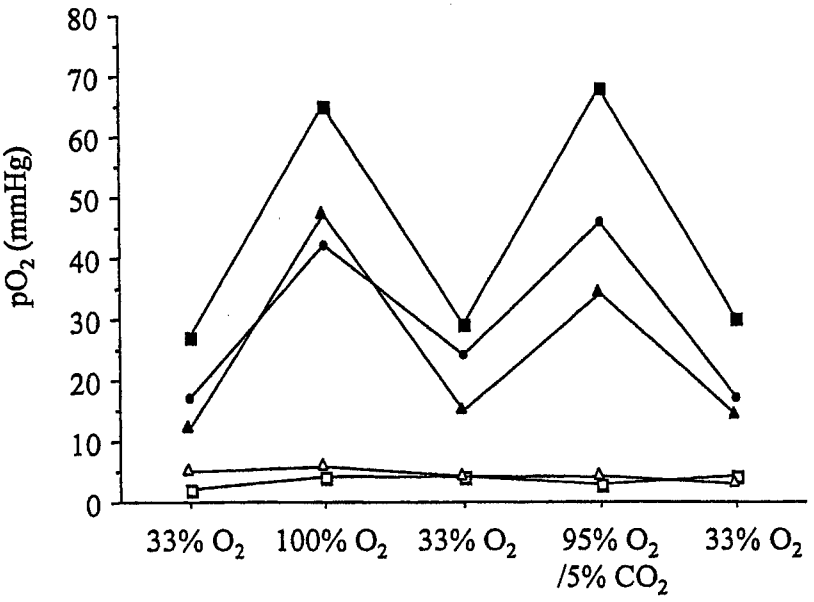

Fig. 7. Electrode measurements of pO_2 in one large tumor from each subline. pO_2 values in five locations in each tumor were measured with respiratory challenge. pO_2 in all the locations in the HI (○) tumor increased remarkably with 100% O_2 or carbogen. In the MAT-Lu (■) tumor, regions with initial $pO_2 > 10$ mm Hg responded significantly, whereas those relatively hypoxic did not.

esthetic (isoflurane in air) (24). The extensive heterogeneity within tumors emphasizes the importance of an imaging approach to examining differential oxygen dynamics. Here, we have used an oxygen electrode to validate the magnitude of changes observed in tumors, and previously we have shown that observation based on optical fiber probes (Oxy-Lite) also gave consistent data (24).

Comparison of repeat measurements with respect to acute interventions is predicated on reproducibility. We have previously shown that individual baseline pO_2 measurements

are usually stable for at least 1 h (10, 52). It has also been shown that pO_2 distributions in tumors are stable over several hours even with respect to repeat anesthesia episodes and movement of the rats out and back into an MRI system (53). We have, however, noted that HFB clears from tumors with a typical half-life of 600 min, and thus, we apply the *ARDVARC* data acquisition protocol to minimize any systematic errors in pO_2 measurements during the 8-min acquisition period. We have shown that there is little macroscopic redistribution over a period of 2.5 h (12).

In agreement with most reports on tumors implanted in rats or mice, we have found that large tumors are significantly more hypoxic. Some clinical studies have failed to show such a correlation. Our recent results (24) from a series of HI tumors, which we followed chronologically for a period of weeks with respect to increasing size, showed a catastrophic fall in pO_2 at some stage between 1 and 2 cm^3. Beyond this size, tumors remained poorly oxygenated. We note that most clinical tumors are much larger, usually >5 cm^3 and sometimes reaching 50 to 100 cm^3 and they may therefore already be at a low pO_2 plateau. We note that some clinical studies have shown a correlation between size and oxygenation (34, 54, 55) and Movsas *et al.* (45) using the Eppendorf Histograph reported a correlation between hypoxia and tumor stage in the prostate.

Limited ketamine (200 μL) was given to each rat i.p. as a relaxant before MR studies. It has been reported that ketamine does not affect mean arterial pressure, heart rate, or cerebral artery blood flow (56). However, methoxyflurane may cause a depression of respiration, tumor blood flow, and heart rate (57). Anesthesia is required to minimize stress and ensure no movement during imaging procedures. Immobilized tumors are vital to allow sequential correlation of specific tumor regions during investigations. Because all rats received the same constant level of anesthesia, we believe that it does not compromise or bias our observations and comparison of different tumor types. Recently, we have switched to isoflurane (24), which may be less vasoactive (57), but we find that HI tumors behave similarly with respect to either anesthesia.

Although we have thus far limited our application of the *FREDOM* approach to fundamental questions of tumor biology in animals, we believe the technique is ready for translation to the clinic. HFB is readily available, exhibits remarkably low toxicity, and could be easily administered to tumors on or near the surface of the body. *FREDOM* is analogous to use of the Eppendorf Histograph in terms of inserting a needle into a tumor, although our needle is considerably finer and no further needle insertion is required for repeated measurements when taken over the next few hours. In terms of patient compliance, Aquino-Parsons *et al.* (49) have already used the Eppendorf Histograph for up to three repeat measurements with respect to respiratory interventions in women with cervical cancer. *FREDOM* does involve sampling a limited region of the tumor by injection of the HFB reporter. However, we have previously shown that pO_2 distributions are similar to those achieved with the Eppendorf Histograph (10). Appropriate injection protocols are required to avoid bias, although for dynamic studies, as presented here, this is less important because each voxel serves as its own control.

To avoid violating the tumor itself, we have previously tested i.v. administration of perfluorocarbon emulsions as reporter molecules (58). However, we and others (58–60) showed that measurements are biased toward well-perfused tumor regions. Histology can be applied to intrinsic markers of hypoxia (61, 62), but this requires biopsy. Moreover, sampling is still involved both in terms of selecting the biopsy site and then choosing representative tissue slices and microscopic fields. Thus, we believe that *FREDOM* is competitive with many current or proposed invasive clinical techniques. While we believe that *FREDOM* is very valuable for animal research and has great potential in the clinic, we are nonetheless also investigating alternative approaches to measuring tumor oxygenation (63, 64). The BOLD approach (9) is very appealing, providing rapid noninvasive images, but quantitative measurements of signal dynamics provide only a qualitative indication of tumor oxygenation; much research remains to be done to relate the observed signal changes to therapeutic outcome. Near-infrared approaches can also interrogate tumor vasculature noninvasively, but hitherto, they have been limited to global observations, providing an indication of average tumor vascular oxygenation only (63).

In conclusion, we have demonstrated that, in comparison with the HI tumor, the faster growing and poorly differentiated MAT-Lu subline of the Dunning R3327 tumor is significantly more hypoxic and the level of hypoxia increases in both sublines with increasing size. Most significantly, we have demonstrated that two tumors derived from the same original parental tumor respond differently to an intervention. This emphasizes the need to assess individual tumors in the clinic in order to optimize a therapeutic regime.

REFERENCES

1. Brown JM. The hypoxic cell: A target for selective cancer therapy—eighteenth Bruce F. Cain memorial award lecture. *Cancer Res* 1999;59:5863–5870.
2. Hall EJ. The oxygen effect and reoxygenation. In: Hall EJ, editor. Radiobiology for the radiologist. Philadelphia: Lippincott; 1994. p. 133–152.
3. Chapman JD, Stobbe CC, Arnfield MR, *et al.* Oxygen dependency of tumor cell killing *in vitro* by light activated photofrin II. *Radiat Res* 1991;126:73–79.
4. Zhong H, Agani F, Baccala AA, *et al.* Increased expression of hypoxia inducible factor-1 alpha in rat and human prostate cancer. *Cancer Res* 1998;58:5280–5284.
5. Rofstad EK, Danielsen T. Hypoxia-induced metastasis of human melanoma cells: Involvement of vascular endothelial

growth factor-mediated angiogenesis. *Br J Cancer* 1999;80: 1697–1707.
6. Stone HB, Brown JM, Phillips T, *et al.* Oxygen in human tumors: Correlations between methods of measurement and response to therapy. *Radiat Res* 1993;136:422–434.
7. Sostman HD, Rockwell S, Sylva AL, *et al.* Evaluation of BA 1112 rhabdomyosarcoma oxygenation with microelectrodes, optical spectrometry, radiosensitivity, and MRS. *Magn Reson Med* 1991;20:253–267.
8. Vaupel P, Kelleher DK, Engel T. Stable bioenergetic status despite substantial changes in blood flow and tissue oxygenation in a rat tumour. *Br J Cancer* 1994;69:46–49.
9. Robinson SP, Collingridge DR, Howe FA, *et al.* Tumor response to hypercapnia and hyperoxia monitored by FLOOD magnetic resonance imaging. *NMR Biomed* 1999;12:98–106.
10. Mason RP, Constantinescu A, Hunjan S, *et al.* Regional tumor oxygenation and measurement of dynamic changes. *Radiat Res* 1999;152:239–249.
11. Hunjan S, Zhao D, Constantinescu A, *et al.* Tumor oximetry: Demonstration of an enhanced dynamic mapping procedure using fluorine-19 echo planar magnetic resonance imaging in the Dunning prostate R3327-AT1 rat tumor. *Int J Radiat Oncol Biol Phys* 2001;49:1097–1108.
12. Mason RP, Rodbumrung W, Antich PP. Hexafluorobenzene: A sensitive ^{19}F NMR indicator of tumor oxygenation. *NMR Biomed* 1996;9:125–134.
13. Eble MJ, Lohr F, Wenz F, *et al.* Tissue oxygen tension distribution in two sublines of the Dunning prostate tumor R3327. In: Vaupel PW, Kelleher DK, Gunderoth M, editors. Tumor oxygenation. Gustav Fischer Verlag, Stuttgart: Funktionsanalyse Biologischer Systeme; 1995. p. 95–105.
14. Peschke P, Hahn EW, Wenz F, *et al.* Differential sensitivity of three sublines of the rat Dunning prostate tumor system R3327 to radiation and/or local tumor hyperthermia. *Radiat Res* 1998;150:423–430.
15. Isaacs J, Isaacs W, Feitz W, *et al.* Establishment and characterization of 7 Dunning prostate cancer cell lines and their use in developing methods for predicting metastatic ability of prostate cancer. *Prostate* 1986;9:261–281.
16. Hahn EW, Peschke P, Mason RP, *et al.* Isolated tumor growth in a surgically formed skin pedicle in the rat: A new tumor model for NMR studies. *Magn Reson Imaging* 1993;11:1007–1017.
17. Vaupel PW, Fortmeyer HP, Runkel S, *et al.* Blood flow, oxygen consumption, and tissue oxygenation of human breast cancer xenografts in nude rats. *Cancer Res* 1987;47:3496–3503.
18. Terris DJ, Minchinton AI, Dunphy EP, *et al.* Computerized histographic oxygen tension measurement of murine tumors. In: Erdmann E, Bruley DF, editors. Oxygen transport to tissue XIV. New York: Plenum; 1992. p. 153–159.
19. Baldwin NJ, Ng TC. Oxygenation and metabolic status of KHT tumors as measured simultaneously by ^{19}F magnetic resonance imaging and ^{31}P magnetic resonance spectroscopy. *Magn Reson Imaging* 1996;14:514–551.
20. Shibamoto Y, Yukawa Y, Tsutsui K, *et al.* Variation in the hypoxic fraction among mouse tumors of different types, size, and site. *Jpn J Cancer Res* 1986;77:908–915.
21. Thews O, Kelleher DK, Vaupel P. Disparate responses of tumour vessels to angiotensin II: Tumour volume-dependent effects on perfusion and oxygenation. *Br J Cancer* 2000;83: 225–231.
22. Yeh KA, Biade S, Lanciano RM, *et al.* Polarographic needle electrode measurements of oxygen in rat prostate carcinomas: Accuracy and reproducibility. *Int J Radiat Oncol Biol Phys* 1995;33:111–118.
23. Hunjan S, Mason RP, Constantinescu A, *et al.* Regional tumor oximetry: ^{19}F NMR spectroscopy of hexafluorobenzene. *Int J Radiat Oncol Biol Phys* 1998;40:161–171.
24. Zhao D, Constantinescu A, Hahn EW, *et al.* Tumor oxygen dynamics with respect to growth and respiratory challenge: Investigation of the Dunning prostate R3327-HI tumor. *Radiat Res* 2001;156:510–520.
25. Thorndyke C, Meeker B, Thomas G, *et al.* The radiation sensitivities of R3327-H and -AT1 rat prostate adenocarcinomas. *J Urol* 1985;134:191–198.
26. Chapman JD, Engelhardt EL, Stobbe CC, *et al.* Measuring hypoxia and predicting tumor radioresistance with nuclear medicine assays. *Radiother Oncol* 1998;46:229–237.
27. Thews O, Kelleher DK, Lecher B, *et al.* Blood flow, oxygenation, metabolic and energetic status in different clonal subpopulations of a rat rhabdomyosarcoma. *Int J Oncol* 1998;13: 205–211.
28. Young S, Marshall R, Hill R. Hypoxia induces DNA overreplication and enhances metastatic potential of murine tumor cells. *Proc Natl Acad Sci USA* 1988;85:9533–9537.
29. Nordsmark M, Hoyer M, Keller J, *et al.* The relationship between tumor oxygenation and cell proliferation in human soft tissue sarcomas. *Int J Radiat Oncol Biol Phys* 1996;35: 701–708.
30. Höckel M, Vaupel P. Tumor hypoxia: Definitions and current clinical, biologic, and molecular aspects. *J Natl Cancer Inst* 2001;93:266–276.
31. Rofstad EK. Microenvironment-induced cancer metastasis. *Int J Radiat* 2000;76:589–605.
32. Raleigh JA, Zeman EM, Calkins DP, *et al.* Distribution of hypoxia and proliferation associated markers in spontaneous canine tumors. *Acta Oncol* 1995;34:849–853.
33. Höckel M, Schlenger K, Aral B, *et al.* Association between tumor hypoxia and malignant progression in advanced cancer of the uterine cervix. *Cancer Res* 1996;56:4509–4515.
34. Fyles AW, Milosevic M, Wong R, *et al.* Oxygenation predicts radiation response and survival in patients with cervix cancer. *Radiother Oncol* 1998;48:149–156.
35. Nordsmark M, Overgaard M, Overgaard J. Pretreatment oxygenation predicts radiation response in advanced squamous cell carcinoma of head and neck. *Radiother Oncol* 1996;41: 31–39.
36. Jaeger KD, Kavanagh M-C, Hill RP. Relationship of hypoxia to metastatic ability in rodent tumors. *Br J Cancer* 2001;84: 1280–1285.
37. Birner P, Schindl P, Obermair A, *et al.* Overexpression of hypoxia-inducible factor 1 is a marker for an unfavorable prognosis in early-stage invasive cervical cancer. *Cancer Res* 2000;60:4693–4696.
38. Brizel DM, Scully SP, Harrelson JM, *et al.* Tumor oxygenation predicts for the likelihood of distant metastases in human soft tissue sarcoma. *Cancer Res* 1996;56:941–943.
39. Giaccia AJ. Hypoxic stress proteins: Survival of the fittest. *Semin Radiat Oncol* 1996;6:46–58.
40. Heacock CS, Sutherland RM. Induction characteristics of oxygen regulated proteins. *Int J Radiat Oncol Biol Phys* 1986; 12:1287–1290.
41. Graeber TG, Osmanian C, Jacks T, *et al.* Hypoxia-mediated selection of cells with diminished apoptotic potential in solid tumours. *Nature* 1996;379:88–91.
42. Koong AC, Denko NC, Hudson KM, *et al.* Candidate genes for the hypoxic tumor phenotype. *Cancer Res* 2000;60:883–887.
43. Catalona WJ, Scott WW. Carcinoma of the prostate. In: Harrison JH, editor. Cancer urology. Philadelphia: WB Saunders; 1979. p. 1085–1124.
44. Chiarado A. National Cancer Institute roundtable on prostate cancer: Future research direction. *Cancer Res* 1991;51:2498–2505.

45. Movsas B, Chapman J, Horwitz E, *et al.* Hypoxic regions exist in human prostate carcinoma. *Urology* 1999;53:11–18.
46. Kallman R, Dorie M. Tumor oxygenation and reoxygenation during radiation therapy: Importance in predicting tumor response. *Int J Radiat Oncol Biol Phys* 1986;12:681–685.
47. Fenton BM. Effects of carbogen plus fractionated irradiation on KHT tumor oxygenation. *Radiother Oncol* 1997;44:183–190.
48. Hartmann K, van der Kleij A, Carl U, *et al.* Effects of hyperbaric oxygen and normobaric carbogen on the radiation response of the rat rhabdomyosarcoma R1H. *Int J Radiat Oncol Biol Phys* 2001;51:1037–1044.
49. Aquino-Parsons C, Green A, Minchinton AI. Oxygen tension in primary gynaecological tumours: The influence of carbon dioxide concentration. *Radiother Oncol* 2000;57:45–51.
50. van der Sanden BJP, Heerschap A, Hoofd L, *et al.* Effect of carbogen breathing on the physiological profile of human glioma xenografts. *Magn Reson Med* 1999;42:490–499.
51. Lanzen JL, Braun RD, Ong AL, *et al.* Variability in blood flow and pO_2 in tumors in response to carbogen breathing. *Int J Radiat Oncol Biol Phys* 1998;42:855–859.
52. Le D, Mason RP, Hunjan S, *et al.* Regional tumor oxygen dynamics: ^{19}F PBSR EPI of hexafluorobenzene. *Magn Reson Imaging* 1997;15:971–981.
53. Hunjan S. In-vivo fluorine nuclear magnetic resonance investigations of tumor oxygen tension and pH [Ph.D. dissertation]. Dallas: University of Texas Southwestern Medical Center; 1999.
54. Lartigau E, Le Ridant AM, Lambin P, *et al.* Oxygenation of head and neck tumors. *Cancer* 1993;71:2319–2325.
55. Hohenberger P, Felger C, Haensch W, *et al.* Tumor oxygenation correlates with molecular growth determinants in breast cancer. *Breast Cancer Res Treatment* 1998;48:97–106.
56. Sasaki K, Cho S, Fukusaki M, *et al.* The effects of propofol with and without ketamine on human cerebral blood flow velocity and CO_2 response. *Anesth Analg* 2000;90:377–382.
57. McKelvey D. Halothane, isoflurane, and methoxyflurane: Physical properties and pharmacology. *Veterinary Technician* 1991;12:21–28.
58. Mason RP, Antich PP, Babcock EE, *et al.* Non-invasive determination of tumor oxygen tension and local variation with growth. *Int J Radiat Oncol Biol Phys* 1994;29:95–103.
59. McIntyre DJO, McCoy CL, Griffiths JR. Tumor oxygenation measurements by ^{19}F MRI of perfluorocarbons. *Curr Sci* 1999;76:753–762.
60. van der Sanden BPJ, Heerschap A, Simonetti AW, *et al.* Characterization and validation of non-invasive oxygen tension measurements in human glioma xenografts by 19F-MR relaxometry. *Int J Radiat Oncol Biol Phys* 1999;44:649–658.
61. Semenza GL. Hypoxia, clonal selection, and the role of HIF-1 in tumor progression. *Crit Rev Biochem Mol Biol* 2000;35:71–103.
62. Loncaster JA, Harris AL, Davidson SE, *et al.* Carbonic anhydrase (CA IX) expression, a potential new intrinsic marker of hypoxia: Correlation with tumor oxygen measurement and prognosis in locally advanced carcinoma of the cervix. *Cancer Res* 2001;61:6394–6399.
63. Liu H, Song Y, Worden KL, *et al.* Noninvasive investigation of blood oxygenation dynamics of tumors by near-infrared spectroscopy. *Appl Optic* 2000;39:5231–5243.
64. Fink K, Yetkin Z, McColl R, *et al.* Brain tumor vascular dynamics: A BOLD MRI investigation. 92nd American Association for Cancer Research (AACR), New Orleans, LA; 2001. p. 388. (Abstr).

RADIATION RESEARCH 159, 621–631 (2003)
0033-7587/03 $5.00

Correlation of Tumor Oxygen Dynamics with Radiation Response of the Dunning Prostate R3327-HI Tumor[1]

Dawen Zhao,[a] Anca Constantinescu,[a] Cheng-Hui Chang,[b] Eric W. Hahn[a] and Ralph P. Mason[a,2]

Departments of [a] Radiology and [b] Radiation Oncology, The University of Texas Southwestern Medical Center, Dallas, Texas 75390

Zhao, D., Constantinescu, A., Chang, C. H., Hahn, E. W. and Mason, R. P. Correlation of Tumor Oxygen Dynamics with Radiation Response of the Dunning Prostate R3327-HI Tumor. *Radiat. Res.* 159, 621–631 (2003).

Our previous studies have shown that oxygen inhalation significantly reduces tumor hypoxia in the moderately well-differentiated HI subline of the Dunning prostate R3327 rat carcinoma. To test our hypothesis that modifying hypoxia could improve the radiosensitivity of these tumors, we performed experimental radiotherapy to compare the tumor response to ionizing radiation alone or in combination with oxygen inhalation. Tumor pO_2 measurements were performed on size-selected tumors several hours before radiotherapy using ^{19}F nuclear magnetic resonance echo planar imaging relaxometry (FREDOM) of the reporter molecule hexafluorobenzene. In common with our previous findings, the larger tumors (>3.5 cm^3) exhibited greater hypoxia than the smaller tumors (<2 cm^3; $P < 0.001$), and oxygen inhalation reduced the hypoxic fraction (<10 Torr): In the larger tumors, hypoxic fraction dropped significantly from a mean baseline value of 80% to 17% ($P < 0.001$). The effect of oxygen administered 30 min before and during irradiation on tumor response to a single 30-Gy dose of photons was evaluated by growth delay. For the smaller tumors, no difference in growth delay was found when treatment was given with or without oxygen breathing. By contrast, breathing oxygen before and during irradiation significantly enhanced the growth delay in the larger tumors (additional 51 days). The differential behavior may be attributed to the low baseline hypoxic fraction (<10 Torr) in small tumors (20%) as a target for oxygen inhalation. There was a strong correlation between the estimated initial pO_2 value and the radiation-induced tumor growth delay ($R > 0.8$). Our histological studies showed a good match between the perfused vessels marked by Hoechst 33342 dye and the total vessels immunostained by anti-CD31 and indicated extensive perfusion in this tumor line. In summary, the present results suggest that the ability to detect modulation of tumor pO_2, in particular, the residual hypoxic fraction, with respect to an intervention, could have prognostic value for predicting the efficacy of radiotherapy. ©

INTRODUCTION

It is recognized that measurement of pretreatment tumor oxygenation can have prognostic value (*1–3*) and that increased tumor pO_2 promotes radiosensitivity (*4, 5*). Many adjuvant interventions have been tested to manipulate tumor oxygenation to improve the response to radiation, e.g. normobaric or hyperbaric oxygen breathing, carbogen alone or combined with nicotinamide, infusion of blood substitutes, and hemoglobin-oxygen affinity modifiers (*3, 6*). While the beneficial effects of such modifiers have sometimes been translated from animal to clinical studies (*7, 8*), many clinical trials have failed to show therapeutic benefit (*9*). This has often been attributed to the inability to identify the cohort of patients who would benefit from adjuvant intervention (*3*). Therefore, accurate evaluation of pretreatment tumor oxygenation and its response to adjuvant intervention may allow therapy to be tailored to individual characteristics. To date the Eppendorf histograph has been the most widely used technique to measure tumor pO_2 in both experimental and clinical studies, and disease-free survival has been correlated with hypoxia in studies of cervical cancer (*1, 2*) and head and neck cancer (*10–12*). The Eppendorf histograph has been considered by some as a "gold standard" for pO_2 measurement, but it is impractical for use in longitudinal studies of specific regions of interest. Longitudinal imaging studies with respect to intervention have been performed in experimental superficial tumors, e.g. window chamber models, but investigations of deeper tissues have been relatively elusive. Historically, electrodes (*13*), or more recently fiber optic probes (*14*) or electron spin resonance (*15*), have been applied to examine dynamic changes at a few (one to four) limited locations. Blood oxygen level-dependent (BOLD) contrast proton MRI is a noninvasive technique to assess tumor vascular oxygenation and heterogeneity in response to intervention, but the

[1] Presented in part at the Forty-Eighth Annual Radiation Research Society Meeting, San Juan, Puerto Rico, April 2001.

[2] Address for correspondence: Department of Radiology, U.T. Southwestern Medical Center, 5323 Harry Hines Blvd., Dallas, TX 75390-9058; e-mail: Ralph.Mason@UTSouthwestern.edu.

method does not provide pO_2 values and interpretation may be complicated by flow (*16*).

We have established an MRI approach to measure tumor oxygen tension quantitatively at multiple locations simultaneously: FREDOM (fluorocarbon relaxometry using echo planar imaging for dynamic oxygen mapping) with hexafluorobenzene (HFB) as a reporter molecule (*17, 18*). This technique allows us to assess baseline pO_2 at multiple specific locations simultaneously within a tumor and also to follow dynamic changes in response to interventions. Our previous work (*19, 20*) using FREDOM showed differential size-related oxygenation of the relatively slowly growing, moderately well-differentiated Dunning prostate R3327 HI rat tumor. Most importantly, we found that oxygen inhalation significantly decreased tumor hypoxia in the HI tumor irrespective of baseline hypoxia. Thus the HI tumor appeared to be an ideal model to test whether our measurements of tumor oxygen dynamics could be correlated with therapeutic outcome.

METHODS

Experiments were reviewed and approved by the Institutional Animal Care and Research Advisory Committee at UT Southwestern.

Tumor Model

Syngeneic Dunning prostate R3327-HI tumors, a moderately well-differentiated and relatively slowly growing subline with a tumor volume doubling time (VDT) of 9 days (*21, 22*), were originally obtained from Dr. J. T. Isaacs, Johns Hopkins University. Tumors were implanted in surgically formed skin pedicles on the foreback of adult male Copenhagen-2331 rats (Harlan, Indianapolis, IN; ~250 g), as described in detail previously (*23*). Thirty-six tumors were grouped at the time of initial measurement as 16 smaller tumors (<2 cm^3; mean = 1.4 ± 0.1 cm^3) and 20 larger tumors (>3.5 cm^3; mean = 6.4 ± 0.7 cm^3).

Tumor Oximetry—FREDOM

Four small tumors and six larger tumors were used for MRI studies, which were performed as described in detail previously (*19*). Briefly, each rat was given 200 μl ketamine hydrochloride (100 mg/ml, Aveco, Fort Dodge, IA) as a relaxant (i.p.) and maintained under general gaseous anesthesia [air and 1.3% isoflurane (Baxter International Inc., Deerfield, IL)]. Hexafluorobenzene (50 μl; Lancaster, Gainesville, FL) that had been deoxygenated by bubbling nitrogen for 5 min before use was injected directly into the tumors using a Hamilton syringe (Reno, NV) with a custom-made fine sharp needle (32 gauge). The HFB was deliberately deposited in both the central and peripheral regions of the tumors to ensure that the interrogated regions would be representative of the whole tumor. Generally, HFB was administered along two or three tracks in the form of a fan in a single central plane of the tumor sagittal to the rat's body. Each animal was placed on its side in a cradle with a thermal blanket to maintain body temperature.

Magnetic resonance experiments were performed using an Omega CSI 4.7 horizontal bore magnet system with actively shielded gradients (Bruker Instrument Inc., Fremont, CA). A tunable ($^1H/^{19}F$) single turn solenoid coil (2 or 3.5 cm in diameter matched to the tumor size) was placed around the tumor-bearing pedicle, and ^1H (200.1 MHz) and ^{19}F (188.3 MHz) images were obtained using three-dimensional (3D) spin-echo sequences to reveal the distribution of HFB within the tumors. After conventional MR imaging, tumor oxygenation was estimated using FREDOM on the basis of ^{19}F pulse burst saturation recovery echo planar imaging (EPI) relaxometry of the HFB (*18*). pO_2 maps with 1.25 mm in-plane voxel resolution were obtained in 8 min. The spin-lattice relaxation rate [R1(s − 1) = 1/T1] was estimated on a voxel-by-voxel basis using a three-parameter monoexponential function, and pO_2 was estimated using the relationship pO_2 (Torr) = (R1 − 0.0835)/0.001876 (*18*). Typically, ~100–300 voxels provided an R1 fit and potential pO_2 value. Since noise itself may give an apparent relaxation curve (R1) fit, data were selected within a region of interest, with a T1 error <2.5 s and a ratio T1 err/T1 <50%. Only those voxels that provided consistently reliable data throughout the measurements were included for further analysis. For nine of the ten tumors, the number of such acceptable voxels ranged from 35 to 150 per tumor. Images from tumor no. 8 showed some motion artifacts, and the requirement for continuously good fits in each voxel throughout the study was relaxed for this data set. Three consecutive 8-min baseline pO_2 measurements were made in 24 min, while the rat breathed air (FO_2 = 21%). Four representative animals (one with a small tumor) also underwent respiratory challenge using 100% O_2, and five pO_2 maps were acquired over 40 min.

Radiation Experiments

Several hours after the MRI measurements, the irradiation was performed with anesthetized rats breathing air or oxygen and 1.3% isoflurane. The TCD_{50} for the HI tumors was reported to be about 50 Gy (*22*), and we chose to use a single dose of 30 Gy. The 30-Gy dose was given at a rate of 2 Gy/min using a 4 MV Varian Clinac 4/100 linear accelerator. Five rats from the small tumor group and seven from the larger tumor group breathed oxygen 30 min prior to and during irradiation, while the same number of rats in each group breathed air. To avoid possible artifacts, the four rats used for the FREDOM pO_2 study were part of the group to receive oxygen during irradiation. A treatment plan was designed to irradiate only the tumors and bolus material was used to improve dose uniformity. Control groups without irradiation consisted of six rats each for the small and large tumor groups. Tumor sizes were measured every 3–7 days using calipers and the volumes were calculated using the formula: volume = $\pi/6\ abc$, where a, b and c are the three respective dimensions. Treatment response was evaluated on the basis of tumor growth, which was determined from the time (T_2) required for each tumor to reach two times the treatment volume (V_0).

Markers of Vascular Endothelium and Perfusion

The blue fluorescent dye Hoechst 33342 (Molecular Probes, Eugene, OR) was injected into the tail vein of three anesthetized rats bearing large tumors at a concentration of 10 mg/kg in 0.9% saline (0.1 ml), and the tumors were excised 1 min later. Tumor specimens were immediately immersed in liquid nitrogen and then stored at −80°C. Immediately after cryostat sectioning (6 μm thick), slices were imaged for Hoechst 33342 under UV light (330–380 nm). On the following day, the same slices were immunostained for the endothelial marker, CD31. Tissue sections were fixed in acetone for 5 min and then washed in phosphate-buffered saline (PBS) for 10 min. A primary mouse anti-rat CD31 monoclonal antibody (1:20 dilution; Serotec, Raleigh, NC) was added and samples were incubated for 2 h at 37°C in a humid box. Slides were then incubated with horseradish peroxidase-conjugated goat anti-mouse secondary antibody (1:50 dilution; Serotec) for 1 h at 37°C. After a wash in PBS, sections were immersed in the AEC substrate (3-amino-9-ethylcarbazole, Vector Laboratories, Burlingame, CA) for 15 min at room temperature. Finally, sections were counterstained with hematoxylin and observed under light microscopy. For fluorescence staining, after 2 h incubation with the primary anti-CD31 antibody, slides were incubated with FITC-conjugated goat anti-mouse secondary antibody (1:100 dilution; Jackson Immunoresearch Laboratories, West Grove, PA) for 1 h at 37°C. After mounting with Vectorshield® medium (Vector Laboratories), the slides were observed under green fluorescence (450–490 nm excitation). Microvascular density (MVD) was evaluated using the "hot spot" technique described by Weidner *et al.* (*24*). The five most vascularized areas in each

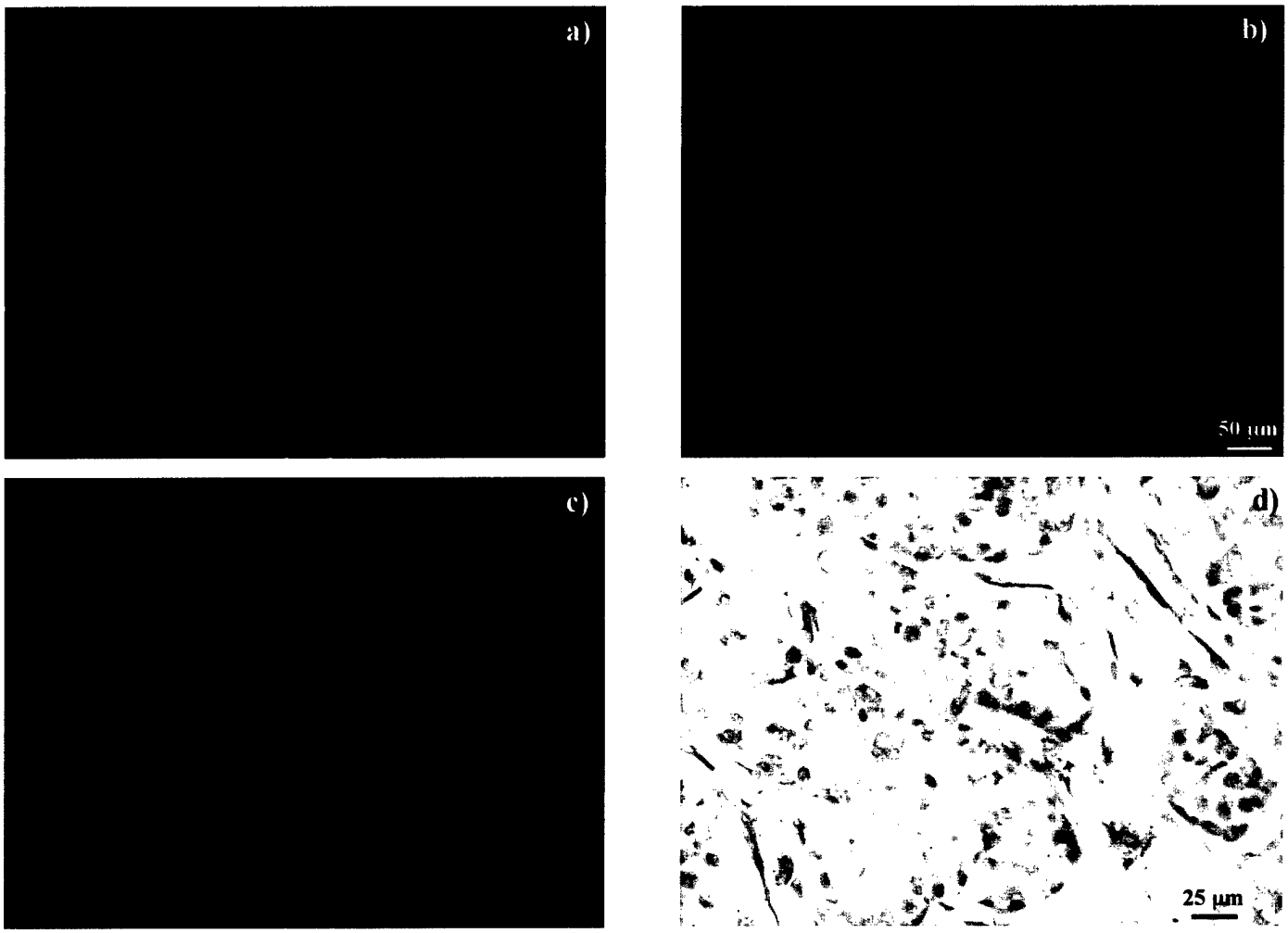

FIG. 1. Immunohistochemical comparison of perfused vessels marked by Hoechst dye 33342 and total vessels detected by anti-CD31. Panel a: Fluorescent image showing extensive distribution of vascular endothelium (green) in a representative large HI tumor (4.5 cm^3). Panel b: The perfused blood vessels marked by blue Hoechst dye in the same region. Panel c: Superimposition of panel b on panel a showing a good overlap between the total vessels (anti-CD31) and the perfused vessels (Hoechst dye). Panel d: Light microscope image showing distribution of vascular endothelium stained by anti-CD31 (pink).

tumor were selected under low-power magnification (4×). MVD was determined by counting the total number of positive CD31-staining cells under high-power magnification (10×; area 0.318 mm^2) and calculating the average number/mm^2.

Statistical Analysis

The statistical significance of changes in oxygenation was assessed using an analysis of variance (ANOVA) on the basis of Fisher's protected least significant difference (PLSD), and the statistical analysis of regression was based on regression and bivariate plots (Statview, SAS Institute Inc., Cary, NC). Kaplan-Meier hazard statistics (Breslow-Gehan-Wilcoxon rank test) were applied to test the differences in times required for tumor growth to two times (T_2) the initial volume at time of treatment. Hypoxic fractions in all the tumors were calculated from the data on oxygen tensions in individual voxels in each pO_2 map. These are presented as HF_5 (fraction of voxels with $pO_2 < 5$ Torr) and HF_{10} (fraction of voxels with $pO_2 < 10$ Torr).

RESULTS

Histology shows that the HI tumor is moderately well-differentiated with uniformly sized tumor cells and pseudoglandular structures. Anti-CD31 immunostaining showed extensive distribution of vascular endothelium (Fig. 1a and d) and a mean MVD = 188 ± 11 (SE)/mm^2. Comparison of the perfused vessels marked by Hoechst 33342 dye with the vessels immunostained by anti-CD31 in the same region indicated extensive perfusion (Fig. 1a and b) and a good correlation (Fig. 1c).

Overlay of ^{19}F images on ^{1}H images (not shown) confirmed that HFB was distributed widely, as reported previously (*19*), but was predominantly in a central slice. An HFB signal was detected from 45 ± 8% of the slice area for the small tumors and 13 ± 2% for the larger tumors. The difference in HFB signal distribution between the small and larger tumors is commensurate with the difference in tumor size given that the same amount of HFB (50 μl) was injected in all tumors irrespective of size. Figure 2 shows a typical map of ^{19}F NMR signal amplitude together with the corresponding T1 and T1 error maps and derived pO_2 map for a representative large tumor (no. 10). The back-

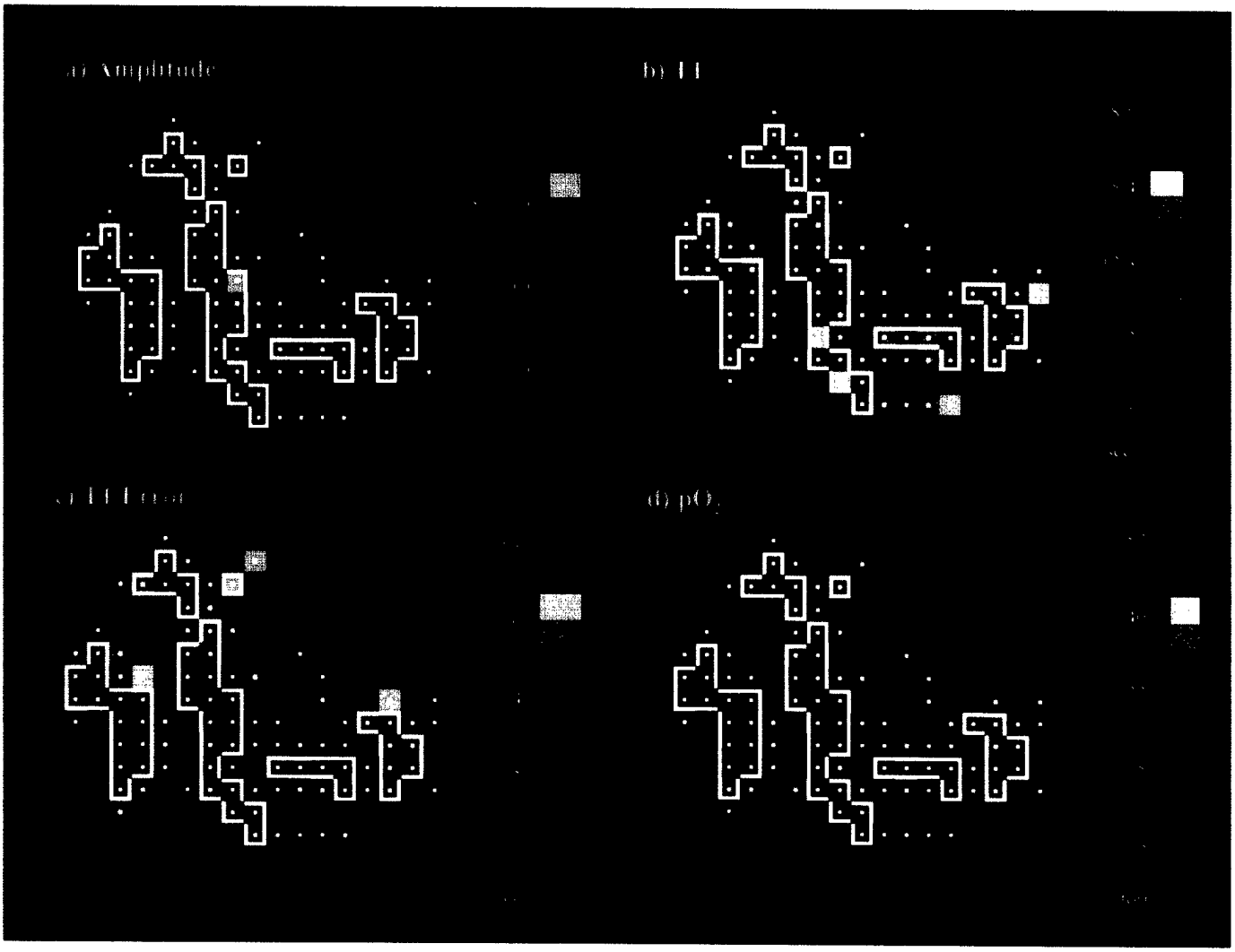

FIG. 2. Maps obtained using the FREDOM approach from a representative large Dunning prostate R3327-HI tumor (9.5 cm^3). Panel a: ^{19}F NMR signal intensity; panel b: spin lattice relaxation times (T1); panel c: estimated errors in T1; and panel d: pO_2 values. Black squares show regions where signal to noise or data quality was so poor that it did not provide a T1 curve fit. Gray voxels show regions that provided a curve fit, but where the uncertainty in the data exceed our criteria (i.e. T1err > 2.5 s or T1err/T1 > 50%). All colored voxels provided a curve fit within the acceptance criteria in this map, but only those voxels within the white regions of interest provided consistently high-quality data throughout the sequence of eight maps acquired during baseline and with oxygen breathing. Further analysis is shown in Fig. 3

ground had a signal amplitude of about 14,000 and the voxels providing reliable pO_2 measurements generally had a signal amplitude in excess of 300,000, providing a minimum signal-to-noise ratio exceeding 20. pO_2 maps of the selected regions obtained from this large tumor with respect to oxygen challenge are shown together with curve fits of selected voxels in Fig. 3. While the animals were breathing air (baseline), the tumor exhibited extensive hypoxia, with 46 of 50 regions (voxels) having pO_2 values less than 10 Torr. After 40 min of oxygen inhalation, the initially hypoxic regions became well oxygenated and only one voxel remained hypoxic (~5 Torr).

Baseline pO_2 distributions obtained from the tumors examined by MRI [four small (363 voxels) and six large (456 voxels) tumors] are presented in Table 1. The small tumors had a mean baseline pO_2 = 29.4 ± 3.2 Torr, with a median of 24.6 ± 3.4 Torr and mean hypoxic fractions of 10 ± 3 and 20 ± 3% for HF_5 and HF_{10}, respectively. In comparison, the larger tumors had mean pO_2 values 3.6 ± 1.5 Torr and median values of 1.3 ± 0.9 Torr, with HF_5 and HF_{10} of 65 ± 5% and 77 ± 4%, respectively. In agreement with our previous studies (*19, 20*), the larger tumors had significantly lower mean pO_2's and higher hypoxic fractions ($P < 0.01$) compared to the small tumors. One of the four small tumors and three of the six large tumors were subjected to a 40-min oxygen challenge; the resulting dynamic changes in mean pO_2 and hypoxic fraction (HF_{10}) are shown in Table 1 and Fig. 4. Baseline pO_2 (mean = 31.0 ± 2.5 Torr; median = 30.0 Torr) in the small tumor increased significantly within 8 min of switching the inspired gas from air to oxygen and reached 180 ± 16 Torr ($P <$ 0.0001; median pO_2 = 177 Torr) after 40 min. All three

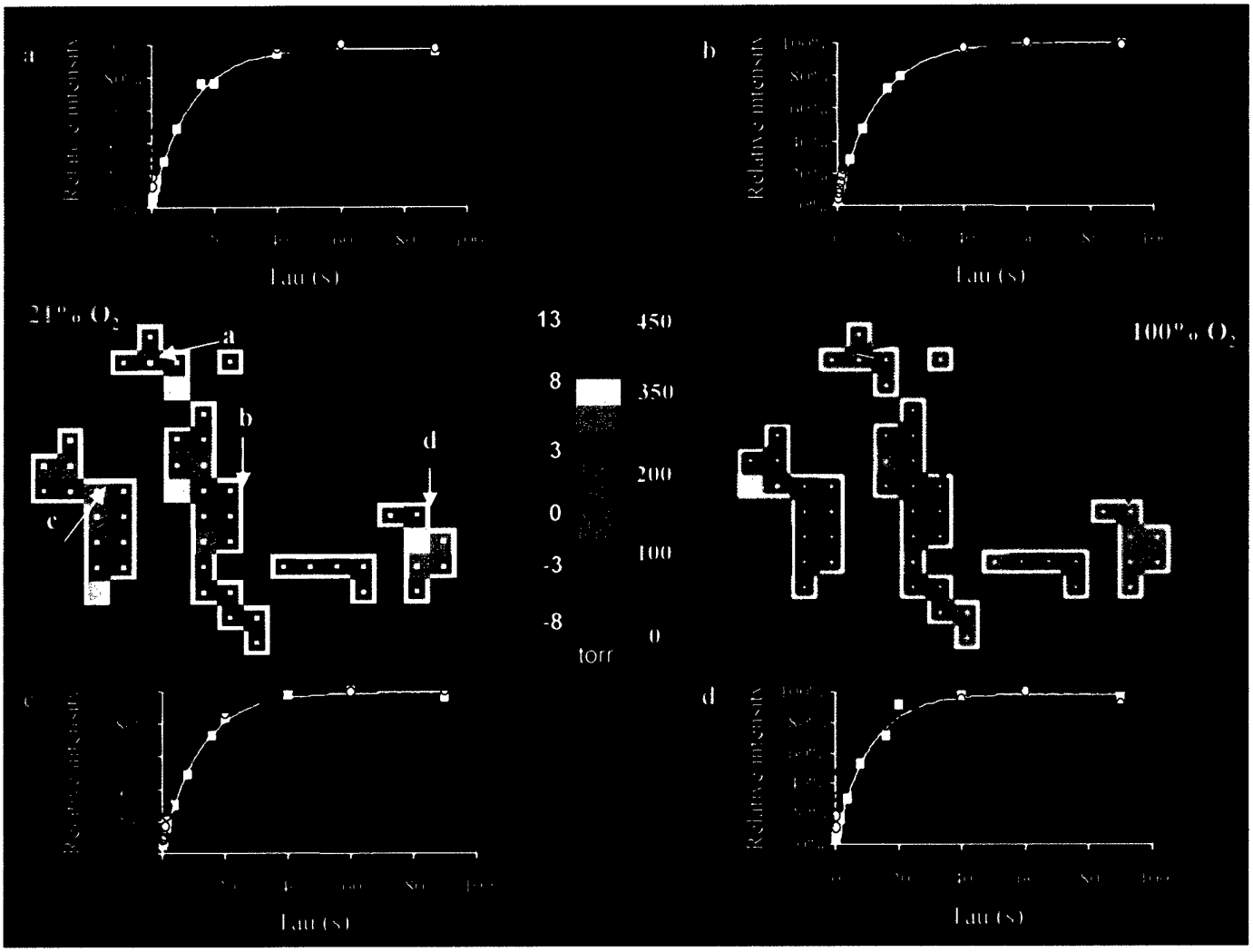

FIG. 3. pO_2 maps (middle row) showing regions of interest from the tumor in Fig. 2, together with T1 curve fits of selected voxels. Left: third baseline map (breathing air: FO_2 = 21%): mean pO_2 = −1.4 ± 0.6 (SE) Torr, median pO_2 = −1.3 Torr. Right: breathing oxygen (FO_2 = 100%): fifth map obtained 32–40 min after switching from air: mean pO_2 = 110 ± 10 Torr ($P < 0.0001$ compared to baseline), median pO_2 = 89 Torr. Since the pO_2 values have very different ranges, separate color scales have been applied. Curve-fitting data are shown for representative voxels and the signal-to-noise ratios quoted for the data points at longest delays. a) baseline T1 = 11.6 ± 0.6 s, signal-to-noise ratio = 44 (white) and the challenged T1 = 2.4 ± 0.2 s (pink), corresponding to pO_2 = 1.3 and 177.2 Torr. Panel b: baseline T1 = 12.5 ± 0.3 s, signal-to-noise ratio = 84, pO_2 = −1.9 and challenge T1 = 8.6 ± 0.3 s, pO_2 = 17.9 Torr. Panel c: baseline T1 = 11.6 ± 0.5 s, signal-to-noise ratio = 39, pO_2 = 1.5 Torr and challenge T1 = 7.0 ± 0.8 s, pO_2 = 31.2 Torr. Panel d: baseline T1 = 10.2 ± 0.7 s, signal-to-noise ratio = 20, pO_2 = 7.9 Torr; the challenge T1 = 2.4 ± 0.5 s, pO_2 = 178.8 Torr.

large tumors had lower baseline pO_2 (range from −1.7 to 5.2 Torr), but the pO_2 increased significantly, with a maximum mean for the three of 102 ± 7 Torr and a median of 71 Torr (Table 1 and Fig. 4). One large tumor reached a maximum pO_2 at 24 min, while the pO_2 continued to rise for the other two through the 40 min (Fig. 4a). Oxygen breathing significantly reduced the HF_5 from 8 to 2% and the HF_{10} from 19% to 4% in the small tumor. In the three larger tumors, the HF_5 and HF_{10} were significantly reduced from 71 ± 9% and 80 ± 8% to 11 ± 5% to 17 ± 7% ($P < 0.01$; Table 1 and Fig. 4b).

Table 2 summarizes tumor growth delay after irradiation alone or in combination with oxygen breathing. Sham-irradiated small control tumors on rats breathing air needed a mean of 7.2 (median 7) days to reach two times (T_2) the treatment volume (V_0). Treatment with radiation alone lengthened the T_2 to a mean of 38.8 ± 9.0 days (median = 28 days), which was not different from the 36.4 ± 6.7 days with radiation plus oxygen (median = 30 days). For the large tumors, with radiation alone, the T_2 was a mean of 30.9 ± 5.5 days (median = 31 days) compared to a mean of 16.7 ± 1.3 days (median = 16 days) in the control tumors (P = 0.06). For large tumors, rats that breathed oxygen 30 min prior to and during irradiation had a significantly increased T_2 of 81.9 ± 14.6 days (median = 77 days, $P < 0.01$). The addition of oxygen produced an enhanced growth delay, with a T_2 ratio of 2.7 (81.9/30.9) compared to radiation alone ($P < 0.01$; Table 2). The Kap-

TABLE 1
pO_2 Measurements and Outcome of Irradiation

Group	Rat no.	Baseline breathing air (21% O_2) pO_2 (Torr) Mean[a] ± SE	Median[a]	HF_5 Mean[a]	HF_{10} ± SE (%)	Oxygen challenge (100% O_2) pO_2 (Torr) Mean ± SE	Median	HF_5 Minimum	HF_{10} (%)	Outcome Treatment	T_2 (days)
Small	1	21.7 ± 1.3	16.2	14 ± 4	26 ± 5	NA	NA	NA	NA	30 Gy	20
(<2 cm³)	2	28.1 ± 1.5	22.0	13 ± 1	20 ± 2	NA	NA	NA	NA	30 Gy	25
	3	31.0 ± 2.5	30.0	8 ± 2	19 ± 2	179.6 ± 16.0[b]	177.4	2	4	30 Gy + O_2	23
	4	37.0 ± 1.5	30.1	3 ± 1	14 ± 2	NA	NA	NA	NA	30 Gy + O_2	47
	Mean	29.4 ± 3.2	24.6 ± 3.4	10 ± 3	20 ± 3						29
Large	5	4.3 ± 1.2	2.0	62 ± 7	74 ± 10	NA	NA	NA	NA	30 Gy	15
(>3.5 cm³)	6	8.8 ± 0.9	5.1	50 ± 7	67 ± 5	NA	NA	NA	NA	30 Gy	16
	7	3.8 ± 0.7	1.3	66 ± 3	80 ± 4	NA	NA	NA	NA	30 Gy	38
	Mean	5.6 ± 1.6[c]	2.8 ± 1.2[c]	59 ± 5[c]	74 ± 4[c]						23
	8	1.3 ± 1.1	0.1	65 ± 3	80 ± 5	107 ± 14[b]	70	15	22	30 Gy + O_2	55
	9	5.2 ± 1.2	0.9	60 ± 7	67 ± 10	895 ± 17[b]	54	17	26	30 Gy + O_2	57
	10	−1.7 ± 2.0	−1.7	88 ± 6	93 ± 5	110 ± 10[b]	89	1	4	30 Gy + O_2	118
	Mean	1.6 ± 2.0[c]	−0.2 ± 0.8[c]	71 ± 9[c]	80 ± 8[c]	102 ± 7[b]	71 ± 10	11 ± 5[b]	17 ± 7[b]		77

Notes. HF_5 or HF_{10}: Hypoxic fraction (fraction of voxels <5 or 10 Torr); HF_5 or HF_{10} minimum: minimum value among the five measurements with respect to oxygen breathing; NA: not measured.

[a] Values represent the mean values across the three baseline observations; T_2: time required to reach two times initial volume (V_0).

[b] $P < 0.01$ from baseline.

[c] $P < 0.01$ from the small tumors.

lan-Meier hazard plots (T_2) indicated that oxygen breathing produced an enhanced growth delay in the large tumors (Fig. 5). The cumulative survival time for the small and large tumors (Fig. 5) truly represents the time for the tumors to reach two times the initial treatment volume. In contrast, for the rats treated with radiation plus oxygen, one animal died before this volume was reached and two animals were euthanized. Each of these animals lived longer than the rats receiving radiation alone. For these animals, the "T_2" was defined as the time they were removed from the study. If anything, this procedure biases the results toward shorter survival times (i.e. less effect of O_2 breathing). Assuming that baseline pO_2 (for air-breathing rats) or the maximum pO_2 values observed during oxygen breathing (for radiation + O_2) using FREDOM represent the pO_2 values at the time of irradiation, we found a strong linear correlation between the pO_2 values and T_2 for the large tumors ($R > 0.8$; Fig. 6). For small tumors, breathing oxygen had

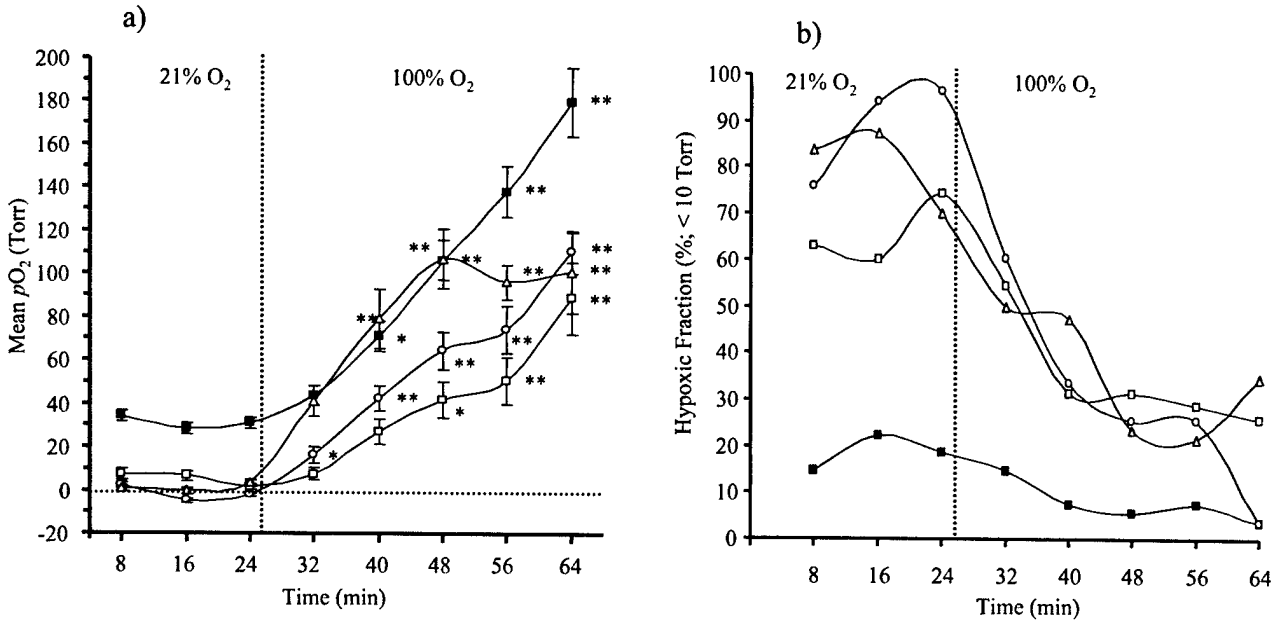

FIG. 4. Changes in oxygenation and hypoxic fraction in response to respiratory challenge. Panel a: Mean ± SE pO_2 obtained from sequential maps of one small (solid) and three large HI (open) tumors with respect to respiratory challenge. *$P < 0.001$, **$P < 0.0001$ compared to mean baseline. Panel b: Corresponding hypoxic fraction (HF_{10}) in these tumors (same symbols) decreased dramatically in response to oxygen breathing.

TABLE 2
Tumor Growth after Radiation alone or Combined with Oxygen Breathing

	Treatment	No.	V_0 (cm^3) Mean ± SE	T_2 (days) Mean ± SE	Median	T_2 ratio
Small	Control (air)	6	1.2 ± 0.2	7.2 ± 0.7	7	
(<2 cm^3)	30 Gy	5	1.4 ± 0.2	38.8 ± 9.0[a]	28	
	30 Gy + O_2	5	1.7 ± 0.4	36.4 ± 6.7[a]	30	0.9
Large	Control	6	4.3 ± 0.2	16.7 ± 1.3	16	
(>3.5 cm^3)	30 Gy	7	6.7 ± 1.3	30.9 ± 5.5	31	
	30 Gy + O_2	7	7.9 ± 1.3	81.9 ± 14.6[b,c]	77	2.7

Notes. V_0: initial tumor volume; T_2: time to two times V_0.
[a] $P < 0.01$ from control group in the small tumors.
[b] $P < 0.001$ from control group.
[c] $P < 0.01$ from irradiation alone group in the large tumors.

no effect on the T_2, and thus we used baseline pO_2 values for the curve, which strengthened the correlation slightly.

DISCUSSION

In this study, we present data which show that the HI tumor, a moderately well-differentiated tumor, responds to oxygen breathing by increased pO_2 and reduced number of hypoxic voxels (<5 or <10 Torr). These data are in agreement with our earlier data (*19, 20*). As before, we show here that smaller tumors (<2 cm^3) are significantly better oxygenated than larger HI tumors (>3 cm^3), but we now demonstrate that this pattern of oxygenation and modulation of oxygen levels is manifested in the radiation responses. With the small HI tumors, a single dose of 30 Gy caused a significant delay in tumor growth (~30 days for T_2), but breathing oxygen produced no additional benefit. We believe this reflects baseline oxygenation: While breathing oxygen did essentially eliminate the hypoxic fraction, it started at a very low level (~20%), and thus most tumor cells were already sensitive to radiation. By contrast, under baseline conditions, larger HI tumors had a substantial hypoxic fraction (HF_{10} = 80%), which was significantly reduced to 17% by breathing oxygen: This resulted in a significantly longer T_2 of about 50 days in rats breathing O_2 (T_2; Table 2). Meanwhile, irradiation of large tumors while rats breathed air produced no significant growth delay, consistent with the large hypoxic fraction, which would be expected to be radioresistant. It may be particularly significant that radiation was similarly effective in small or large tumors when the HF_{10} < 20%.

Since Gray *et al.* (*25*) demonstrated that hypoxic cells are radioresistant, and noting that solid tumors are often hypoxic (*4*), there have been extensive efforts to increase tumor oxygenation (*5*). Intuitively, one might expect breathing elevated oxygen to improve tumor oxygenation and hence enhance the response to radiation. However, some previous investigations have found little or no therapeutic benefit in animals or in the clinic (*9, 26*). Indeed, a meta-analysis of 83 clinical trials involving over 10,000

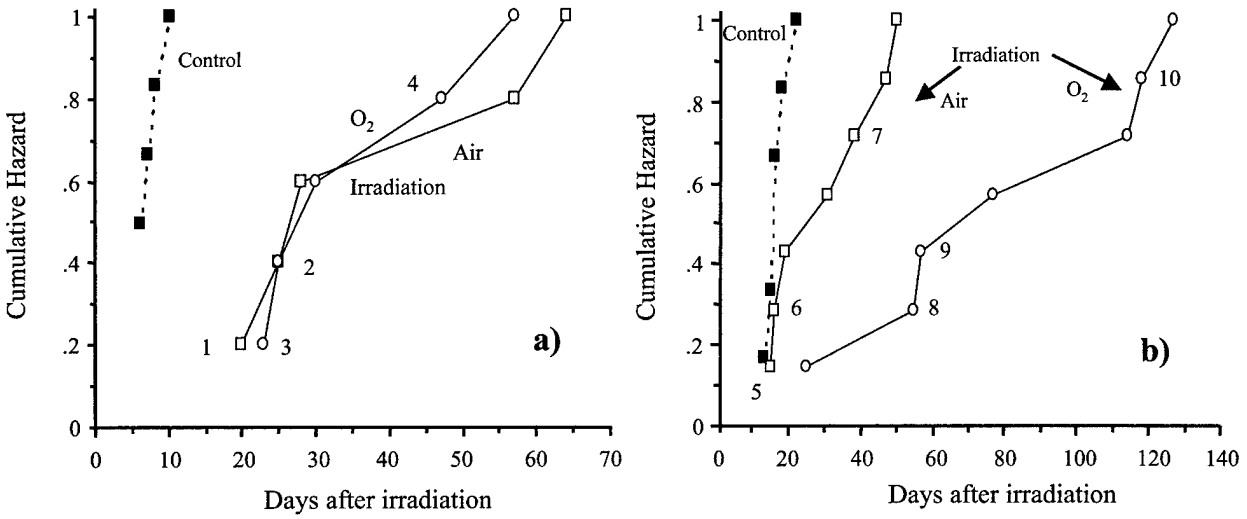

FIG. 5. The Kaplan-Meier hazard plots indicate time required to reach two times the initial size (T_2). Panel a: For small tumors, significant growth delays were observed in irradiated tumors compared to sham-irradiated control tumors ($P < 0.01$), but oxygen breathing did not have an additional beneficial effect. Panel b: By contrast, a significant growth delay (51 days; $P < 0.01$) was observed in large HI tumors when rats breathed oxygen 30 min prior to and during irradiation. The animals are denoted as in Table 1.

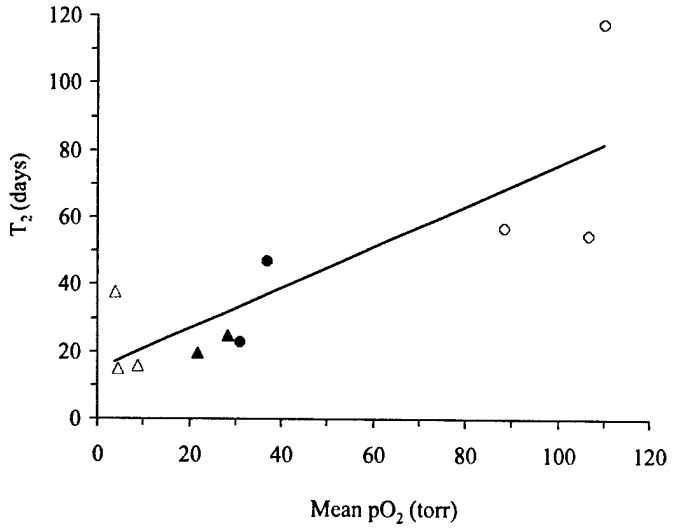

FIG. 6. T_2 as a function of the estimated pO_2 values at time of irradiation showed strong correlation ($R > 0.8$). For the six large tumors (open), baseline pO_2 values were used for the group receiving radiation alone ($n = 3$, triangle), while oxygen-modified pO_2 values were used for the group receiving radiation plus oxygen ($n = 3$, circle). For small tumors (filled), baseline pO_2 values were used for both groups (radiation alone ($n = 2$, triangle) and with oxygen ($n = 2$, circle) because oxygen breathing did not improve radiosensitivity.

patients showed a only modest benefit that was restricted to specific tumor types (*3*). As others have speculated, this marginal effect may have resulted from the inability to identify those patients who would benefit from elevated oxygen. As we have seen, the effect of irradiation of large HI rat tumors was enhanced by oxygen inhalation, but the effect would have been masked in a non-stratified population by the small tumors, which showed no effect. Current application of the Eppendorf histograph provides the capacity to identify hypoxic tumors, and some institutions are incorporating pO_2 measurements into treatment planning. As a consequence, evidence is mounting that tumor oxygenation is a useful prognostic indicator of patient survival and disease-free survival in cervical cancer (*1, 2*) and head and neck cancer (*10–12*). Initial studies also suggest that the level of hypoxia in breast (*27*), prostate (*28*) and brain (*29*) tumors may ultimately have prognostic value. Thus identifying patients with hypoxic tumors is of some importance, but what may be of greater value is to identify those tumors that respond with reduced hypoxia while the patients are breathing oxygen or carbogen.

Generally, pO_2 measurements have been used to assess baseline pO_2 only, but Aquino Parsons *et al.* (*30*) have tested the ability to detect modulation of pO_2 accompanying adjuvant interventions. Repeat histograph investigations of a group of women with cervical cancer demonstrated improved tumor oxygenation when all subjects breathed carbogen (rather than air). Oxygen and carbogen (oxygen mixed with 2.5% or 5% CO_2) were also compared, with as many as three series of measurements made in each tumor, but of necessity, parallel regions were examined because this approach is highly invasive (*30*). In their study, both fractions of CO_2 in the carbogen appeared equally effective. Pure oxygen had little effect on the severely hypoxic fraction, i.e. the fraction of readings <2.5 Torr.

Other studies have shown that the effect of carbogen on radiosensitivity and/or oxygenation appears to be slightly superior to pure oxygen in some tumor types (*31–33*). However, our own previous studies have generally found oxygen and carbogen to have a similar influence on oxygenation of rat prostate tumors irrespective of tumor subline (e.g. Dunning prostate R3327-AT1, HI or MAT-Lu) or size (*18–20*) and agrees well with recent work published by Thews *et al.* (*34*). Thews *et al.* reported no significant differences in oxygenation of an experimental mouse tumor when the animals were breathing 100% O_2 compared to 1, 2.5 or 5% CO_2 plus O_2.

The value of examining dynamic changes is emphasized by reports that efficacy of adjuvant interventions can be influenced by timing, e.g. preirradiation breathing time, and indeed, some studies (*33, 35*) have shown that after an initial increase in pO_2, a zenith is reached, followed by a decline. We created pO_2 maps every 8 min, and over a 40-min breathing time, the mean pO_2 in our HI tumors increased continually and the HF_{10} declined significantly in three of the four tumors ($P < 0.01$; Fig. 4). This finding is in line with our observations using both FREDOM and fiber-optic probes (*19, 20*).

In common with our previous investigations (*19, 20*), we found that the large Dunning prostate R3327 HI tumors were significantly less well oxygenated than smaller ones: Mean and median pO_2 values were lower and the hypoxic fraction was greater (Table 1). The representative tumors used for pO_2 measurement in this study exhibited both baseline pO_2 distributions and responses to oxygen inhalation that were not statistically distinguishable from our earlier observations (*19*). Thus, while both inter- and intratumor heterogeneity were observed, the HI tumors in this study behaved in a consistent manner. This is important, since we measured pO_2 in representative tumors and have assumed that the other experimental tumors in the groups exhibited similar oxygen distributions and dynamics.

As observed previously (*19, 20*), HI tumors show a remarkable response to oxygen inhalation: Even in large tumors, the hypoxic fraction <10 Torr (HF_{10}) decreased rapidly from values greater than 60% to as low as 4% (Fig. 4). To us, this reflects a well-developed vasculature. Indeed, histology showed an extensive vasculature that is well perfused as revealed by the anti-CD31 staining (PECAM) and extensive distribution of Hoechst 33342 dye (Fig. 1). The general histological appearance of the HI tumors is the same as reported by others (*21, 22*).

Others have examined the radiosensitivity of the Dunning prostate sublines H, HI and AT1 (*22, 36*). Peschke *et al.* (*22*) reported that the well-differentiated and less hypoxic H and HI sublines were more sensitive to radiation

than the anaplastic AT1, but they did not examine the influence of tumor size.

Dynamic measurements are particularly valuable for assessing the time course of changes with respect to interventions. Historically, single electrodes were applied (*13*), and more recently multiple locations have been interrogated with fiber-optic probes (*19, 37*). Dynamic studies using EPR have examined a single location within a tumor (*15, 38*), and permanent sensor implants have permitted chronic studies of a single location over hours and days. EPR measurement of pO_2 at a single location has been used to evaluate the time course of increasing hypoxia and of reoxygenation after irradiation of a mouse tumor (*15, 39*). Most significantly, the timing of sequential doses in a two-dose split regimen could be optimized to exploit the observed reoxygenation (*15*).

We showed previously that HFB shows little macroscopic redistribution over a period of hours (*40*). It does clear from the tumors with a typical half-life of HFB of about 10 h, though some tumors show essentially no detectable clearance over a period of 6 h (*41, 42*). Microscopically, Oil Red O (ORO)-labeled HFB appeared as discrete droplets by histological observation (*17*). Clearance of HFB precludes long-term studies of chronic oxygenation unless further doses of HFB are administered. However, it does allow us to examine acute changes with respect to various interventions ranging from respiratory challenge with inhaled gases to vasoactive agents (*43*) and vascular targeting drugs (*44*). Short-term changes in pO_2 after irradiation have also been examined (*45*). Other perfluorocarbon reporter molecules show longer tissue residence, and we previously used perfluorotributylamine to follow chronic changes during tumor growth over a period of weeks (*46*). The perfluorocarbons administered i.v. sequester in the well-perfused regions of the tumor (*47*).

In common with other oximetry approaches, FREDOM involves sampling regions of a tumor, which should be representative of the whole. We showed previously that these data are consistent with the Eppendorf histograph approach (*17*). We aim to sample both central and peripheral tumor regions by administering the HFB in the form of a fan along several tracks across a central plane of the tumor. As seen in Fig. 2, many more voxels give a potential pO_2 value than are used for the analysis. We apply specific thresholding criteria to select only those data points providing a "good" curve fit. Comparison of maps a and d in Fig. 2 shows that the data selected generally correspond to regions of higher signal intensity, which ensures a better signal-to-noise ratio and better data quality, as also demonstrated previously (*48*). Importantly, however, there does not appear to be any correlation between the signal amplitude and the pO_2 values themselves, since that might imply that the HFB acts as an oxygen reservoir. Beyond the data thresholding, we also normally select only those data points that provide consistently high-quality data to ensure that the same voxels are interrogated throughout a series of measurements. Occasionally, an animal (and its tumor) will move slightly during a long time series of measurements. In this case the requirement of consistently high-quality curve fits throughout the data set for individual voxels fails since the tissues have moved relative to the voxel grid. Such motion is immediately apparent when examining the images. There is a choice of eliminating such a data set or relaxing the acceptance criteria. In this study, the motion was seen in only one tumor (no. 8) and the acceptance criteria were relaxed to include the data, based on pO_2 population distribution, rather than absolute spatial continuity. It is important to recognize that all methods of pO_2 measurement include a degree of sampling. In some approaches, this involves the selective placement and tracking of electrodes, in others the choice of locations for biopsy and the number of microscopic fields of view. Sampling can be avoided by obtaining global measurements, as commonly acquired using near infrared approaches, but this may itself mask the fundamental tumor heterogeneity (*49*). Thus we believe that the FREDOM approach, which provides pO_2 measurements at multiple individual locations simultaneously and reproducibly, can be a robust method worthy of further applications.

In view of tumor heterogeneity, the general trend among pO_2 measurements has been toward measuring pO_2 distributions, and the Eppendorf histograph is considered by some to be a gold standard. It is the only technique to have widespread clinical application so far. While it precludes assessment of changes at individual locations within the tumor, strong correlations have been reported between median pO_2 or HF_{10} and surviving fraction based on the clonogenic assay (*50*). We showed previously that pO_2 distributions measured using FREDOM are not dissimilar from those obtained using the histograph (*17*). We believe that FREDOM could offer an enhanced examination in the future, since needle insertion is required only once and acute dynamic studies can be conducted at multiple individual locations simultaneously. We do, however, recognize that access to clinical ^{19}F MRI is presently limited and costly.

Fyles *et al.* (*2*) showed that hypoxia in small cervical cancers had little impact on outcome, while it was highly significant for large tumors. More recently, they also reported that the finding is pertinent only to node-negative patients (*51*). Thus it is reasonable to search for additional prognostic factors other than tumor size (*2*), and recent reports suggest that in certain cases lactate concentration (*52*), apoptosis (*53*), microvascular density (*24*), expression of proteins such as HIF-1 (*54*), or carbonic anhydrase (CA IX) (*55*) could provide additional stratification. Our differentiation of small and large tumors based on the response to respiratory intervention agrees with the report of Fyles *et al.* (*2*), but we are seeking additional parameters to stratify tumors.

Since human prostate cancer can have a high hypoxic fraction (*28*), the ability to monitor changes in pO_2 could have important implications in therapeutic strategies. In

particular, radiotherapy could benefit from intensity-modulated treatment based on regional variation in pO_2.

We have found that changes in pO_2 coincide with modulation of therapeutic efficacy. An alternative explanation could simply note that "large" tumors responded, whereas smaller ones did not, and indeed, several studies have shown that tumor size is a strong prognostic indicator in the clinic. In this tumor type, as we have shown in several other tumor types, small tumors tend to be well oxygenated, while larger tumors are relatively hypoxic. Thus we have not been able to test small baseline hypoxic tumors or well-oxygenated large ones. It will ultimately be important to explore other tumor types in which pO_2 and tumor size are not related. However, Fig. 6 does show a strong correlation irrespective of size between mean pO_2 and growth delay after irradiation, and thus we believe that pO_2 is an important parameter predicting therapeutic outcome.

In conclusion, our results suggest that the ability to detect modulation of tumor pO_2, in particular, the residual hypoxic fraction, with respect to an intervention, could have prognostic value for improving the efficacy of radiotherapy. If the findings we present here are confirmed in prostate cancer patients, it would suggest the therapeutic value of monitoring tumor baseline and dynamic pO_2. Tumors like the HI can be modulated and might be expected to show improved response to radiotherapy with oxygen or carbogen inhalation prior to therapy. These results further demonstrate the value of FREDOM as a prognostic tool to assess *in vivo* dynamic changes in regional pO_2. We hope our new data showing the predictive value of FREDOM with respect to dynamic measurements provides an impetus to develop this technique further, e.g. to examine its usefulness in more diverse tumor types, encourage evaluation in other laboratories, and translate measurements to clinical settings.

ACKNOWLEDGMENTS

We are grateful to Drs. Mark Jeffrey and Matthew Merritt for maintaining the MR system, Dr. Kenneth Gall for radiotherapy, Dr. Sophia Ran for valuable advice regarding histology, Lan Jiang for assistance with data analysis, and Drs. Peter Peschke (DKFZ, Heidelberg) and Peter Antich for ongoing collegial support. This research was supported in part by NCI R01 79515 and DOD Prostate Cancer Initiative Postdoctoral Award (DAMD 170110108) (DZ).

Received: June 7, 2002; accepted: January 6, 2003

REFERENCES

1. M. Höckel, K. Schlenger, B. Aral, M. Mitze, U. Schäffer and P. Vaupel, Association between tumor hypoxia and malignant progression in advanced cancer of the uterine cervix. *Cancer Res.* **56**, 4509–4515 (1996).
2. A. W. Fyles, M. Milosevic, R. Wong, M.-C. Kavanagh, M. Pintile, A. Sun, W. Chapman, W. Levin, L. Manchul and R. P. Hill, Oxygenation predicts radiation response and survival in patients with cervix cancer. *Radiother. Oncol.* **48**, 149–156 (1998).
3. J. Overgaard and M. R. Horsman, Modification of hypoxia-induced radioresistance in tumors by the use of oxygen and sensitizers. *Semin. Radiat. Oncol.* **6**, 10–21 (1996).
4. J. M. Brown, The hypoxic cell: A target for selective cancer therapy. *Cancer Res.* **59**, 5863–5870 (1999).
5. M. Höckel and P. Vaupel, Tumor hypoxia: Definitions and current clinical, biologic, and molecular aspects. *J. Natl. Cancer Inst.* **93**, 266–276 (2001).
6. P. Vaupel, D. K. Kelleher and O. Thews, Modulation of tumor oxygenation. *Int. J. Radiat. Oncol. Biol. Phys.* **42**, 843–848 (1998).
7. A. Rojas, V. K. Hirst, A. S. Calvert and H. J. Johns, Carbogen and nicotinamide as radiosensitizers in a murine mammary carcinoma using conventional and accelerated radiotherapy. *Int. J. Radiat. Oncol. Biol. Phys.* **3**, 357–365 (1996).
8. J. H. A. M. Kaanders, L. A. M. Pop, H. A. M. Marres, I. Bruaset, F. J. A. van den Hoogen, M. A. W. Merkx and A. J. van der Kogel, ARCON: Experience in 215 patients with advanced head-and neck cancer. *Int. J. Radiat. Oncol. Biol. Phys.* **52**, 769–778 (2002).
9. P. Rubin, J. Hanley, H. M. Keys, V. Marcial and L. Brady, Carbogen breathing during radiation therapy: The Radiation Therapy Oncology Group study. *Int. J. Radiat. Oncol. Biol. Phys.* **5**, 1963–1970 (1979).
10. D. M. Brizel, G. S. Sibly, L. R. Prosnitz, R. L. Scher and M. W. Dewhirst, Tumor hypoxia adversely affects the prognosis of carcinoma of the head and neck. *Int. J. Radiat. Oncol. Biol. Phys.* **38**, 285–289 (1997).
11. M. Nordsmark, M. Overgaard and J. Overgaard, Pretreatment oxygenation predicts radiation response in advanced squamous cell carcinoma of head and neck. *Radiother. Oncol.* **41**, 31–39 (1996).
12. V. Rudat, B. Vanselow, P. Wollensack, C. Bettscheider, S. Osman-Ahmet, M. J. Eble and A. Dietz, Repeatability and prognostic impact of the pretreatment pO_2 histography in patients with advanced head and neck cancer. *Radiother. Oncol.* **57**, 31–37 (2000).
13. C. W. Song, I. Lee, T. Hasegawa, J. G. Rhee and S. H. Levitt, Increase in pO_2 and radiosensitivity of tumors by Fluosol and carbogen. *Cancer Res.* **47**, 442–446 (1987).
14. J. Bussink, J. H. A. M. Kaanders, A. M. Strik and A. J. van der Kogel, Effects of nicotinamide and carbogen on oxygenation in human tumor xenografts measured with luminescence based fiberoptic probes. *Radiother. Oncol.* **57**, 21–30 (2000).
15. J. A. O'Hara, F. Goda, E. Demidenko and H. M. Swartz, Effect on regrowth delay in a murine tumor of scheduling split-dose irradiation based on direct pO_2 measurements by electron paramagnetic resonance oximetry. *Radiat. Res.* **150**, 549–556 (1998).
16. S. P. Robinson, F. A. Howe, L. M. Rodrigues, M. Stubbs and J. R. Griffiths, Magnetic resonance imaging techniques for monitoring changes in tumor oxygenation and blood flow. *Semin. Radiat. Oncol.* **8**, 198–207 (1998).
17. R. P. Mason, A. Constantinescu, S. Hunjan, D. Le, E. W. Hahn, P. P. Antich, C. Blum and P. Peschke, Regional tumor oxygenation and measurement of dynamic changes. *Radiat. Res.* **152**, 239–249 (1999).
18. S. Hunjan, D. Zhao, A. Constantinescu, E. W. Hahn, P. P. Antich and R. P. Mason, Tumor oximetry: Demonstration of an enhanced dynamic mapping procedure using fluorine-19 echo planar magnetic resonance imaging in the Dunning prostate R3327-AT1 rat tumor. *Int. J. Radiat. Oncol. Biol. Phys.* **49**, 1097–1108 (2001).
19. D. Zhao, A. Constantinescu, E. W. Hahn and R. P. Mason, Tumor oxygen dynamics with respect to growth and respiratory challenge: Investigation of the Dunning prostate R3327-HI tumor. *Radiat. Res.* **156**, 510–520 (2001).
20. D. Zhao, A. Constantinescu, E. W. Hahn and R. P. Mason, Differential oxygen dynamics in two diverse Dunning prostate R3327 rat tumor sublines (MAT-Lu and HI) with respect to growth and respiratory challenge. *Int. J. Radiat. Oncol. Biol. Phys.* **53**, 744–756 (2002).
21. J. Isaacs, W. Isaacs, W. Feitz and J. Scheres, Establishment and characterization of 7 Dunning prostate cancer cell lines and their use in developing methods for predicting metastatic ability of prostate cancer. *Prostate* **9**, 261–281 (1986).
22. P. Peschke, E. W. Hahn, F. Wenz, F. Lohr, F. Braunschweig, G. Wolber, I. Zuna and M. Wannenmacher, Differential sensitivity of three sublines of the rat Dunning prostate tumor system R3327 to radiation and/or local tumor hyperthermia. *Radiat. Res.* **150**, 423–430 (1998).

23. E. W. Hahn, P. Peschke, R. P. Mason, E. E. Babcock and P. P. Antich, Isolated tumor growth in a surgically formed skin pedicle in the rat: A new tumor model for NMR studies. *Magn. Reson. Imaging* **11**, 1007–1017 (1993).
24. N. Weidner, J. Folkman, F. Pozza, P. Bevilacqua, E. N. Allred and D. H. Moore, Tumor angiogenesis: A new significant and independent prognostic indicator in early-stage breast carcinoma. *J. Natl. Cancer Inst.* **84**, 1875–1887 (1992).
25. L. H. Gray, A. Conger, M. Ebert, S. Hornsey and O. Scott, The concentration of oxygen dissolved in tissues at time of irradiation as a factor in radiotherapy. *Br. J. Radiol.* **26**, 638–648 (1953).
26. G. Stuben, M. Stuschke, K. Knuhmann, M. R. Horsman and H. Sack, The effect of combined nicotinamide and carbogen treatments in human tumor xenografts: Oxygenation and tumor control studies. *Radiother. Oncol.* **48**, 143–148 (1998).
27. P. Okunieff, M. Höckel, E. P. Dunphy and P. W. Vaupel, Oxygen tension distributions are sufficient to explain the local response of human breast tumors treated with radiation alone. *Int. J. Radiat. Oncol. Biol. Phys.* **26**, 631–636 (1993).
28. B. Movsas, J. Chapman, E. Horwitz, W. Pinover, R. Greenberg, A. Hanlon, R. Iyer and G. Hanks, Hypoxic regions exist in human prostate carcinoma. *Urology* **53**, 11–18 (1999).
29. R. Rampling, G. Cruickshank, A. D. Lewis, S. A. Fitzsimmons and P. Workman, Direct measurement of pO_2 distribution and bioreductive enzymes in human malignant brain tumors. *Int. J. Radiat. Oncol. Biol. Phys.* **29**, 427–431 (1994).
30. C. Aquino-Parsons, A. Green and A. I. Minchinton, Oxygen tension in primary gynaecological tumours: The influence of carbon dioxide concentration. *Radiother. Oncol.* **57**, 45–51 (2000).
31. J. L. Lanzen, R. D. Braun, A. L. Ong and M. W. Dewhirst, Variability in blood flow and pO_2 in tumors in response to carbogen breathing. *Int. J. Radiat. Oncol. Biol. Phys.* **42**, 855–859 (1998).
32. B. J. P. van der Sanden, A. Heerschap, L. Hoofd, A. W. Simonetti, K. Nicolay, A. van der Toorn, W. N. M. Colier and A. J. van der Kogel, Effect of carbogen breathing on the physiological profile of human glioma xenografts. *Magn. Reson. Med.* **42**, 490–499 (1999).
33. H. D. Suit, N. Marshall and D. Woerner, Oxygen, oxygen plus carbon dioxide, and radiation therapy of a mouse mammary carcinoma. *Cancer* **30**, 1154–1158 (1972).
34. O. Thews, D. K. Kelleher and P. Vaupel, Dynamics of tumor oxygenation and red blood cell flux in response to inspiratory hyperoxia combined with different levels of inspiratory hypercapnia. *Radiother. Oncol.* **62**, 77–85 (2002).
35. S. Falk, R. Ward and N. Bleehen, The influence of carbogen breathing on tumor tissue oxygenation in man evaluated by computerized pO_2 histography. *Br. J. Cancer* **66**, 919–924 (1992).
36. C. Thorndyke, B. Meeker, G. Thomas, W. Laky, M. McPhee and J. Chapman, The radiation sensitivities of R3327-H and -AT1 rat prostate adenocarcinomas. *J. Urol.* **134**, 191–198 (1985).
37. J. Bussink, J. H. A. M. Kaanders, A. M. Strik, B. Vojnovic and A. J. van der Kogel, Optical sensor-based oxygen tension measurements correspond with hypoxia marker binding in three human tumor xenograft lines. *Radiat. Res.* **154**, 547–555 (2000).
38. B. Gallez, B. F. Jordan, C. Baudelet and P. D. Mission, Pharmacological modification of the partial pressure of oxygen in the murine tumors: Evaluation using *in vivo* EPR oximetry. *Magn. Reson. Med.* **42**, 627–630 (1999).
39. J. A. O'Hara, R. D. Blumenthal, O. Y. Grinberg, E. Demidenko, S. Grinberg, C. M. Wilmot, A. M. Taylor, D. M. Goldenberg and H. M. Swartz, Response to radioimmunotherapy correlates with tumor pO_2 measured by EPR oximetry in human tumor xenografts. *Radiat. Res.* **155**, 466–473 (2001).
40. D. Le, R. P. Mason, S. Hunjan, A. Constantinescu, B. R. Barker and P. P. Antich, Regional tumor oxygen dynamics: ^{19}F PBSR EPI of hexafluorobenzene. *Magn. Reson. Imaging* **15**, 971–981 (1997).
41. R. P. Mason, W. Rodbumrung and P. P. Antich, Hexafluorobenzene: A sensitive ^{19}F NMR indicator of tumor oxygenation. *NMR Biomed.* **9**, 125–134 (1996).
42. S. Hunjan, R. P. Mason, A. Constantinescu, P. Peschke, E. W. Hahn and P. P. Antich, Regional tumor oximetry: ^{19}F NMR spectroscopy of hexafluorobenzene. *Int. J. Radiat. Oncol. Biol. Phys.* **40**, 161–171 (1998).
43. D. Zhao, A. Constantinescu, L. Jiang, E. W. Hahn and R. P. Mason, Prognostic radiology: Quantitative assessment of tumor oxygen dynamics by MRI. *Am. J. Clin. Oncol.* **24**, 462–466 (2001).
44. R. P. Mason, S. Ran and P. E. Thorpe, Quantitative assessment of tumor oxygen dynamics: Molecular imaging for prognostic radiology. *J. Cell. Biochem.* **87**, 45–53 (2002).
45. R. P. Mason, S. Hunjan, D. Le, C. Constantinescu, B. R. Barker, P. S. Wong, P. Peschke, E. W. Hahn and P. P. Antich, Regional tumor oxygen tension: Fluorine echo planar imaging of hexafluorobenzene reveals heterogeneity of dynamics. *Int. J. Radiat. Oncol. Biol. Phys.* **42**, 747–750 (1998).
46. R. P. Mason, P. P. Antich, E. E. Babcock, A. Constantinescu, P. Peschke and E. W. Hahn, Noninvasive determination of tumor oxygen tension and local variation with growth. *Int. J. Radiat. Oncol. Biol. Phys.* **29**, 95–103 (1994).
47. D. J. O. McIntyre, C. L. McCoy and J. R. Griffiths, Tumor oxygenation measurements by ^{19}F MRI of perfluorocarbons. *Curr. Sci.* **76**, 753–762 (1999).
48. B. R. Barker, R. P. Mason, N. Bansal and R. M. Peshock, Oxygen tension mapping by ^{19}F echo planar NMR imaging of sequestered perfluorocarbon. *J. Magn. Reson. Imaging* **4**, 595–602 (1994).
49. H. Liu, Y. Song, K. L. Worden, X. Jiang, A. Constantinescu and R. P. Mason, Noninvasive investigation of blood oxygenation dynamics of tumors by near-infrared spectroscopy. *Appl. Optic* **39**, 5231–5243 (2000).
50. D. W. Siemann, I. M. Johansen and M. R. Horsman, Radiobiological hypoxia in the KHT sarcoma: Predictions using the Eppendorf histograph. *Int. J. Radiat. Oncol. Biol. Phys.* **40**, 1171–1176 (1998).
51. A. Fyles, M. Milosevic, M. Hedley, M. Pintile, W. Levin, L. Manchul and R. P. Hill, Tumor hypoxia has independent predictor impact only on patients with node-negative cervix cancer. *J. Clin. Oncol.* **20**, 680–687 (2002).
52. S. Walenta, M. Wetterling, M. Leherke, G. Schwichert, K. Sundfør, E. K. Rofstad and W. Mueller-Klieser, High lactate levels predicts likelihood of metastasis, tumor regrowth, and patient survival in human cervix cancers. *Cancer Res.* **60**, 916–927 (2000).
53. M. Höckel, K. Schlenger, S. Höckel and P. Vaupel, Hypoxic cervical cancers with low apoptotic index are highly aggressive. *Cancer Res.* **59**, 4525–4528 (1999).
54. H. Zhong, F. Agani, A. A. Baccala, E. Laughner, N. Rioseco-Camacho, W. B. Isaacs, J. W. Simons and G. L. Semenza, Increased expression of hypoxia inducible factor-1 alpha in rat and human prostate cancer. *Cancer Res.* **58**, 5280–5284 (1998).
55. J. A. Loncaster, A. L. Harris, S. E. Davidson, J. P. Logue, R. D. Hunter, C. C. Wycoff, J. Pastorek, R. J. Ratcliffe, I. J. Stratford and C. M. L. West, Carbonic anhydrase (CA IX) expression, a potential new intrinsic marker of hypoxia: Correlation with tumor oxygen measurement and prognosis in locally advanced carcinoma of the cervix. *Cancer Res.* **61**, 6394–6399 (2001).

Tumor oxygen dynamics:

correlation of *in vivo* MRI with histological findings

Dawen Zhao, Sophia Ran[+], Anca Constantinescu, Eric W. Hahn and Ralph P. Mason

Departments of Radiology and [+]Pharmacology, U.T. Southwestern Medical Center, Dallas, TX

Correspondence:
Ralph P. Mason, Ph.D., C. Chem.,
Department of Radiology,
UT Southwestern Medical Center,
5323 Harry Hines Blvd.,
Dallas, TX 75390-9058
Tel: (214) 648-8926
Fax: (214) 648-2991
E-mail: Ralph.Mason@UTSouthwestern.edu

Running title: Oxygen dynamics in prostate tumors

Keywords: ^{19}F nuclear magnetic resonance (NMR), oxygen tension, prostate tumor, immunohistochemistry, hypoxia

Abbreviations: EPI: Echo Planar Imaging; *FREDOM:* Fluorocarbon Relaxometry using Echo planar imaging for Dynamic Oxygen Mapping; HF: Hypoxic Fraction; HFB: Hexafluorobenzene; VDT: Volume Doubling Time

Abstract

Tumor oxygenation has long been recognized as a significant factor influencing cancer therapy. We recently established a novel magnetic resonance *in vivo* approach to measuring regional tumor oxygen tension: *FREDOM* (Fluorocarbon Relaxometry using Echo planar imaging for Dynamic Oxygen Mapping) using hexafluorobenzene, as the reporter molecule. We have now investigated oxygen dynamics in the two Dunning prostate R3327 rat tumor sublines AT1 and H. *FREDOM* revealed considerable intra-tumoral heterogeneity in the distribution of pO_2 values in both sublines. The anaplastic faster growing AT1 tumors were more hypoxic compared with the size-matched well differentiated and slower growing H tumors. Respiratory challenge with oxygen produced significant increases in mean and median pO_2 in all the H tumors ($p<0.001$), but no response in half of the larger AT1 tumors (>3 cm^3). Immunohistochemical studies using the hypoxia marker pimonidazole and the vascular endothelial cell marker CD31 confirmed that the H tumors had more extensive vasculature and less hypoxia than the AT1 tumors. These results further validate the utilization of *FREDOM* to monitor tumor oxygenation and concur with the hypothesis that the level of hypoxia is related to tumor growth rate and poor vascularity.

Introduction

It is well recognized that hypoxia in solid tumors affects response to radiotherapy [1-3] and some chemotherapeutic drugs [4]. Recent evidence, in experimental and clinical studies, indicates that tumor hypoxia might also be a mechanism for malignant progression and metastasis in solid tumors [5,6]. Given the importance of oxygen, many techniques for monitoring pO_2 have been developed [7]. While each method has specific attributes, many are highly invasive, and impractical for longitudinal studies of specific regions of interest.

We recently demonstrated the feasibility of measuring tumor oxygenation based on ^{19}F NMR echo planar imaging (EPI) following direct intratumoral injection of the reporter molecule hexafluorobenzene (HFB): *FREDOM* (Fluorocarbon Relaxometry using Echo planar imaging for Dynamic Oxygen Mapping) [8]. This technique allows us to not only simultaneously examine multiple specific locations within a tumor, but also observe dynamic changes at individual locations with respect to intervention. Our previous studies of Dunning R3327 prostate rat tumor sublines have demonstrated that the faster growing metastatic MAT-Lu tumors were more hypoxic than the relatively well differentiated and slower growing HI tumors [9]. In order to further investigate the potential correlation between hypoxia and tumor malignant progression, we have now studied and compared tumor oxygen tension dynamics in two other Dunning prostate rat tumor sublines: the well differentiated slower growing H and the anaplastic fast growing AT1, which derives originally from the course of passage of the H [10].

There is a close relationship between hypoxia and vascular extent in solid tumors, and it is widely accepted that tumor hypoxia results in part from poor vascularity [11]. Immunohistochemistry based on bioreductive chemical markers and vascular endothelial cell markers can reveal spatial patterns of tumor hypoxia and vasculature, as well as their relationship

at the cellular level [12-14]. We have now compared direct pO_2 measurements using *FREDOM* with histological investigations of hypoxia and vasculature using pimonidazole and anti-CD31 antibody and show that the macroscopic dynamic imaging is consistent with the histological microstructure.

Methods

Experiments were approved by the Institutional Animal Care and Research Advisory Committee.

Tumor Model

Two sublines of the Dunning prostate R3327 adenocarcinoma were selected: H, a well differentiated, slow growing tumor with volume doubling time (VDT) of 16 days [15], and AT1, an anaplastic, faster growing subline with VDT of 5 days [10]. Tumors were originally obtained from Dr. J. T. Isaacs (Johns Hopkins, Baltimore) and provided to us by Dr. P. Peschke (DKFZ, Heidelberg, Germany). Tumors were implanted in a skin pedicle surgically created on the foreback of adult male Copenhagen-2331 rats (~250 g, Harlan), as described in detail previously [16]. Tumors were allowed to grow and investigated by MRI when about 1 cm^3 or when greater than 3 cm^3 (~10 mm or > 20 mm diameter). Twelve H tumors, including six small (size range 0.6 ~ 1.5 cm^3) and six large (range 3.0 ~ 4.6 cm^3), and thirteen AT1 tumors, including seven small (range 0.7 ~ 1.8 cm^3) and six large (range 3.0 ~ 5.2 cm^3) were investigated. In preparation for MRI, each rat was given ketamine hydrochloride (200 µl; 100 mg/ml, Aveco, Fort Dodge, IA) as a relaxant (i.p.) and maintained under general gaseous anesthesia [1 dm^3/min air and 1.3% isoflurane (Baxter International Inc., Deerfield, IL)]. Hexafluorobenzene (50 µl, Lancaster, Gainesville, FL), was deoxygenated by bubbling nitrogen for 5 mins before use, and injected directly into the tumors using a Hamilton syringe (Reno, NV) with a custom-made fine sharp

needle (32G), as described in detail previously [9]. Generally, HFB was administered along three tracks in the form of a fan in a single central plane of the tumor coronal to the rat's body. The needle was inserted manually to penetrate across the whole tumor and withdrawn ~1 mm to reduce pressure, and 3 µl HFB was deposited. The needle was repeatedly withdrawn a further 2-3 mm and additional HFB was deposited. Typically, HFB was deliberately deposited at about 16 individual locations per tumor, in both the central and peripheral regions of the tumors to ensure that the interrogated regions would be representative of the whole tumor. Each animal was placed on its side in a cradle with a thermal blanket to maintain body temperature.

Tumor Oximetry - FREDOM

Magnetic resonance experiments were performed using an Omega CSI 4.7 horizontal bore magnet system with actively shielded gradients (Bruker Instrument Inc., Fremont, CA). A tunable ($^{1}H/^{19}F$) MR coil, 2 or 3 cm in diameter matched to the tumor size (constructed from a cylindrical copper tube about 2 cm deep and acting as a single turn solenoid) was placed around the tumor-bearing pedicle. Proton images were obtained for anatomical reference using a three-dimensional (3D) spin-echo sequence. The coil was then retuned in place to 188.27 MHz, and corresponding ^{19}F MR images were obtained. Overlaying the ^{19}F MR images on the corresponding proton images revealed the distribution of HFB.

Following conventional MR imaging, tumor oxygenation was estimated on the basis of ^{19}F pulse burst saturation recovery (PBSR) EPI relaxometry of the HFB, as described previously [8]. The *ARDVARC* (Alternated R1 Delays with Variable Acquisitions to Reduce Clearance effects) data acquisition protocol was applied to optimize data quality. This approach provided pO_2 maps with 1.25 mm in plane voxel resolution in 8 minutes with typically ~50-150 individual pO_2 measurements (voxels per tumor). The spin-lattice relaxation rate [R1 (s^{-1}) = 1/T1] was

estimated on a voxel-by-voxel basis using a three-parameter monoexponential function, and pO_2 was estimated using the relationship pO_2 (torr) = (R1 – 0.0835)/0.001876 [8]. Three consecutive baseline pO_2 measurements were made over 24 minutes, while the rats breathed air. The inhaled gas was then altered to oxygen (100% O_2) and pO_2 maps were immediately acquired with no equilibration period. Five consecutive maps were acquired over 40 mins. The gas was then returned to air, and five further maps were acquired over 40 mins.

Histology

Histological studies were performed on large AT1 and H tumors.

Necrosis

For H&E staining, tumor tissues were fixed in 10% formalin, embedded in paraffin and sectioned (4 μm). Tumor necrotic regions were identified on the H&E stained slides examined under low magnification (2X objective). All fields (~30) in each section were captured by a digital camera and processed using Metaview software (Universal Imaging Corporation, West Chester, PA). Fields were calibrated according to magnification, areas occupied by necrotic cells were outlined, calculated and expressed in mm^2. The area of the entire cross-section was determined manually. The proportion of necrotic areas (% necrosis) was calculated as follows: sum of all necrotic areas in a single cross-section divided by total area of cross-section and multiplied by 100. Five slides representing each tumor type were analyzed and the percentage of necrosis was calculated and averaged for each tumor.

Immunohistochemical detection of hypoxia

Pimonidazole hydrochloride (Hypoxyprobe™-1, NPI, Inc., Belmont, MA) was injected into the tail vein at a dose of 60 mg/kg. Ninety min later, rats were anesthetized and then perfused for 20 min with physiological saline containing 5 mM $CaCl_2$. For immunohistochemistry, the tissues

were immediately immersed in liquid nitrogen and stored at -80 °C. After cryostat sectioning (6 μm thick), tumor sections were fixed in acetone for 5 min and then re-hydrated in phosphate buffer saline containing 0.1% Tween-20 (PBST) for 10 min. Monoclonal antibody Mab1 (NPI, Inc., Belmont, MA) that detects pimonidazole-protein adducts was diluted 1:100 and added to frozen sections followed by incubation for 2 hr at 37 °C. Slides were then incubated for 1 hr at 37 °C with horseradish peroxidase (HRP)- conjugated goat anti mouse secondary antibody (1: 100 dilution; Serotec, Raleigh, NC). After a PBST wash, sections were immersed in AEC substrate (3-amino-9-ethylcarbazole, Vector Laboratories, Inc., Burlingame, CA) for 15 min at room temperature. Finally, sections were counterstained with hematoxylin and observed under light microscopy. Hypoxic fraction was determined as area positively stained for pimonidazole relative to the total tissue area using Metaview software.

Blood Vessel Density

Mouse anti rat CD31 monoclonal antibody (1:20; Serotec, Raleigh, NC) and HRP- conjugated goat anti mouse secondary antibody (1:100) were used to detect tumor blood vessels on 6 μm sections immediately adjacent to those used for detection of hypoxia. Vascular density was evaluated using the 'hot spot' technique described by Weidner *et al.* [17]. The five most vascularized areas in each tumor were selected under low magnification (4×). Vascular density was determined by counting the total number of structures positive for CD31 using 10X objective (area 0.318 mm^2) and calculating the mean number of vessels per mm^2.

Statistical Analysis

The statistical significance of changes in oxygenation was assessed using an Analysis of Variance (ANOVA) on the basis of Fisher's Protected Least Significant Difference (PLSD; Statview, SAS Inst. Inc., Cary, NC). Where appropriate, the Student's t-test was applied. Hypoxic

fractions ($HF_{2.5;\ 5;\ 10}$ < 2.5; 5; 10 torr) measured by *FREDOM* in all the tumors were calculated from the fraction of hypoxic voxels in each pO_2 map. All data are quoted ± s.e.

Results

Tumor Oximetry - FREDOM

Overlay of ^{19}F on ^{1}H images (not shown) confirmed that HFB was widely distributed, predominantly in a central slice and occupied voxels representing 5 to 10% of the whole tumor. In the series of EPI relaxation data sets, typically ~50-300 voxels provided an R1 fit, and potential pO_2 value. Since even noise may give an apparent relaxation curve (R1) fit, data were selected within a region of interest, and having T1 error < 2.5 s and ratio T1 error/T1 < 50%. With respect to respiratory interventions, only those voxels, which provided consistently reliable data during the time course, were included for further analysis. The number of such acceptable voxels ranged from 11 to 74 per tumor. Figure 1 shows typical pO_2 maps of the selected regions obtained from representative small H and AT1 tumors under baseline air breathing and during oxygen challenge. During air breathing, both tumors exhibited extensive heterogeneity in pO_2 distribution, but the H tumor was better oxygenated than the AT1 tumor ($p<0.001$). Upon switching to oxygen breathing, both tumors responded with significantly increased mean pO_2 ($p<0.001$).

Data for small and large tumors in the H and AT1 sublines are pooled as histograms in Figs. 2 and 3, respectively. For the H tumors (Fig. 2), a total of 219 voxels from the six small H tumors were pooled and gave a mean baseline pO_2 = 31 ± 2 torr (median = 27 torr), which was significantly greater ($p<0.001$) than for the six larger H tumors (159 voxels), which had a value of 14 ± 1 torr (median = 12 torr). For the AT1 subline (Fig. 3), the seven small tumors (280

voxels) had a mean pO_2 of 14 ± 1 torr (median = 11 torr), which was significantly greater ($p<0.001$), compared to the six large AT1 tumors (149 voxels; mean = 4 ± 1 torr, median = 3 torr). Comparison of the pooled mean baseline pO_2 between the two sublines showed that both the small and large groups of AT1 tumors had significantly lower mean pO_2 than the size-matched H groups ($p<0.001$). Oxygen breathing produced significant increase in mean pO_2 in all the tumor groups ($p<0.001$). However, hypoxic fractions ($pO_2 < 2.5$ torr; $2.5 < pO_2 < 5$ torr; $5 < pO_2 < 10$ torr) behaved differently between the H and AT1 tumors. Specifically, for the larger tumors, the hypoxic fractions of all the ranges in the H tumors (18%; 8%; 18%) decreased dramatically to less than 5%, whereas no distinct changes were observed in the large AT1 tumors (Figs. 2 and 3).

Uniquely, *FREDOM* allows the oxygen dynamics at multiple individual locations to be followed non-invasively and simultaneously, specifically revealing the fate of initially hypoxic regions. Voxels with initial $pO_2 < 10$ torr through all the three baseline measurements were followed with respect to respiratory challenge for both H (92 voxels) and AT1 (248 voxels) sublines (Figs. 4a and 4b). Fig. 4a shows that oxygen breathing produced a significant increase in mean pO_2 for these initially hypoxic regions in both the H (mean baseline $pO_2 = 3.9 \pm 0.4$ torr; maximum pO_2 observed with oxygen = 54.7 ± 4.6 torr) and the AT1 (mean baseline $pO_2 = 1.2 \pm 0.1$ torr; maximum $pO_2 = 17.9 \pm 2.3$ torr) tumors ($p<0.01$). However, comparison of the median pO_2 for these voxels showed a dramatic increase in the H tumors (baseline $pO_2 = 4.1$ torr to maximum $pO_2 = 46.2$ torr), versus only a small increase in the corresponding regions of the AT1 tumors (baseline $pO_2 = 1.5$ torr to maximum $pO_2 = 5.3$ torr). We also examined these hypoxic voxels grouped as having baseline $pO_2 < 5$ torr or in the range 5 to 10 torr. For the AT1 tumors, both subsets behaved equivalently and in line with the trace shown in Fig. 4a. For the H tumors,

each subset showed a significant increase, but the pO_2 achieved was significantly higher for those voxels, which started in the 5-10 torr group. Moreover, figure 4b shows that about 90% initially hypoxic regions became well oxygenated with oxygen breathing in the H tumors, whereas > 60% of the hypoxic regions in the AT1 tumors remained. Hypoxic regions in the groups of small and large AT1 tumors did not behave significantly differently ($p>0.3$).

pO_2 data were also compared on the basis of differences between individual tumors, as shown in Table 1. As with the pooled data, for both the H and AT1 tumors, the large tumors were significantly more hypoxic than the smaller tumors, and the AT1 tumors were significantly less well oxygenated than the size-matched H tumors ($p<0.05$; Tables 1 and 2). With respect to oxygen challenge, all the tumors in the H subline and the small AT1s showed significant increases in global mean pO_2 ($p<0.001$), while three of the six larger AT1 tumors did not respond to oxygen. The mean and median pO_2 increased, and the $HF_{5\ or\ 10}$ decreased significantly in the H and the small AT1 tumors with oxygen inhalation ($p<0.05$; Table 1). Mean pO_2 of the group of six large tumors did increase, but only reached a $p<0.1$ level of significance.

Immunohistochemistry

AT1 tumors were significantly more hypoxic than the H tumors of comparable size (Fig. 5 and Table 2). The positive staining for pimonidazole in the AT1 tumors was primarily detected in tumor cells located in perinecrotic regions and more than 100 μm away from blood vessels, which were recognized by the anti CD31 antibody (Fig. 5C and D). The total number of vessels per mm^2 was 139± 30 (range 88 to 227) in the better oxygenated H tumors, which was significantly higher than for the more hypoxic AT1 tumors (45± 13/mm^2, range 28 to 71; $p<0.05$; Fig. 5 and Table 2). This difference in vascularity also coincided with the greater necrotic fraction: about 7% area in the AT1 tumors compared with only 2% in the H tumors (Table 2).

Discussion

The anaplastic and faster growing AT1 tumors were significantly more hypoxic than the well differentiated and slower growing H tumors from which they were originally derived. These results are consistent with previous reports comparing oxygenation and radiation sensitivity of the AT and H sublines. Based on electrode polarographic pO_2 measurements, the H subline was found to be considerably less hypoxic [18]. This coincided with ^{31}P NMR showing greater phosphocreatine and less inorganic phosphate (Pi) in H tumors [19]. Moreover, radiation sensitivity of AT, but not H tumors could be enhanced by misonidazole [20], suggesting a lack of hypoxia in the H tumors. We have ourselves examined AT1 tumors previously during development of the ^{19}F MRI oximetry technique [8,21]. The mean and median pO_2 values reported now and previously are remarkably similar, together with distribution histograms and hypoxic fractions. In all cases, we have found that larger tumors are significantly less well oxygenated than small tumors, and indeed, this was also observed in other Dunning prostate R3327 tumors sublines (MAT-Lu and HI) [9,22] and rat breast tumors [23]. Yeh *et al.* [18] found no such correlation with size for either subline based on electrode oximetry, but ^{31}P NMR did show metabolic hypoxiation in larger AT tumors [19]. Inter laboratory comparison must recognize differences in techniques and procedures. The histology of our tumors is very similar to that of Chapman *et al.* [18,20] and growth of the H tumors is comparable. However, we work with the AT1 subline [10], as opposed to the AT, and we find a volume doubling time of 5 days as opposed to 2 or 3 days [20]. In comparing our own previous data, we have now altered our anesthesia protocol to a baseline of air/isoflurane as opposed to 33% oxygen in nitrous oxide with metafane [8,21]. Nonetheless, the pO_2 distributions appear very similar.

In addition to providing tumor baseline pO_2, the *FREDOM* technique allows the study of oxygen dynamics in response to interventions, *e.g.*, respiratory challenge. Our results show that oxygen breathing produced significant increase in mean pO_2 in all the H tumors and the small AT1 tumors, while the change was only borderline significant in the larger AT1 tumors (Table 1). Most interestingly, the initially hypoxic regions in the H tumors responded significantly to become well oxygenated with oxygen challenge, whereas no distinct reduction in hypoxic fractions was observed in the large AT1 tumors (Table 1 and Fig. 4a and b). The AT1 tumor data coincides with our previous observations in this subline [21].

There is increasing evidence that tumor malignant progression may be associated with a hypoxic microenvironment [5,6,24]. Several recent clinical studies have demonstrated a positive relationship between the presence of hypoxia and poor outcome associated with malignant progression and metastasis in several cancers, *e.g.*, advanced squamous cell carcinoma of the cervix [3,25,26], and sarcomas and carcinomas from head, neck and soft tissue [27]. Studies of breast cancer have not all been consistent, *e.g.*, early work by Vaupel *et al.* [28] showed no correlation between grade or stage and pO_2 using the Eppendorf Histograph. By contrast, a recent report from Hohenberger *et al.* [29] indicated that mean pO_2 and hypoxic fraction in breast tumors were associated with both grade and stage. The results of Höckel *et al.* [3] in advanced cervical cancer patients showed a lack of correlation between tumor oxygenation and differentiation or stage, but a significantly positive correlation of tumor oxygenation and malignant progression. In an animal model, Thews *et al.* [30] reported that a higher differentiated rhabdomyosarcoma subline F1 of the BA-HAN-1 was less well oxygenated than the undifferentiated G8 subline. While Thew's results show the opposite trend to the observations we report here, it is important to note that the F1 and G8 tumors each grow relatively rapidly. In our

studies the higher differentiated tumors grow much more slowly. Several other studies have shown evidence that tumor malignant progression, *e.g.*, local invasion, destructive growth and metastasis, may be associated with hypoxic microenvironment in both experimental models [5,24,31,32] and the clinic [25,26,33]. A recent study by Movsas *et al.* [34] using the Eppendorf Histograph showed that increasing levels of hypoxia were related to increasing clinical stage of human prostate carcinomas, but trends with respect to grade did not reach significance. Eble *et al.* [35] found that the moderately well differentiated Dunning rat prostate HI subline was better oxygenated than the anaplastic AT1 subline and Yeh *et al.* [18] found that the well differentiated H subline was better oxygenated than the anaplastic AT. Our previous study of two other Dunning prostate R3327 rat tumor sublines showed that the poorly differentiated, faster growing (VDT = 2.7 days) and metastatic MAT-Lu tumors were less well oxygenated than the moderately differentiated and slower growing (VDT = 9 days) HI tumors. Similar to the results here, breathing hyperoxic gas (oxygen or carbogen) significantly increased the oxygenation and reduced the hypoxic fraction in the HI tumors, but to a much lessor extent in the metastatic MAT-Lu tumors [9]. This would tend to support the hypothesis that tumor hypoxia is associated with parameters such increased growth rate and level of differentiation (grade). As in our previous studies [9,22,23] of various tumor types, tumor size, which is a major component of tumor staging, showed a strongly inverse relationship to oxygenation.

Many experimental and clinical studies have demonstrated that reoxygenation of hypoxic tumor cells contributes to improved radiation sensitivity for tumor therapy [36,37]. Whether initially hypoxic regions of a tumor can be modified to become better oxygenated has long been considered a key indicator for outcome of irradiation. Examining the initially hypoxic regions (pO_2 values < 10 torr) showed that more than 90% of the hypoxic regions in the H tumors

became better oxygenated in response to oxygen breathing. In contrast, about 60% of such regions from the AT1 tumors remained unchanged (Fig. 4b). Thus, one would expect that radiosensitivity of the H tumors might be significantly improved with pretreatment oxygen breathing, whereas beneficial effect in the AT1 tumors would be less. In fact, measurements in HI tumors with respect to our recent experimental radiotherapy have validated the hypothesis. We found that oxygen breathing before and during a 30 Gy single dose irradiation significantly enhanced the radiosensitivity by prolonging the tumor growth delay in large HI tumors [38]. Intriguingly, breathing oxygen had no benefit in small HI tumors coinciding with a very small baseline hypoxic fraction. By analogy, one would expect that patients with hypoxic tumors like the large H and HI would show enhanced local control by irradiation in combination with oxygen breathing. Actually, recent clinical data have shown promising results in advanced head and neck cancers accomplished by accelerated radiotherapy with the carbogen and nicotinamide (ARCON) schedule. The phase II trial demonstrated that the ARCON has significantly improved 3-year local control rates to 80% for larynx, 69% for hypopharynx, 88% for oropharynx cancers [39] and those patients with hypoxic tumors received the greatest benefit from the ARCON paradigm [33].

Comparison of figure 4a and b shows the mean pO_2 in the initially hypoxic regions from both the H and the AT1 tumors continued to increase during the course of 40 min oxygen breathing, while the corresponding hypoxic fraction in both sublines dropped to a minimum value within 24 min and then remained stable. This discrepancy suggests that hypoxic regions may be divided into two categories: those, which are modulated by oxygen within 24 mins and continue to show increase at later times, versus those, which are unresponsive. This information could be valuable for guiding and planning radiotherapy. In our previous studies of the Dunning

prostate rat tumors, we found that oxygen or carbogen breathing produced a similar effect on tumor oxygenation across all the sublines MAT-Lu, AT1, and HI [8,9,21,22,40]. Our irradiation study validated that oxygen breathing significantly improved radiosensitivity in initially hypoxic large HI tumors [38].

Hexafluorobenzene has many strengths as a reporter molecule: MR interrogation is non-destructive, HFB exhibits remarkably low toxicity and is readily available. From an MR perspective HFB is ideal, having a single resonance, high sensitivity to pO_2 and minimal sensitivity to temperature [41]. The high vapor pressure produces a short biological half-life ($T_{1/2}$ ~ 600 mins) [40], but there is little macroscopic redistribution over a period of 2.5 h allowing effective investigations of acute interventions [41]. The Hamilton syringe with a custom-made fine sharp needle (32G) was designed to minimize tissue damage. Our current data, as well as our previous observations, have demonstrated the stability of local pO_2 measurements under baseline conditions. *FREDOM* oximetry has been validated by various techniques in previous studies, *e.g.*, similar baseline pO_2 distribution in the AT1 tumors acquired by Eppendorf Histograph [21] and comparable oxygen dynamics with oxygen or carbogen challenge observed in HI tumors using the fiber-optic OxyLite^{TM} [22] or oxygen electrodes [9].

Tumor oxygenation may be investigated at many levels ranging from induced gene expression, to cellular microscopy and macroscopic techniques. Ultimately, correlation with outcome is relevant to clinical application, as has been demonstrated for measurements using the Eppendorf Histograph [3,26,27] and most recently pimonidazole binding [33]. We have previously shown that pO_2 measurements using *FREDOM* were similar to the Histograph and now we show that hypoxic fractions are commensurate with pimonidazole binding. The anaplastic faster growing AT1 tumors had significantly higher pimonidazole binding (18%) than

the well differentiated slower growing H tumors (5%, $p<0.05$), consistent with the *FREDOM* measurements. However, as shown in Table 2, the hypoxic fractions $HF_{2.5,\ 5,\ and\ 10}$ measured by *FREDOM* for the large AT1 tumors were far greater than the extent of pimonidazole binding. Others have also reported such discrepancies using Histograph or OxyLite™ [12,42]. Histograph assessment of oxygenation does not differentiate hypoxic live tissues from necrotic regions leading to overestimation of tumor hypoxia [43,44]. However, in our tumors the level of necrosis is relatively small, and would not account for the disparity. It has also been suggested that diffusion may limit the distribution of bioreductive hypoxia markers leading to underestimation of tumor hypoxia [45] and, in addition, nitroimidazole binding may be influenced by levels of both nitroreductase and thiol [46]. Furthermore, a pO_2 threshold value for hypoxic marker binding is not clearly defined *in vivo*. There may also be differences in sensitivity to chronic versus acute hypoxia and the time required for efficient pimonidazole labeling. Bennewith *et al.* [47] have now shown significantly greater pimonidazole binding when assessed following 96 h continuous oral availability, as opposed to a single dose *i.v* or *i.p.* followed by tissue harvest after 6 h. Here, we followed the manufacturer's recommendations of a 90 min. delay between *i.v.* administration and sacrifice. Despite the lack of absolute correspondence, a general positive correlation in assessments of tumor hypoxia has been reported between Histograph or OxyLite™ and pimonidazole binding by others [12,44], and now by us, here.

Tumor hypoxia results in part from inadequate blood vessel development and solid tumors appear not grow beyond a critical size of ~1 mm^3 without evoking angiogenesis [48]. Figure 5 shows a typical case of insufficient blood vessels in a region of an AT1 tumor, which results in hypoxia, and eventually necrosis with increased distance away from the vessels. The anti-CD31 staining for vascular endothelial cells showed that the more hypoxic AT1 tumors had lower

vascular density than the better oxygenated H tumors (Table 2). This result is in agreement with other reports in various animal or human tumors indicating greater hypoxia at reduced vascular density[11,44]. However, some studies have shown the opposite trend [17,49], may be because hypoxia stimulates angiogenesis generating greater neovasculature. Here, we have applied histological approaches to assess hypoxia in relation to vascular density. Others have examined additional pertinent parameters including vascular perfusion, *e.g.*, using distribution of the Hoechst 33342 dye [14,38] and even dynamic changes by applying pairs of distinct hypoxia markers (CCI-103F and pimonidazole) sequentially before and after an intervention to reveal dynamic response (pulse chase double labeling) [14]. Specifically, they were able to detect changes in tumor hypoxia following interventions designed to modulate hypoxia such as breathing hyperoxic gas and hydralazine. Ultimately, dynamic studies will be of great importance and the availability and correlation of many diverse techniques revealing tissue and cellular properties on various scales from whole tumor to microscopic resolution will be pertinent.

The *FREDOM* approach to tumor oximetry has the great advantage of facilitating non-invasive assessment of changes in pO_2 in response to interventions, as shown here for breathing hyperoxic gases and previously for vasoactive agents, such as hydralazine [50], or vascular targeting agents [51]. The method is inherently quantitative, but it does require introduction of small quantities (~ 50 µl) of the reporter molecule HFB. Another drawback for potential clinical application, is the current lack of a ^{19}F NMR channel on most clinical MRI scanners. Currently, we estimate at least 20 research instruments in the world have a clinical ^{19}F EPI capability and this will increase dramatically with the popularity of high field systems (*e.g.*, 3 T). Our own institution is installing its first clinical ^{19}F MRI capability in spring 2003 and we envisage

clinical application of the *FREDOM* in the near future. We are currently investigating Investigational New Drug approval for HFB.

We and others are also searching for alternative non-invasive approaches. Near infrared reveals changes in vascular oxygenation with high time resolution, but currently little spatial discrimination [52]. BOLD (Blood Oxygen Level Dependant) contrast ^{1}H MRI provides spatial resolution and is sensitive to changes in vascular oxygenation, but also is sensitive to changes in tumor blood flow and tumor blood volume (FLOOD) [53]. Moreover, correlation between changes in signal intensity and direct measures of pO_2 have shown a qualitative relationship, but poor indication of absolute pO_2 [54,55]. In some cases correlation has been shown between pO_2 and DCE (Dynamic Contrast Enhanced) ^{1}H MRI [56,57], but while DCE can reveal changes in vascular flow and permeability, it must be recognized that tissue pO_2 represents a balance between oxygen delivery and consumption, and thus, such correlations are unlikely to be valid across diverse tumor types.

In conclusion, we have demonstrated that in comparison with the H tumor, the anaplastic faster growing AT1 subline of the Dunning R3327 tumor is significantly more hypoxic. Comparable data using histological markers of hypoxia and vascular endothelium further validate the assessment of tumor oxygenation by *FREDOM*. We believe this approach can provide valuable insight into tumor physiology and response to interventions, assisting in the development of novel therapeutic strategies. Ultimately, *FREDOM* should have application in the clinical setting.

Acknowledgments

We are grateful to Dr. Matthew Merritt for maintaining the MR system, Ms. Maria Sambade for assistance with histology, Dr. Peter Peschke (DKFZ, Heidelberg) for providing tumor cells

and Dr. Philip Thorpe for laboratory facilities. Research supported in part by NIH RO1 CA79515 (NCI)/ EB002762 (NIBIB), DOD Prostate Cancer Initiative Postdoctoral Award (DAMD 170110108) (DZ) and performed in conjunction with Cancer Imaging Program P20 CA 86354.

References

1. Brown JM, and Giaccia AJ (1994). Tumor hypoxia: the picture has changed in the 1990s. *Int. J. Radiat. Biol.* **65**, 95-102.

2. Denekamp J. (1989). Physiological hypoxia and its influence on radiotherapy. In *The Biological Basis of Radiotherapy, 2nd ed.*, GG Steel, GE Adams, and A Horwich, Eds. Elsevier, Amsterdam. pp. 115-143.

3. Höckel M, Schlenger K, Aral B, Mitze M, Schäffer U, and Vaupel P (1996). Association between tumor hypoxia and malignant progression in advanced cancer of the uterine cervix. *Cancer Res.* **56**, 4509-4515.

4. Sartorelli AC (1988). Therapeutic attack of hypoxic cells of solid tumors: Presidential address. *Cancer Res.* **48**, 775-778.

5. De Jaeger K, Kavanagh MC, and Hill RP (2001). Relationship of hypoxia to metastatic ability in rodent tumors. *Br. J. Cancer* **84**, 1280-1285.

6. Höckel M, and Vaupel P (2001). Tumor hypoxia: Definitions and current clinical, biologic, and molecular aspects. *J. Natl. Cancer Inst.* **93**, 266-276.

7. Stone HB, Brown JM, Phillips T, and Sutherland RM (1993). Oxygen in human tumors: correlations between methods of measurement and response to therapy. *Radiat. Res.* **136**, 422-434.

8. Hunjan S, Zhao D, Constantinescu A, Hahn EW, Antich PP, and Mason RP (2001). Tumor Oximetry: demonstration of an enhanced dynamic mapping procedure using fluorine-19 echo planar magnetic resonance imaging in the Dunning prostate R3327-AT1 rat tumor. *Int. J. Radiat. Oncol. Biol. Phys.* **49**, 1097-1108.

9. Zhao D, Constantinescu A, Hahn EW, and Mason RP (2002). Differential oxygen dynamics in two diverse Dunning prostate R3327 rat tumor sublines (MAT-Lu and HI) with respect to growth and respiratory challenge. *Int. J. Radiat. Oncol. Biol. Phys.* **53**, 744-756.

10. Isaacs J, Isaacs W, Feitz W, and Scheres J (1986). Establishment and characterization of 7 Dunning prostate cancer cell lines and their use in developing methods for predicting metastatic ability of prostate cancer. *Prostate* **9**, 261-281.

11. Vaupel P, Kallinowski F, and Okunieff P (1989). Blood flow, oxygen and nutrient supply, and metabolic microenvironment of human tumors: a review. *Cancer Res.* **49**, 6449-6465.

12. Raleigh JA, Chou SC, Arteel GE, and Horsman MR (1999). Comparison among pimonidazole binding, oxygen electrode measurements, and radiation response in C3H mouse tumors. *Radiat. Res.* **151**, 580-589.

13. Evans SM, Hahn S, Pook DR, Jenkins WT, Chalian AA, Zhang P, Stevens C, Weber R, Weinstein G, Benjamin I, Mirza N, Morgan M, Rubin S, McKenna WG, Lord EM, and Koch CJ (2000). Detection of hypoxia in human squamous cell carcinoma by EF5 binding. *Cancer Res.* **60**, 2018-2024.

14. Ljungkvist ASE, Bussink J, Rijken PFJW, Raleigh JA, Denekamp J, and Van Der Kogel AJ (2000). Changes in tumor hypoxia measured with a double hypoxic marker technique. *Int. J. Radiat. Oncol. Biol. Phys.* **48**, 1529-1538.

15. Peschke P, Hahn EW, Wenz F, Lohr F, Braunschweig F, Wolber G, Zuna I, and Wannenmacher M (1998). Differential sensitivity of three sublines of the rat Dunning prostate tumor system R3327 to radiation and/or local tumor hyperthermia. *Radiat. Res.* **150**, 423-430.

16. Hahn EW, Peschke P, Mason RP, Babcock EE, and Antich PP (1993). Isolated tumor growth in a surgically formed skin pedicle in the rat: A new tumor model for NMR studies. *Magn. Reson. Imaging* **11**, 1007-1017.

17. Weidner N (1995). Intratumor microvessel density as a prognostic factor in cancer. *Am. J. Pathol.* **147**, 9-19.

18. Yeh KA, Biade S, Lanciano RM, Brown DQ, Fenning MC, Babb JS, Hanks GE, and Chapman JD (1995). Polarographic needle electrode measurements of oxygen in rat prostate carcinomas: accuracy and reproducibility. *Int. J. Radiat. Oncol. Biol. Phys.* **33**, 111-118.

19. Chapman JD, McPhee MS, Walz N, Chetner MP, Stobbe CC, Soderlind K, Arnfield M, Meeker BE, Trimble L, and Allen PS (1991). Nuclear magnetic resonance spectroscopy and sensitizer-adduct measurements of photodynamic therapy-induced ischemia in solid tumors. *J. Natl. Cancer Inst.* **83**, 1650-1659.

20. Thorndyke C, Meeker B, Thomas G, Laky W, McPhee M, and Chapman J (1985). The radiation sensitivities of R3327-H and -AT1 rat prostate adenocarcinomas. *J. Urol.* **134**, 191-198.

21. Mason RP, Constantinescu A, Hunjan S, Le D, Hahn EW, Antich PP, Blum C, and Peschke P (1999). Regional tumor oxygenation and measurement of dynamic changes. *Radiat. Res.* **152**, 239-249.

22. Zhao D, Constantinescu A, Hahn EW, and Mason RP (2001). Tumor oxygen dynamics with respect to growth and respiratory challenge: Investigation of the Dunning prostate R3327-HI tumor. *Radiat. Res.* **156**, 510-520.

23. Song Y, Constantinescu A, and Mason RP (2002). Dynamic breast tumor oximetry: the development of prognostic radiology. *Technol. Cancer Res. Treat.* **1**, 1-8.

24. Rofstad EK (2000). Microenvironment-induced cancer metastasis. *Int. J. Radiat.* **76**, 589-605.

25. Birner P, Schindl P, Obermair A, Plank C, Breitenecker G, and Oberhuber G (2000). Overexpression of hypoxia-inducible factor 1 is a marker for an unfavorable prognosis in early-stage invasive cervical cancer. *Cancer Res.* **60**, 4693-4696.

26. Fyles A, Milosevic M, Hedley M, Pintile M, Levin W, Manchul L, and Hill RP (2002). Tumor hypoxia has independent predictor impact only on patients with node-negative cervix cancer. *J. Clin. Oncol.* **20**, 680-687.

27. Brizel DM, Scully SP, Harrelson JM, Layfield LJ, Bean JM, Prosnitz LR, and Dewhirst MW (1996). Tumor oxygenation predicts for the likelihood of distant metastases in human soft tissue sarcoma. *Cancer Res.* **56**, 941-943.

28. Vaupel PW, Schlenger K, Knoop C, and Höckel M (1991). Oxygenation of human tumors: evaluation of tissue oxygen distribution in breast cancers by computerized O_2 tension measurements. *Cancer Res.* **51**, 3316-3322.

29. Hohenberger P, Felger C, Haensch W, and Schlag PM (1998). Tumor oxygenation correlates with molecular growth determinants in breast cancer. *Breast Cancer Res. Treatment* **48**, 97-106.

30. Thews O, Kelleher DK, Lecher B, and Vaupel P (1998). Blood flow, oxygenation, metabolic and energetic status in different clonal subpopulations of a rat rhabdomyosarcoma. *Int. J. Oncol.* **13**, 205-211.

31. Young S, Marshall R, and Hill R (1988). Hypoxia induces DNA overreplication and enhances metastatic potential of murine tumor cells. *Proc. Natl. Acad. Sci. USA* **85**, 9533-9537.

32. Cairns RA, Kalliomaki T, and Hill RP (2001). Acute (cyclic) hypoxia enhances spontaneous metastasis of KHT murine tumors. *Cancer Res.* **61**, 8903-8908.

33. Kaanders JHAM, Wijffels KIEM, Marres HAM, Ljungkvist ASE, Pop LAM, van den Hoogen FJA, de Wilde PCM, Bussink J, Raleigh JA, and van der Kogel AJ (2002). Pimonidazole binding and tumor vascularity predict for treatment outcome in head and neck cancer. *Cancer Res.* **62**, 7066-7074.

34. Movsas B, Chapman J, Greenberg R, Hanlon A, Horwitz E, Pinover W, Stobbe C, and Hanks G (2000). Increasing levels of hypoxia in prostate carcinoma correlate significantly with increasing clinical stage and patient age: an Eppendorf pO_2 study. *Cancer* **89**, 2018-2024.

35. Eble MJ, Lohr F, Wenz F, Krems B, Bachert P, and Peschke P (1995). Tissue oxygen tension distribution in two sublines of the Dunning prostate tumor R3327. In *Tumor Oxygenation.* PW Vaupel, DK Kelleher, and M Gunderoth, Eds. Funktionsanalyse Biologischer Systeme, Gustav Fischer Verlag, Stuttgart. pp. 95-105.

36. Kallman R, and Dorie M (1986). Tumor oxygenation and reoxygenation during radiation therapy: importance in predicting tumor response. *Int. J. Radiat. Oncol. Biol. Phys* **12**, 681-685.

37. Fenton BM (1997). Effects of carbogen plus fractionated irradiation on KHT tumor oxygenation. *Radiother Oncol* **44**, 183-190.

38. Zhao D, Constantinescu A, Chang CK, Hahn EW, and Mason RP. Correlation of tumor oxygen dynamics with radiation response of the Dunning prostate R3327-HI tumors. *Radiat. Res.* **159**, in press 2003.

39. Kaanders JHAM, Pop LAM, Marres HAM, Bruaset I, van den Hoogen FJA, Merkx MAW, and van der Kogel AJ (2002). ARCON: experience in 215 patients with advanced head-and-neck cancer. *Int. J. Radiat. Oncol. Biol. Phys.* **52**, 769-778.

40. Hunjan S, Mason RP, Constantinescu A, Peschke P, Hahn EW, and Antich PP (1998). Regional tumor oximetry: ^{19}F NMR spectroscopy of hexafluorobenzene. *Int. J. Radiat. Oncol. Biol. Phys.* **40**, 161-171.

41. Mason RP, Rodbumrung W, and Antich PP (1996). Hexafluorobenzene: a sensitive ^{19}F NMR indicator of tumor oxygenation. *NMR Biomed.* **9**, 125-134.

42. Bussink J, Kaanders JHAM, Strik AM, Vojnovic B, and van der Kogel AJ (2000). Optical sensor-based oxygen tension measurements correspond with hypoxia marker binding in three human tumor xenograft lines. *Radiat. Res.* **154**, 547-555.

43. Evans SM, Hahn S, Hahn SM, Magarelli DP, and Koch CJ (2001). Hypoxic heterogeneity in human tumors: EF5 binding, vasculature, necrosis, and proliferation. *Am. J. Clin. Oncol.* **24**, 467-472.

44. Lyng H, Sundfor K, and Rofstad EK (1997). Oxygen tension in human tumours measured with polarographic needle electrodes and its relationship to vascular density, necrosis and hypoxia. *Radiother. Oncol.* **44**, 163-169.

45. Olive PL (1994). Radiation-induced reoxygenation in the SCC VII murine tumor: evidence for a decrease in oxygen consumption and an increase in tumor perfusion. *Radiother. Oncol.* **32**, 37-46.

46. Jenkins WT, Evans SM, and Koch CJ (2000). Hypoxia and necrosis in rat 9L glioma and Morris 7777 hepatoma tumors: comparative measurements using EF5 binding and the Eppendorf needle electrode. *Int. J. Radiat. Oncol. Biol. Phys.* **46**, 1005-1017.

47. Bennewith KL, Raleigh JA, and Durand RE (2002). Orally administered pimonidazole to label hypoxic tumor cells. *Cancer Res.* **62**, 6827-6830.

48. Folkman J (1974). Tumor angiogenesis. *Adv. Cancer Res.* **19**, 331-358.

49. Semenza GL (2002). HIF-1 and tumor progression: pathophysiology and therapeutics. *Trends Mol. Med.* **8**, S62-67.

50. Zhao D, Constantinescu A, Jiang L, Hahn EW, and Mason RP (2001). Prognostic radiology: quantitative assessment of tumor oxygen dynamics by MRI. *Am. J. Clin. Oncol.* **24**, 462-466.

51. Mason RP, Ran S, and Thorpe PE (2002). Quantitative assessment of tumor oxygen dynamics: Molecular Imaging for Prognostic Radiology. *J. Cell. Biochem.* **87**, 45-53.

52. Kim JG, Zhao D, Song Y, Constantinescu A, Mason RP, and Liu H (2003). Interplay of tumor vascular oxygenation and tumor pO_2 observed using NIRS, oxygen electrode, and ^{19}F MR pO_2 Mapping. *J. Biomed. Optics* **8**, 53-62.

53. Howe FA, Robinson SP, Rodrigues LM, and Griffiths JR (1999). Flow and oxygenation dependent (FLOOD) contrast MR imaging to monitor the response of rat tumors to carbogen breathing. *Magn. Reson. Imaging* **17**, 1307-1318.

54. Baudelet C, and Gallez B (2002). How does blood oxygen level-dependent (BOLD) contrast correlate with oxygen partial pressure (pO_2) inside tumors? *Magn. Reson. Med.* **48**, 980-986.

55. Fan X, River JN, Zamora M, Al-Hallaq HA, and Karczmar GS (2002). Effect of carbogen on tumor oxygenation: combined fluorine-19 and proton MRI measurements. *Int. J. Radiat. Oncol. Biol. Phys.* **54**, 1202-1209.

56. Cooper RA, Carrington BM, Loncaster JA, Todd SM, Davidson SE, Logue JP, Luthra AD, Jones AP, Stratford I, Hunter RD, and West CML (2000). Tumor oxygenation levels correlate with dynamic contrast-enhanced magnetic resonance imaging parameters in carcinoma of the cervix. *Radiother. Oncol.* **57**, 53-59.

57. Wang Z, Su M-Y, and Nalcioglu O (2002). Applications of dynamic contrast enhanced MRI in oncology: measurement of tumor oxygen tension. *Technol. Cancer Res. Treat.* **1**, 29-38.

Legends

Figure 1

pO_2 maps obtained using *FREDOM*. Distinct heterogeneity was seen in these representative small H (1.1 cm^3) and AT1 (1.5 cm^3) tumors under baseline conditions, when the anesthetized rats breathed air. The H tumor (baseline mean pO_2 = 20.3 ± 2.2 (se) torr) was significantly better oxygenated than the AT1 tumor (baseline mean pO_2 = 5.3 ± 0.9 torr, $p < 0.001$). In response to oxygen inhalation, pO_2 increased significantly in both the H and the AT1 tumors [mean pO_2 = 46.7 ± 3.7 torr ($p < 0.001$) and 17.2 ± 3.8 torr ($p < 0.005$), respectively]. In each case, the fourth measurement after switching to oxygen breathing is shown. Colored voxels were selected by applying threshold criteria to each ensuing high quality data throughout the time course. Gray voxels provided a T1 curve fit, but with large errors.

Figure 2

Histograms of tumor oxygenation pooled for the H tumors. Data from six small (219 voxels) and six large (159 voxels) H tumors obtained using *FREDOM* show distinct heterogeneity. The small tumors were significantly better oxygenated (mean = 31 ± 2 torr, median = 27 torr) than the large tumors (mean = 14 ± 1 torr, median = 12 torr; $p<0.001$). In response to respiratory challenge with oxygen, both mean and median pO_2 in each group increased significantly ($p<0.001$). Arrows indicate mean (x) and median (m) pO_2, respectively. The bin numbers show the maximum pO_2 for each category. Cumulative frequencies are shown by curves.

Figure 3

Histograms of tumor oxygenation pooled for the AT1 tumors. Seven small tumors (280 voxels) showed significantly higher baseline pO_2 (mean = 14 ± 1 torr, median = 11 torr) than the six large tumors (149 voxels; mean = 4 ± 1 torr, median = 3 torr; $p< 0.001$). With respect to oxygen challenge, mean pO_2 in both groups increased significantly ($p<0.001$). However, the median pO_2 in the large tumors only increased from 3 to 8 torr. Comparison with the H tumors (Fig. 2) showed that both the groups of small and large AT1 tumors were less well oxygenated ($p<0.001$). Arrows indicate mean (x) and median (m) pO_2, respectively.

Figure 4

Dynamic oxygenation at individual locations with initial pO_2 <10 torr (hypoxic) in response to oxygen breathing. **A.** A total of 92 initially hypoxic voxels from both the small (n=31) and the large (n=61) H tumors, and 248 hypoxic voxels from the small (n=131) and large AT1 (n=117) tumors were followed with respect to gas challenge. The mean pO_2 in each subline increased immediately after oxygen breathing, and reached a mean pO_2 = 55 ± 5 (se) torr in H versus 18 ± 2 torr in AT1, respectively ($p<0.001$) after 40 mins. **B.** Dynamic hypoxic fraction (HF_{10} < 10 torr) in the initially hypoxic regions of the H tumors decreased to a minimum < 10%, 24 min after switching to oxygen inhalation, whereas > 60% initially hypoxic regions remained in the AT1 tumors (* $p<0.001$).

Figure 5

Distribution of pimonidazole and CD31 in representative large H and AT1 tumors **A.** Well differentiated H tumor comprising multiple glandular structures and connective stroma.

Immunostaining for hypoxia marker, pimonidazole showed few positive cells. **B.** Anti-CD31 staining (brown) demonstrated relatively well distributed vascular endothelial cells in a consecutive 6 μm section. **C.** The anaplastic AT1 tumor is composed of non-glandular structure and fewer stromal cells. Typical distribution of hypoxia in the AT1, recognized as positive staining for pimonidazole (brown), was observed at some distance from blood vessels stained for CD31 (**D**, arrow) and located adjacent to necrotic regions (N).

Table 1 Comparison of pO_2 data in individual R3327 Dunning Prostate Rat Tumors

Tumor Subline	Size	No.	Baseline (21% O_2)				Oxygen challenge (100% O_2)			
			pO_2 (torr)		Hypoxic Fractions (%)		pO_2 (torr)		Hypoxic Fractions (%)	
			Mean ± SE	Median	HF_5	HF_{10}	Mean ± SE	Median	HF_5	HF_{10}
H	Small	6	33.8 ± 4.4	30.1 ± 4.4	9 ± 2	16 ± 2	137.2 ± 22.9†	121.1 ± 21.2†	1 ± 1†	3 ± 1†
	Large	6	12.7 ± 1.1*	11.4 ± 1.6*	31 ± 4*	46 ± 5*	83.1 ± 16.2†	68.5 ± 20.0†	7 ± 3†	10 ± 4†
AT1	Small	7	10.4 ± 2.1^{+}	7.9 ± 2.3^{+}	42 ± 7^{+}	61 ± 7^{+}	62.4 ± 13.1$^{+\dagger}$	55.4 ± 21.0^{+}	19 ± 7$^{+\dagger}$	24 ± 9$^{+\dagger}$
	Large	6	3.5 ± 1.2^{*+}	2.1 ± 1.0^{*+}	65 ± 5^{*+}	83 ± 3^{*+}	40.6 ± 20.1	23.2 ± 15.5	46 ± 11^{+}	59 ± 14^{+}

Small : < 1.5 cm^3; Large: > 3 cm^3; $HF_{5 \text{ or } 10}$: Hypoxic fraction (< 5 or 10 torr)

* $p < 0.05$ from the small group; $^{+}$ $p < 0.05$ from the H tumors; † $p < 0.05$ from baseline

Table 2 Comparison of hypoxic fraction with histology

Tumor Subline	*FREDOM* Hypoxic fraction (%) $HF_{2.5}$	HF_5	HF_{10}	Histology Necrosis (%)	Hypoxia marker Pimonidazole (%)	Vascular density CD31 (/mm^2)
H	21 ± 3	31 ± 4	46 ± 5	2 ± 1	5 ± 1	139 ± 30
AT1	51 ± 5*	65 ± 5*	83 ± 3*	7 ± 1	18 ± 4*	45 ± 13*

$HF_{2.5, 5 \text{ or } 10}$: Hypoxic fraction (< 2.5, 5 or 10 torr); * $p < 0.05$ from H tumors.

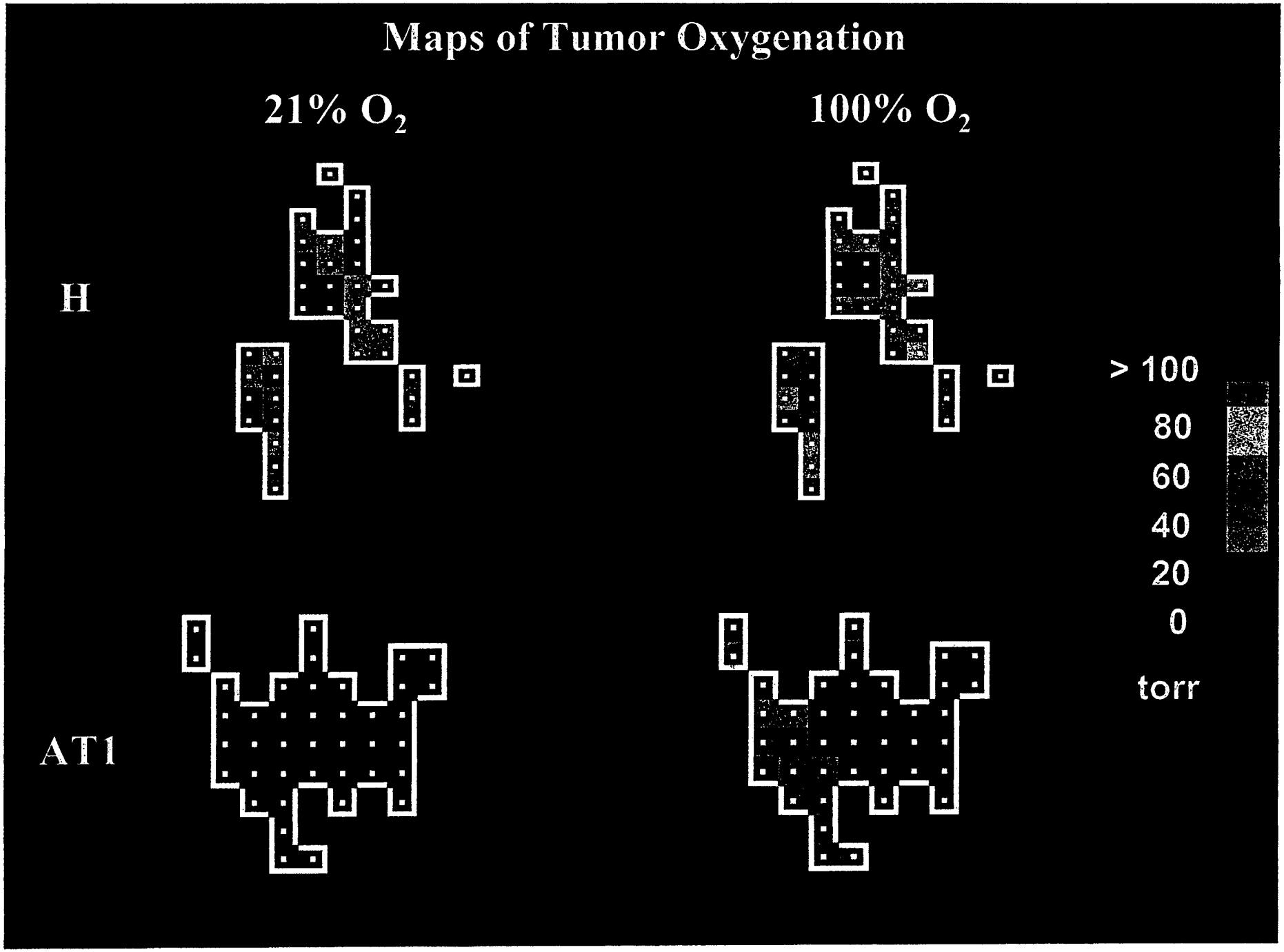
Maps of Tumor Oxygenation
21% O_2
100% O_2
H
AT1
> 100
80
60
40
20
0
torr

Fig. 2

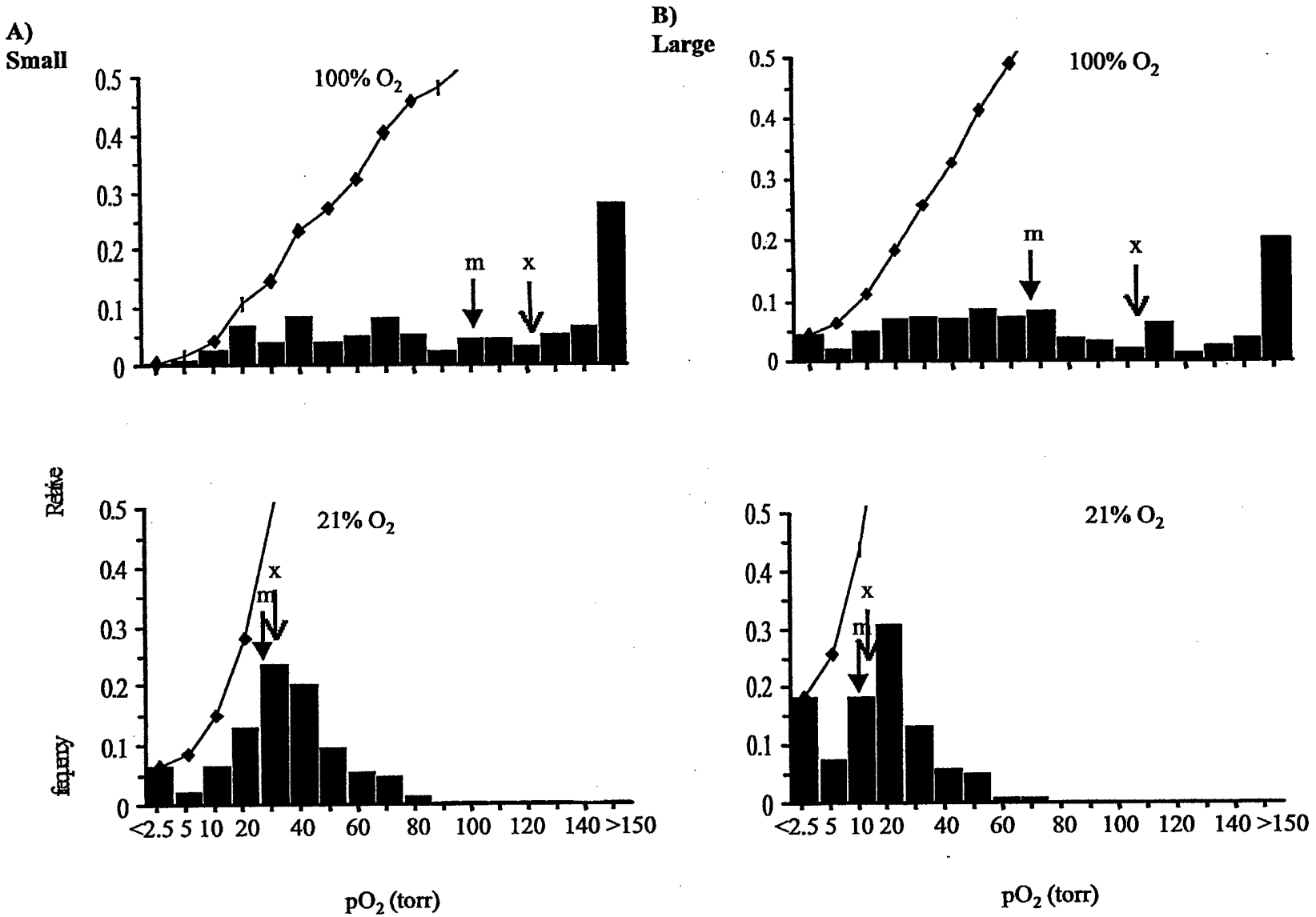
A)
Small
B)
Large
100% O_2
21% O_2
m
x
0.5
0.4
0.3
0.2
0.1
0
Relative frequency
<2.5 5 10 20 40 60 80 100 120 140 >150
pO_2 (torr)

Fig. 3

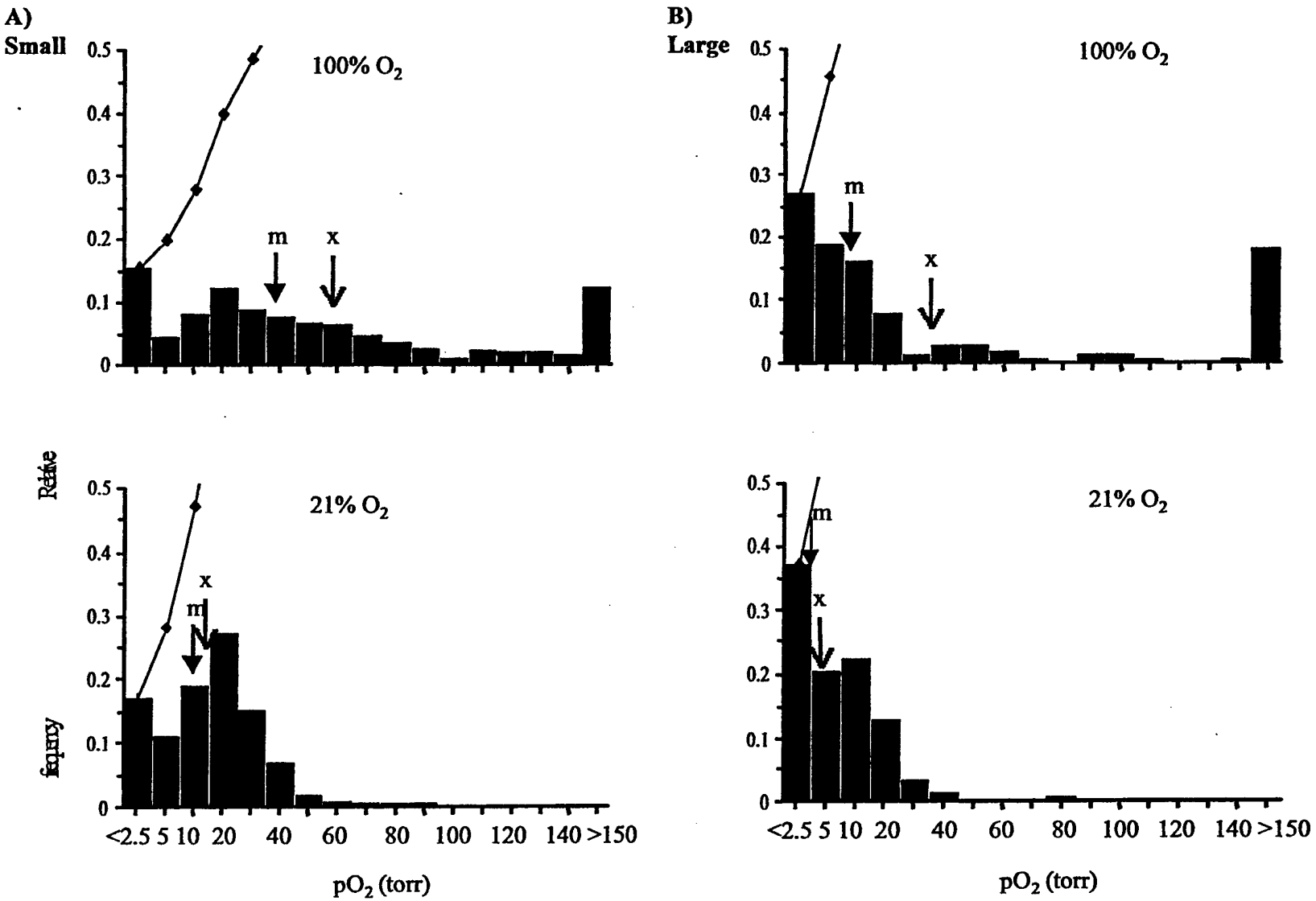
A)
Small
100% O_2
m
x
21% O_2
x
m
Relative frequency
0.5
0.4
0.3
0.2
0.1
0
<2.5 5 10 20 40 60 80 100 120 140 >150
pO_2 (torr)
B)
Large
100% O_2
m
x
21% O_2
m
x
<2.5 5 10 20 40 60 80 100 120 140 >150
pO_2 (torr)

Fig. 4a

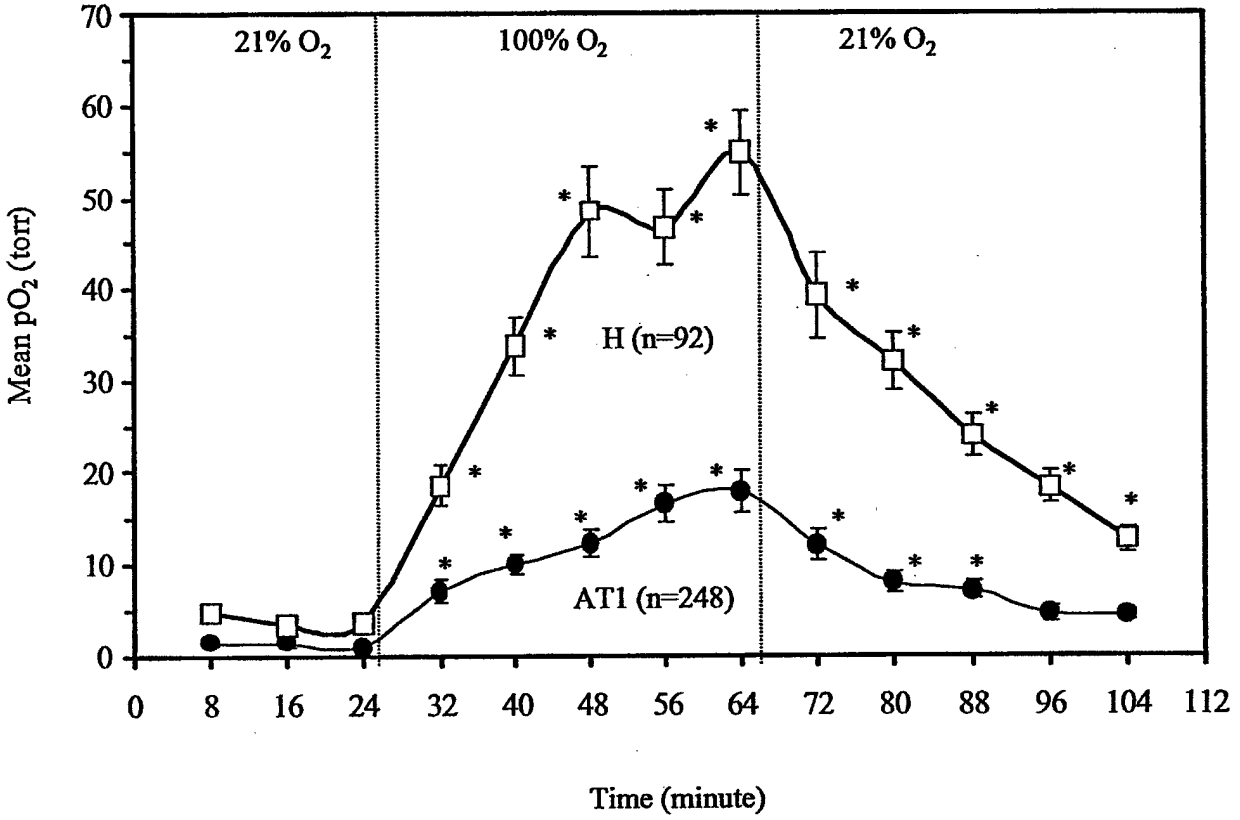
21% O_2
100% O_2
21% O_2
H (n=92)
AT1 (n=248)
Mean pO_2 (torr)
Time (minute)
0
10
20
30
40
50
60
70
0
8
16
24
32
40
48
56
64
72
80
88
96
104
112

Fig. 4b

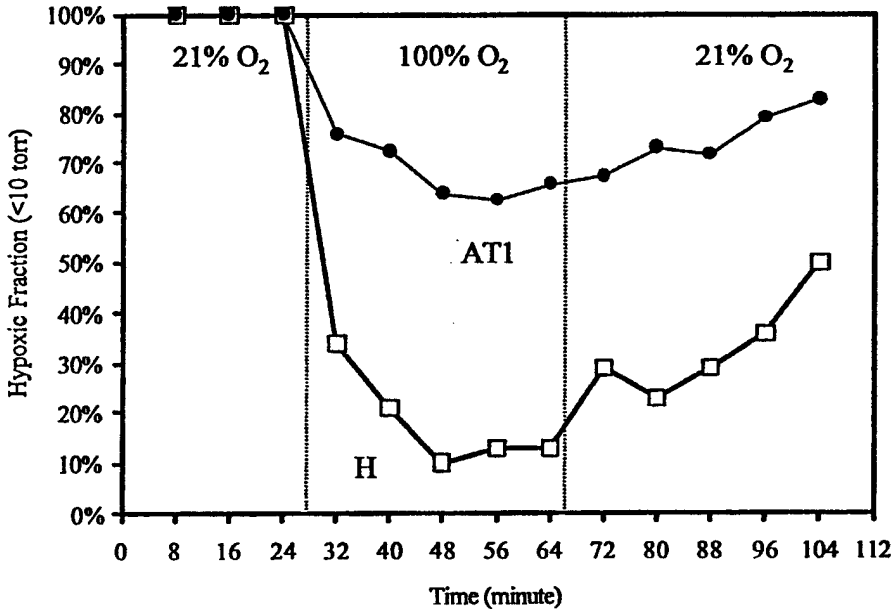
100%
90%
80%
70%
60%
50%
40%
30%
20%
10%
0%
Hypoxic Fraction (<10 torr)
21% O2
100% O2
21% O2
AT1
H
0
8
16
24
32
40
48
56
64
72
80
88
96
104
112
Time (minute)

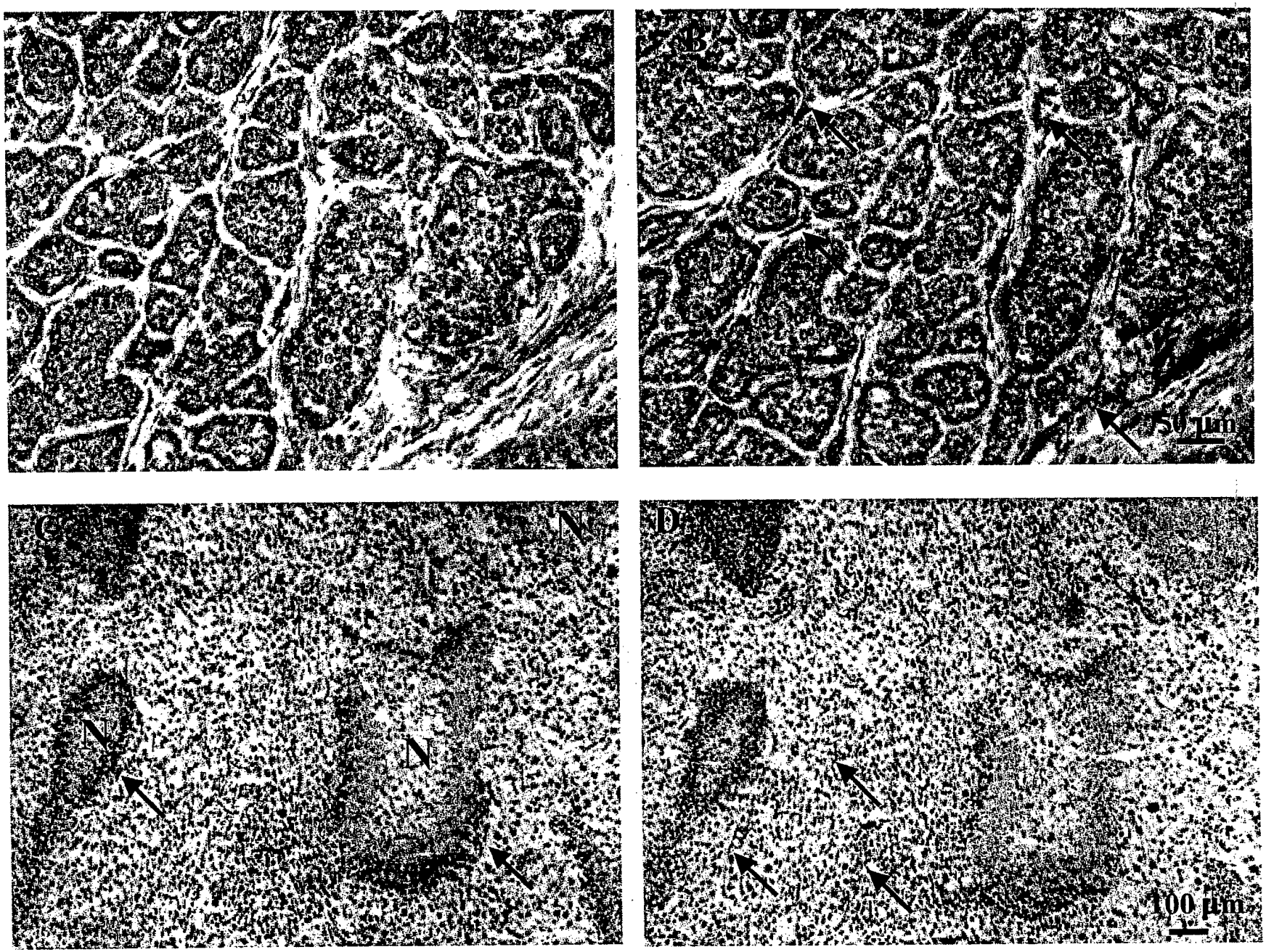
B
50 µm
C
N
N
N
D
100 µm

PROCEEDINGS

New Discoveries in Prostate Cancer Biology and Treatment

December 5-9, 2001
The Registry Resort
Naples, Florida

Conference Co-Chairpersons

KENNETH J. PIENTA
University of Michigan
Comprehensive Cancer Center
Ann Arbor, MI

ROBERT H. GETZENBERG
University of Pittsburgh
Pittsburgh, PA

DONALD S. COFFEY
Johns Hopkins Hospital
Baltimore, MD

In vivo MRI monitoring of prostate tumor vasculature and oxygen dynamics
Dawen Zhao, Lan Jiang, Anca Constantinescu, Eric W. Hahn and Ralph P. Mason, Department of Radiology, U.T. Southwestern Medical Center, Dallas, TX 75390.

Hypoxic cells in solid tumors, has long been recognized as a significant factor influencing response to cancer therapy and prognosis. We recently established a novel magnetic resonance approach to measuring regional tumor oxygen tension: *FREDOM* (Fluorocarbon Relaxometry using Echo planar imaging for Dynamic Oxygen Mapping) using hexafluorobenzene, as the reporter molecule (1, 2). Recognizing the intimate interplay of tumor oxygenation and blood flow, we began investigations to compare regional changes in pO_2, vascular oxygenation and blood flow. Here, we compare perfusion and oxygen dynamics in two Dunning R3327 prostate rat tumor sublines (3): the well differentiated slower growing H subline (Tpot ~ 20 days) and the anaplastic faster growing AT1 subline (Tpot ~ 4.6 days). MRI experiments were performed on a 4.7 T MR system. Vascular oxygen dynamics were assessed using BOLD (Blood Oxygen Level Dependant) contrast ^1H MRI. A series of echo planar images was acquired, while the rat breathed air and in response to respiratory challenge with oxygen (1 dm^3/min). Differences in signal intensity enhancement in response to oxygen inhalation were found between the H (40%) and the AT1 (25%) tumors ($p<0.05$). Increased signal may be interpreted as increased HbO_2. Following a re-equilibration period, dynamic Gd-DTPA contrast-enhanced (DCE) MRI was performed using a spin-echo T1-weighted pulse sequence. The data also revealed significantly higher signal enhancement in H (38%) compared to AT1 (15%) tumors ($p<0.05$). Finally, *FREDOM* performed on the same 4 mm thick tumor section revealed considerable intra tumoral heterogeneity in the distribution of pO_2 values. H tumors had a higher mean baseline pO_2 (30.5 ± 1.6 mmHg) than size-matched AT1 (13.6 ± 0.5 mmHg) tumors ($p<0.001$). Further, although both tumor types responded to respiratory challenge, oxygen inhalation produced a significantly higher maximum pO_2 ($p<0.001$) in H (121.6 ± 6.8 mmHg) compared with AT1 (58.3 ± 3.8 mmHg) tumors. Immunohistochemical studies using the hypoxic marker (pimonidazole) and the vascular endothelial cell marker (CD31) verified that the H subline with 2% positive pimonidazole binding is better oxygenated than the AT1 subline (11%), and vascular density is also higher in H than AT1 tumors. In summary, we believe that the BOLD and DCE MRI, which provide a qualitative index of vascular oxygenation and flow, when combined with quantitative data on tissue oxygenation by ^{19}F MR provide valuable insight into tumor physiology, specifically related to the proficiency of the vascular component and is relevant to treatment response and prognosis. References: 1. Hunjan, S., Zhao, D., Constantinescu, A., Hahn, E. W., Antich, P. P., and Mason, R. P. Int. J. Radiat. Oncol. Biol. Phys. 49, 1097-1108, 2001. 2. Zhao, D., Constantinescu, A., Hahn, E. W., and Mason, R. P. Radiat. Res. 157, in the press 2002. 3. Isaacs, J., Isaacs, W., Feitz, W., and Scheres, J. Prostate 9, 261-81, 1986. (Supported by the DOD Prostate Cancer Initiative (DAMD 170110108) and NCI RO1 79515)

FOURTH INTERNATIONAL SYMPOSIUM ON ANTI-ANGIOGENIC AGENTS

Recent Advances and Future Directions in Cell Biology and Clinical Research

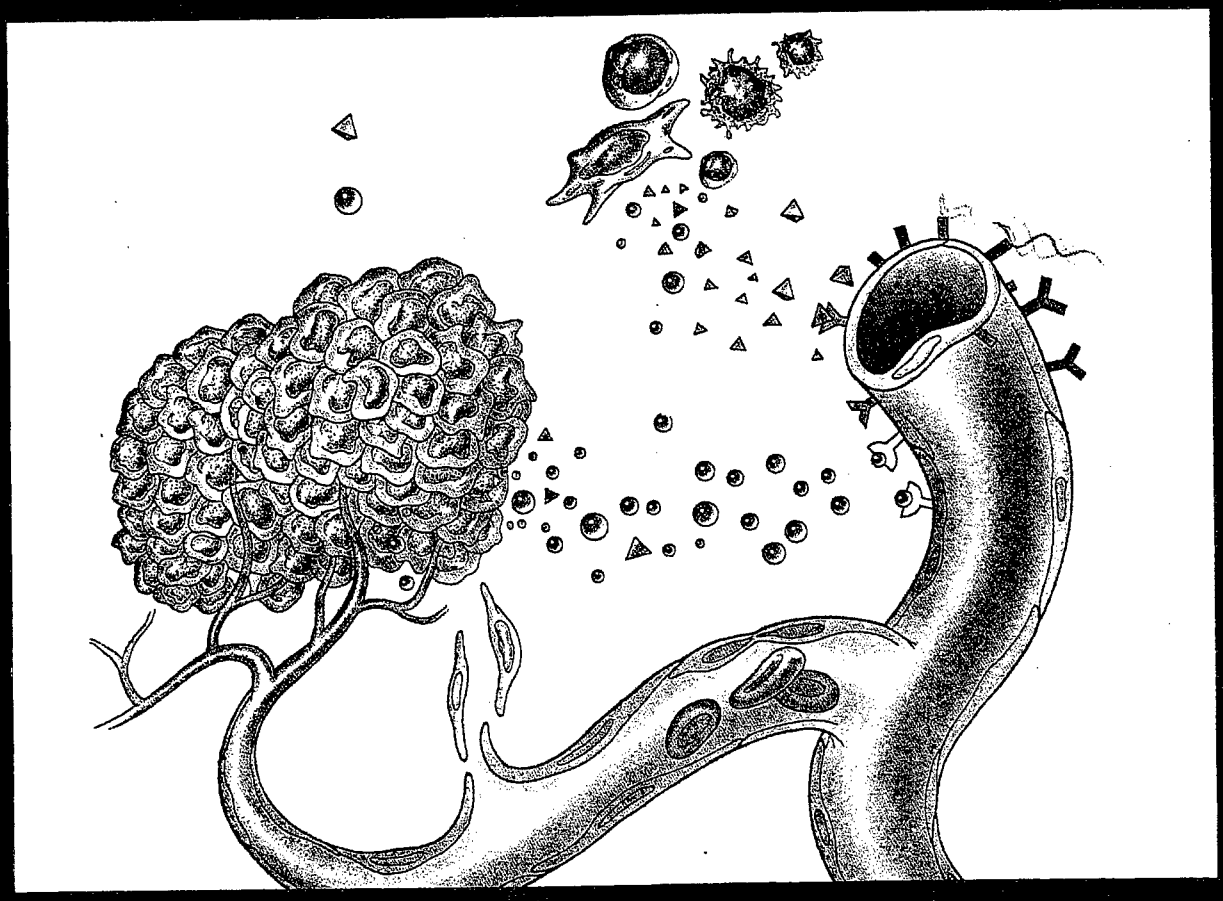

The Adam's Mark Hotel
Dallas, Texas

SPONSORED BY

CBCE®

In vivo MRI Monitoring of Prostate Tumor Vasculature and Oxygen Dynamics

Dawen Zhao, Lan Jiang, Anca Constantinescu, Eric W. Hahn and Ralph P. Mason

Department of Radiology

The University of Texas Southwestern Medical Center, Dallas, TX 75390

Introduction

Hypoxic cells in solid tumors have long been recognized as a significant factor influencing response to cancer therapy and prognosis. We have recently established a novel magnetic resonance approach to measuring regional tumor oxygen tension, *FREDOM* (fluorocarbon Relaxometry using Echo planar imaging for Dynamic Oxygen Mapping) with hexafluorobenzene, as a reporter molecule (1, 2). Recognizing the intimate interplay of tumor oxygenation and blood flow, we have initiated BOLD (Blood Oxygen Level Dependent) contrast 1H MRI and DCE (Dynamic Contrast Enhanced) MRI to compare regional changes in pO_2, vascular oxygenation and flow. Moreover, immunohistochemical approaches using bioreductive chemical probes of hypoxia and vascular endothelium markers have been used to estimate tumor hypoxia and vasculature. Here, we apply various approaches to compare tumor hypoxia and vasculature in two Dunning R3327 prostate rat tumor sublines: (1) the relatively well differentiated slower growing H subline (Tpot ~18 days) and the anaplastic and fast growing AT1 subline (Tpot 4.8 days).

Methods

In vivo MRI Studies: Dunning prostate tumors were implanted in skin pockets on the forefoot of male Copenhagen rats. When the tumors reached ~1 cm diameter (~0.8 cm^3), hexafluorobenzene (HFB, 80 µl) was injected directly into the tumor. A size matched 1H/19F single turn solenoid coil was placed around the tumor and MR experiments were performed using a 4.7 T magnet with actively shielded gradients. Vascular oxygen dynamics were assessed using *BOLD* centered 1H MRI. A series of echo planar 2 mm coronal section images was acquired, while the rat breathed air and then during respiratory challenge with oxygen (1 dm^3/min). Following a reequilibration period with air inhalation for 10 mins, a bolus of Gd-DTPA (0.1 mmol/kg, Magnevist™) was injected through a tail vein catheter (27 G butterfly, Abbott Labs) without moving the rat. Again, a series of T1-weighted 2 mm coronal echo planar images was acquired to reveal dynamic contrast enhanced MRI. Tumor oxygenation was assessed using *FREDOM* of HFB with 8 minute time resolution. A series of pO_2 maps was acquired over a period of 1 hour with respiratory challenge, and corresponding regional pO_2 was estimated using the relationship: pO_2 (mmHg) = (R1-0.09359)/0.001678 (1).

Immunohistochemistry: Pimonidazole hydrochloride (Hypoxyprobe™-1, HPI, Inc., Belmont, MA) was injected in the tail vein at a dose of 60 mg/kg. 90 min later the animal was perfused for 20 min with 0.1 mM $CaCl_2$ in 0.9% saline. Tumors were excised and immediately immersed in liquid nitrogen and then stored in -80 °C freezer until use. A series of 8 µm frozen sections from several regions of each tumor was immunostained for hypoxia (pimonidazole) and microvascular density (mouse anti rat CD31, Serotec Inc. Raleigh, NC).

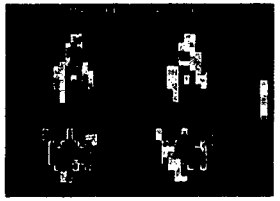

Figure 1 pO_2 maps by *FREDOM*

Distinct heterogeneity was seen in these representative H (1.4 cm diameter) and AT1 (1.8 cm diameter) tumors under baseline conditions when anesthetized rats breathed air. The H tumor (baseline mean pO_2 = 17.9 ± 1.8(sd) mmHg) was better oxygenated than the AT1 tumor (baseline mean pO_2 = 6.3 ± 0.8 mmHg). In response to oxygen inhalation, pO_2 increased significantly in both the H (mean pO_2 = 82.0 ± 3.6 mmHg, $p < 0.0001$) and the AT1 tumors (mean pO_2 = 17.2 ± 3.6 mmHg, $p < 0.005$)

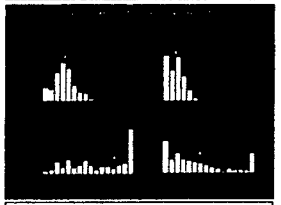

Figure 2 Histograms of tumor oxygenation.

Data from an H (A) was ranged from 1.5 to 1.8 cm diameter) and tumor AT1 (B, size from 1.3 to 1.8 cm diameter) tumors obtained using *FREDOM* show distinct heterogeneity in response to respiratory challenge with oxygen, both mean and median pO_2 increased significantly. Arrows indicate mean (a) and median (m) pO_2, respectively

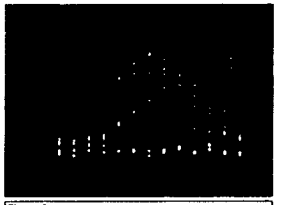

Figure 3 Local response to respiratory intervention

Variation in pO_2 with respiratory challenge for individual regions shown as initially well oxygenated or hypoxic regions from an AT1 (dotted line) and H tumor (solid), respectively. All the well oxygenated regions in the two sublines increased significantly in pO_2 in response to oxygen breathing. While the hypoxic regions from AT1 tumor did not, H tumor did increase with gas challenge.

Figure 4 Proton MRI of tumor vascular dynamics.

Echo planar images (EPI) of representative H and AT1 tumors. In response to respiratory challenge, each tumor showed a BOLD effect as revealed in the normalized subtraction maps (right). DCE also showed contrast changes. In the AT1 tumor, major response to each intervention occurred in ductal regions. By contrast, predominant DCE and BOLD effects occurred in vascular regions in the H tumor

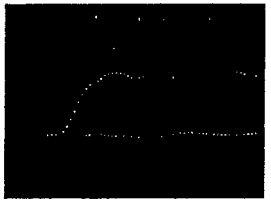

Figure 5 Tumor vascular dynamics.

Variation in mean H MR signal intensity in response to breathing oxygen (BOLD) or Magnevist™ bolus (DE) for groups of H and AT1 tumors. In each case the BOLD response is delayed by ~ 45 s compared with DE. Both BOLD and DE effects were greater in H tumors than AT1. The light blue lines shows stability of signal in the absence of intervention. Lines indicate mean ± se

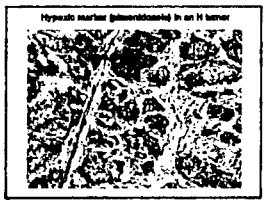

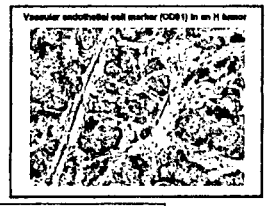

Figure 6 Comparison of pimonidazole and CD31 in a representative H tumor

Well differentiated H tumor containing multiple glandular structures and connective tissue. Immunostaining for hypoxic marker, pimonidazole (left) showed few positive cells. Anti-CD31 (brown, right) demonstrated relatively well distributed vascular endothelial cells in a representative 8 µm section

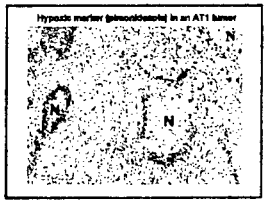

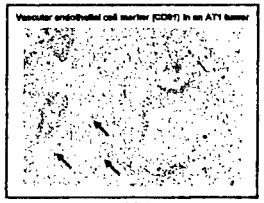

Figure 7 Comparison of pimonidazole and CD31 in a representative AT1 tumor

Anaplastic AT1 tumor is composed of non-glandular structure and fewer stromal cells. Typical distribution of hypoxia in the AT1, recognized as positive staining for pimonidazole (brown, left), was observed at some distances from blood vessels stained for CD31 (arrows, right) and located adjacent to necrotic regions (N). Compared with the level of hypoxia and vasculature in the H tumors, the AT1 tumors have a higher labelling index for pimonidazole (11% versus 2%) and lower vascular density.

University of Texas SOUTHWESTERN Medical Center at Dallas

For further information, you may contact

Ralph.Mason@utsouthwestern.edu

Conclusions

Methodology

- *FREDOM* allows us to measure quantitative pO_2 values at multiple locations simultaneously
- *FREDOM* allows us to monitor dynamic changes at individual locations with respect to interventions.
- Non-invasive *BOLD* and DCE MRI qualitatively evaluate tumor vascular oxygenation and perfusion.
- Immunohistochemical approach provides an assessment of tumor hypoxia and vasculature at the cellular level.

Tumor physiology

- Slower growing, well differentiated H tumors had higher baseline pO_2 compared to faster growing, anaplastic AT1 tumors.
- Respiratory challenge using oxygen produced a significant increase ($p < 0.0001$) in tumor oxygenation.
- *BOLD* and DCE showed that the H subline was better perfused than AT1.
- Comparable results by immunohistochemistry supported our MRI findings.

Discussion

We believe that a combination of *BOLD* and DCE together with quantitative tissue oxygenation by *FREDOM* will provide a better understanding of tumor physiology, specifically related to the proficiency of the vascular component and is relevant to treatment response and prognosis.

References

1. Hurjtjen, B., Zhao, D., Constantinescu, A., Hahn, E. W., Ardbill, P. P., and Mason, R. P. Int. J. Radiat. Oncol. Biol. Phys. 49, 1097-1106, 2001
2. Zhao, D., Constantinescu, A., Hahn, E. W., and Mason, R. P. Radiat. Res. 158, 510-20, 2001.
3. Isaacs, J., Isaacs, W., Feitz, W., and Scherns, J. Prostate 9, 261-91, 1986.

Acknowledgment

This work was supported by the DOD Prostate Cancer Initiative (DAMD 170110108) and NCI RO1 78518. We are grateful to Drs. Peter Ardbill, Sophie Ren and Mark Jeffrey for cellegial support.

PROGRAM & ABSTRACTS

Forty-ninth Annual Meeting of the Radiation Research Society

and the

Twentieth Annual Meeting of the North American Hyperthermia Society

April 20–April 24, 2002
Reno Hilton

In Joint Sponsorship with the Radiological Society

pump). Each tumor-bearing rat was placed under continuous gas anesthesia, using air + ~ 2% Isoflurane, then administered EF5 at -3 hr before X-ray at time '0'. At -40 min. DDFP or saline was administered over 30 min. at 23 microliter/min. At -10 min., the anesthetic gas was either continued with air (for controls) or switched to carbogen (95% O2 + 5% CO2). The tumor was then irradiated and processed for evaluation of radiation response by an *in vivo-in vitro* assay. The EF5 binding period was used to quantify the pre-existing level of tumor hypoxia. The animals were only subjected to carbogen for the last few minutes of the 3 hr EF5 drug exposure, at the time of irradiation. Carbogen alone provided only minimal sensitization. Similarly, DDFP treatment with air was not different than controls without drug. However, DDFP plus carbogen caused dramatic sensitization, and has provided a highly significant decrease in surviving fraction. The response for tumors in the DDFP + carbogen group was the same as for Morris 7777 cells irradiated in air after disaggregation from the tumor, e.g. a completely aerobic radiation response. DDFP plus carbogen appears to completely reverse the hypoxic cell radioresistance in this tumor model. To our knowledge, no previous study has achieved such a complete elimination of radioresistance. For example, misonidazole and etanidazole have only been useful for providing modest sensitization of very radioresistant tumors, and would not provide any sensitization to tumors of intermediate hypoxia.

(P10-86) Hypoxia Marker Binding Predicts for Outcome in Cancer of the Cervix. C. Aquino-Parsons[1], J.P. Banath[1,*], J.A. Raleigh[2,*] and P.L. Olive[1,*]. [1]British Columbia Cancer Agency, 600 W. 10th Ave., Vancouver, B.C. V5Z 1L3. [2]University of North Carolina, Chapel Hill, NC 27599.

Low tumor oxygenation measured using oxygen microelectrodes is known to be predictive for poor outcome in cancer of the cervix. To determine whether the hypoxia marker, pimonidazole, would show a similar predictive ability, patients with invasive epithelial cervical cancers, FIGO stages Ib to IVa, were given pimonidazole hydrochloride as an i.v. infusion (0.5 gm/m^2) 24 hours before tumor biopsy. Patients were subsequently treated with the current standard course of radiation and weekly cisplatinum. After incisional biopsy, a single cell suspension was prepared from approximately 100 mg tumor, and cells were fixed in 70% ethanol. Flow analysis of these samples was performed using anti-pimonidazole antibody, and histograms were analyzed using a curve fitting program that defined hypoxic cells as those that bound on average 10 times more pimonidazole antibody than the well-oxygenated cells of the tumor. In 68 tumor biopsies analyzed for pimonidazole binding, the percentage of hypoxic cells ranged from 0 to 23% with a mean of 5.9%. In 45 patients where follow-up time has now exceeded 1 year, none of the 8 patients with tumors containing less than 1.5% hypoxic cells has yet shown evidence of disease. However, local recurrence and/or metastases were observed in 25% of the remaining 37 patients. These results support the use of hypoxia markers to identify patients with cervical cancer that will respond well to treatment.

(P10-87) Comparison of hypoxia and microvascular density in the slow growing well differentiated H vs. the faster growing anaplastic AT1 Dunning Prostate R3327 rat tumor. D. Zhao[1,*], E.W. Hahn[1,*], S. Ran[2], A. Constantinescu[1] and R.P. Mason[1,*]. [1]Department of Radiology, U.T. Southwestern Medical Center, Dallas, TX 75390. [2]Department of Pharmacology, U.T. Southwestern Medical Center, Dallas, TX 75390.

Tumor oxygenation status is recognized as a significant factor influencing the outcome of radiation therapy. A major program in our laboratory is to understand basic physiological mechanisms that are associated with the level of hypoxia in tumors, by using tumors having diverse growth rates and histology. Here, we compare oxygen dynamics in two Dunning prostate R3327 rat tumor sublines: the well differentiated slower growing H subline (Tpot 16 days) and the anaplastic faster growing AT1 subline (Tpot 5 days). The tumors were transplanted to surgically formed skin pedicles located on the foreback of adult male Copenhagen rats and examined when they were 2~3 cm diameter. We used *FREDOM* tumorally, as the reporter molecule to measure regional tumor oxygen tension using a 4.7 T MR system. We also carried out immunohistochemical studies using pimonidazole to determine the level and distribution of hypoxia and the vascular endothelial cell marker CD31 to determine the micro-vascular density. As expected, *FREDOM* revealed considerable intra tumoral heterogeneity in the distribution of pO_2 values. H tumors had a higher mean baseline pO_2 (12.7 ± 1.1 mmHg) than size-matched AT1 (3.9 ± 1.5 mmHg) tumors ($p<0.001$). The HF<10 mmHg was 45.7 ± 4.8 percent in the H tumors compared to 83.2 ± 3.5 per cent for the AT1 tumors ($p<0.001$). Two percent of the tumor cells in the H tumors were bound with pimonidazole compared to the AT1 subline in which 11% of the cells were pimonidazole positive. Microvascular density (MVD) was also higher in H vs. AT1 tumors. In summary, these results concur with our working hypothesis that the level of hypoxia is related to tumor growth rate and in turn to the vascular architecture. Supported by the DOD Prostate Cancer Initiative (DAMD 170110108) and NCI RO1 79515.

(P10-88) Comparison of the Comet Assay and Eppendorf Electrode to Measure Tumor Oxygenation in Head and Neck Cancer Patients. M.J. Dorie[1,*], D. Terris[2,*], H. Pinto[3], D. Bloch[3], Q.T. Le[1], J.M. Brown[1,*] and M.S. Kovacs[1,*]. [1]Department of Radiation Oncology, Stanford University, Stanford, CA 94305. [2]Department of Surgery, Stanford University, Stanford, CA 94305. [3]Department of Medicine, Stanford University, Stanford, CA 94305. [4]Department of Health Research and Policy, Stanford University, Stanford, CA 94305.

As part of a clinical trial of the addition of tirapazamine to chemoradiotherapy of node positive stage IV head and neck cancer, we measured the oxygenation of the neck nodes prior to treatment using both the Eppendorf oxygen electrode and the induction of DNA single strand breaks (SSBs) after a dose of 5 Gy using the alkali comet assay. The median oxygenation (by Eppendorf) was 11.8 mmHg for the tumors and 51.9 mmHg for the normal subcutaneous tissue. In addition to fine needle aspirates taken 1, 2 and 3 minutes after the 5 Gy dose, we took samples prior to irradiation to establish a baseline comet tail moment, and irradiated these samples *in vitro* to establish the tail moment distribution in fully oxygenated cells following 5 Gy. We analyzed the comet distributions using median tail moment (MTM) after removal of baseline contamination due to the presence of unirradiated cells in the sample. We found a highly significant correlation between the MTM values for 1 and 2 minutes ($r^2=0.66$, $p<0.0001$) thereby demonstrating the reliability of the assay. The slope of this line is consistent with the expected half-life of 3 minutes for the repair of radiation-induced SSBs. A comparison of the *in vivo* and *in vitro* MTM data indicates that the inter-tumor variation in DNA damage is not due to differences in intrinsic radiosensitivity between tumors, but rather due to variation in oxygenation from tumor to tumor. However, we found no correlation between the Eppendorf median pO_2 and the comet MTM ($r^2=0.09$). The data for tumor oxygenation determined by the comet assay and clinical outcome will be presented.

(P10-89) Tumor hypoxia assessment in breast cancer. M.A. Varia[1,*], S.C. Chou[1], C.A. Ballenger[2], S. Maygarden[3], L. Licht[1] and J.A. Raleigh[1,*]. [1]Department of Radiation Oncology, Universityof North Carolina, Chapel Hill, NC 27599. [2]Department of Radiation Oncology, Duke University Medical Center, Durahm, NC 27710. [3]Department of Pathology, University of North Carolina, Chapel Hill, NC 27599.

As tumor hypoxia predicts for poor prognoses in human cancers, there is increasing interest in developing methods of hypoxia assessment. Several clinical studies show the presence of tumor hypoxia in uterine cervical carcinoma, head and neck cancer, and soft tissue sarcomas, however little is known about the presence of tumor hypoxia in breast cancer, the most common cancer in women. We have initiated studies of tumor hypoxia assessment in human breast cancer using pimonidazole as the hypoxia marker. Patients with biopsy confirmed breast carcinoma are enrolled in

INTERNATIONAL SOCIETY FOR MAGNETIC RESONANCE IN MEDICINE

Tenth Scientific Meeting and Exhibition

18 – 24 May 2002

Honolulu, Hawai'i, USA

Program

INTERNATIONAL SOCIETY FOR
ISMRM
MAGNETIC RESONANCE IN MEDICINE

Measurement of tumor oxygen dynamics correctly predicts beneficial adjuvant intervention for radiotherapy in Dunning prostate R3327-HI tumors

D. Zhao, A. Constantinescu, K.C. Chang, K. Gall, E.W. Hahn, and R.P. Mason,
Departments of Radiology and Radiation Oncology, U.T. Southwestern Medical Center, Dallas, TX, USA

It is generally recognized that accurate measurement of tumor oxygenation could predict response to radiotherapy. We have recently established a magnetic resonance approach to measuring regional tumor oxygen tension *FREDOM* (Fluorocarbon Relaxometry using Echo planar imaging for Dynamic Oxygen Mapping) with hexafluorobenzene, as a reporter molecule. *FREDOM* data showed that the hypoxic fraction in large Dunning prostate R3327-HI tumors decreased significantly with oxygen inhalation. Here, we tested the effect of the adjuvant intervention of oxygen inhalation on radiotherapy of these tumors. Radiation induced growth delay corresponded with decreased hypoxic fraction.

Introduction: It is recognized that tumor hypoxia influences the outcome of radiation therapy, and increased tumor oxygenation promotes radiosensitivity. We have developed a method to measure tumor oxygen tension quantitatively and now demonstrate its prognostic value with respect to radiation induced tumor growth delay. The *FREDOM* approach exploits the strong sensitivity of the ^{19}F NMR spin lattice relaxation rate of the reporter molecule hexafluorobenzene to pO_2 (1). Our earlier studies showed that oxygen inhalation significantly decreased tumor hypoxia in the moderately well differentiated subline of Dunning prostate R3327-HI rat carcinoma (2). To test our hypothesis that oxygen inhalation is an effective adjuvant intervention for radiotherapy, we compared tumor response to ionizing radiation alone or in combination with oxygen inhalation.

Methods: Syngeneic Dunning prostate R3327-HI tumors (moderately well differentiated, volume doubling time 9 days; TCD_{50} ~ 50 Gy) were implanted in surgically formed skin pedicles on the foreback of male Copenhagen rats. Tumors were measured thrice weekly with calipers. Tumors were allowed to grow to ~1 cm diameter (~0.6 cm^3) or 2 cm diameter (> 3.5 cm^3), at which time they were divided into groups for irradiation. Prior to irradiation, pO_2 was assessed in selected tumors using *FREDOM*. Hexafluorobenzene (50 µl) was injected directly into the tumor. A size matched $^1H/^{19}F$ single turn solenoid coil was placed around the tumor and MR experiments were performed using a 4.7 T magnet with actively shielded gradients. Tumor oxygenation was assessed using ^{19}F PBSR-EPI of HFB with 8 minute time resolution. For those rats, which would breathe oxygen during irradiation, a respiratory challenge with oxygen was performed to assess the response of tumor pO_2. Regional pO_2 was estimated using the relationship: pO_2 (torr) = (R1-0.0835)/0.001876.

Several hours after MRI measurements, irradiation was performed using a single dose (30 Gy) at 6 MeV on a Siemens KDS linear accelerator. Half the rats breathed oxygen for 30 min prior to and during irradiation, while the others breathed air. A treatment plan was designed to irradiate the tumors only and bolus material was used to improve dose uniformity.

Results: In common with our previous findings (2), the larger tumors (> 3.5 cm^3) exhibited greater hypoxia than the smaller tumors (< 2 cm^3). Baseline mean and median pO_2 were 28.4 ± 1.1 torr and 25.3 torr in the smaller tumors, but significantly lower in the larger tumors (4.6 ± 1.0 torr and 1.7 torr; $p < 0.001$). With oxygen inhalation, pO_2 increased significantly in both the smaller (mean = 179.6 ± 16 torr; median = 177.4 torr) and the larger tumors (mean = 110.2 ± 13.6 torr; median = 70.1 torr). For all tumors, irradiation produced a significant growth delay compared with sham irradiated controls, but for small tumors oxygen inhalation had no additional effect. By contrast, for the larger tumors, oxygen inhalation produced enhanced growth delay (enhancement ratio = 2.4).

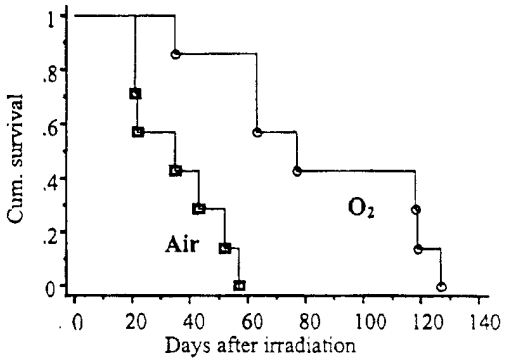

For large HI tumors a significant growth delay (50 days; $p < 0.01$) was observed when rats inhaled oxygen during irradiation. The Kaplan Meier survival plot indicates time to reach 3 x initial size (or earlier sacrifice, as needed).

Discussion: When rats breathed oxygen during irradiation, large HI tumors exhibited a significantly longer growth delay than those breathing air. For small tumors, no difference was observed. The differential behavior may be attributed to the low baseline hypoxic fraction (< 10 torr) in small tumors (20%) as a target for oxygen inhalation. Meanwhile, hypoxic fraction in the larger tumors dropped significantly from a mean baseline value 80% to a final value 21% after 40 min oxygen breathing ($p < 0.001$). These data suggest that the ability to detect modulation of tumor pO_2, in particular, the residual hypoxic fraction, with respect to an intervention, could have prognostic value for improving the efficacy of radiotherapy. These results further demonstrate the value of *FREDOM* to assess *in vivo* dynamic changes in regional pO_2 as a prognostic tool.

References:

1. Hunjan, S., Zhao, D., Constantinescu, A., Hahn, E. W., Antich, P. P., and Mason, R. P. *Int. J. Radiat. Oncol. Biol. Phys.* 49, 1097-1108, 2001.

2. Zhao, D., Constantinescu, A., Hahn, E. W., and Mason, R. P. *Radiat. Res.* 156, 510-520, 2001.

Acknowledgment: Supported by DOD Prostate Cancer Initiative (DAMD 170110108) and NCI RO1 79515.

The Tumor Microenvironment and Its Impact on Cancer Therapies
8th International Workshop

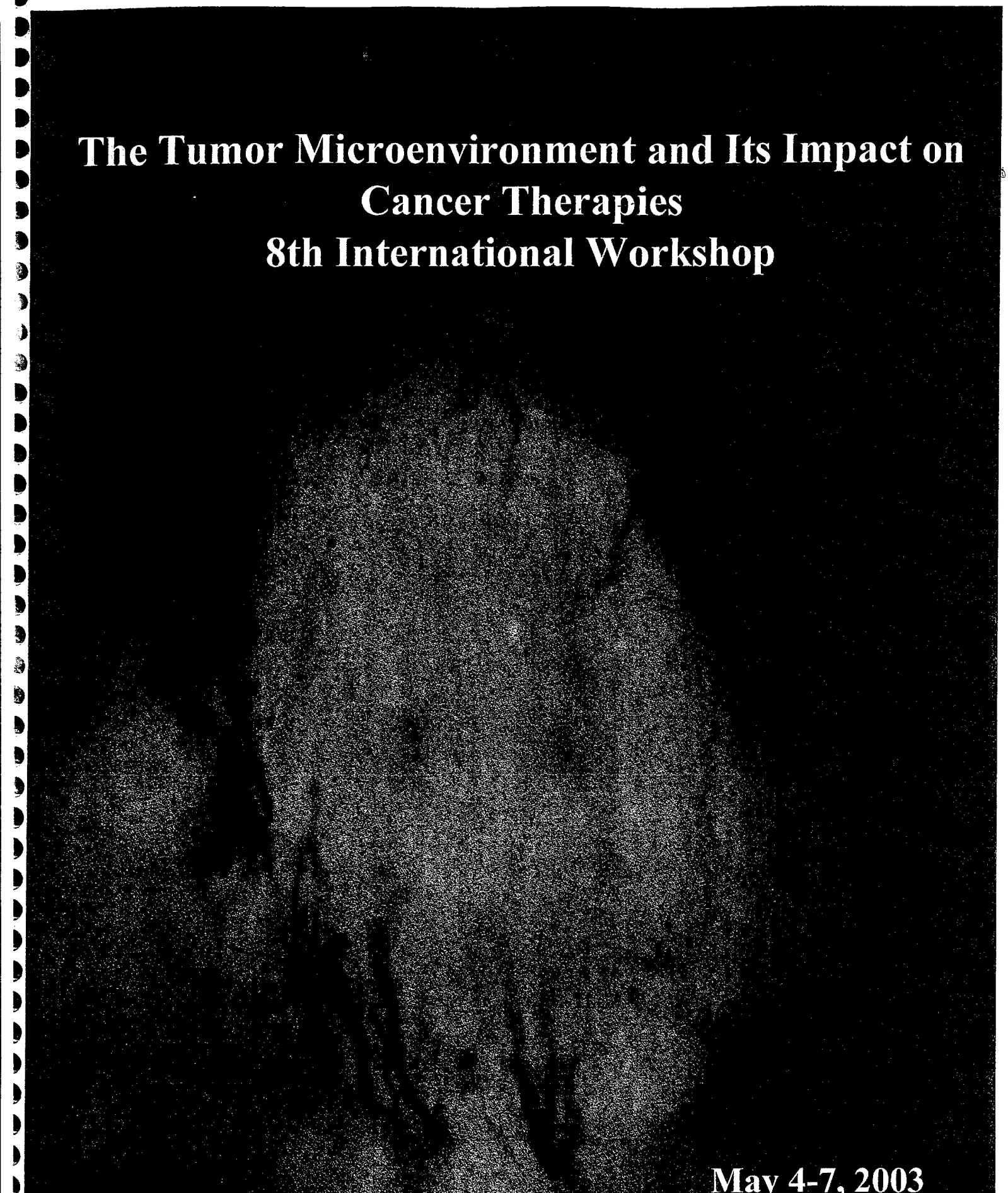

May 4-7, 2003

MRI EVALUATION OF METRONOMIC CHEMOTHERAPY: THE ANTITUMOR EFFECTS OF COMBINED LOW-DOSE CYCLOPHOSPHAMIDE AND THALIDOMIDE ON PROSTATE TUMORS

DAWEN ZHAO, SOPHIA RAN[+], ANCA CONSTANTINESCU, ERIC W. HAHN, AND RALPH P. MASON
DEPARTMENTS OF RADIOLOGY AND [+]PHARMACOLOGY,
UT SOUTHWESTERN MEDICAL CENTER, DALLAS, TX 75390, USA

Several reports suggest that continuous low dose administration of certain cytotoxic agents, so-called "metronomic" chemotherapy can strongly potentiate the efficacy of anti-angiogenic or anti-vascular therapies. We believe that non-invasive approaches (imaging) can greatly enhance the understanding of the mode of action and efficacy of a specific treatment protocol. We have used Dynamic Contrast Enhanced (DCE) Magnetic Resonance Imaging (MRI) to explore changes in the vasculature of Dunning R3327-AT1 prostate rat tumors during a metronomic schedule. Therapy comprised low-doses of the chemotherapeutic agent, cyclophosphamide (CTX; 20 mg/kg p.o. daily) singly or in combination with the angiogenic inhibitor, thalidomide (60 mg/kg i.p. twice a week).

AT1 tumors are relatively fast growing undifferentiated tumors with a volume doubling time of 4.6 days. The syngeneic tumors were implanted in skin pedicles on the foreback of male Copenhagen rats. When tumors reached ~1 cm diameter (~0.6 cm^3) DCE MRI was performed using a 4.7 T MR system and a bolus injection of Gd-DTPA (0.1 mmol/kg, Magnevist) through a tail vein catheter. The tumors showed considerable heterogeneity with greater and more rapid contrast changes in the tumor periphery, than the center. Metronomic therapy was initiated the following day and tumor growth monitored with calipers. After 7 days of treatment, DCE-MRI revealed significant changes in the central regions of the tumors, where contrast changes were now much less and slower. The contrast response of the tumor rim was, however, essentially, as before. At this stage, little difference in tumor size was apparent, but ultimately there was a significant growth delay in the AT1 tumors receiving combined metronomic treatment, compared with the control group (30 days; $p<0.05$).

Histological sections with H&E staining confirmed that the combined treatment caused a large amount of necrosis in the central regions, leaving a thin peripheral region alive. This tumor type normally has only isolated central micro necroses. Interestingly, vascular thrombosis was observed in numerous tumor microvessels in the groups treated with thalidomide alone or the metronomic combination. Apoptotic endothelial cells detected by an antibody against apoptosis marker, caspase 3, were evident in the vessels packed with thrombi. Immunohistochemical studies also showed significantly increased number of apoptotic tumor cells and decreased number of dividing cells that are identified by anti-PCNA antibody.

In summary, non-invasive DCE MRI revealed intra-tumoral heterogeneity in *situ, in vivo* and changes in temporo-spatial dynamics, which may give an early indication of treatment response and ultimately allow scheduling, dosage and drug combination to be optimized.

Supported by the DOD Prostate Cancer Initiative (DAMD 170110108) (DZ) and NCI RO1 79515.